Titre: Title:	Viscous-inviscid interaction on wings at low speeds
Auteur: Author:	Pascal Tram
Date:	1992
Type:	Mémoire ou thèse / Dissertation or Thesis
Référence: Citation:	Tram, P. (1992). Viscous-inviscid interaction on wings at low speeds [Mémoire de maîtrise, Polytechnique Montréal]. PolyPublie. https://publications.polymtl.ca/57028/

URL de PolyPublie: PolyPublie URL:	https://publications.polymtl.ca/57028/
Directeurs de recherche: Advisors:	Ion Paraschivoiu
Programme: Program:	Génie mécanique

UNIVERSITÉ DE MONTRÉAL

Viscous-Inviscid Interaction on Wings

at Low Speeds

par

Pascal TRAN

DÉPARTEMENT DE GÉNIE MÉCANIQUE

ÉCOLE POLYTECHNIQUE

RAPPORT DE PROJET PRÉSENTÉ EN VUE DE L'OBTENTION

DU GRADE DE MAITRE EN INGÉNIERIE (M.Ing.)

GÉNIE MÉCANIQUE

Avril 1992

SOMMAIRE

La réalisation d'une aile pour une application spécifique requiert l'étude de l'écoulement autour de cette aile afin de déterminer différents paramètres aérodynamiques tels la distribution de pression et de vitesse ainsi que les forces sur l'aile. L'industrie aéronautique est donc intéressée à développer des moyens permettant de faire ces calculs le plus précisément possible tout en étant assez économique en temps et en argent. Si on tient compte de la viscosité et de la compressibilité de l'air, il faudrait résoudre les équations de Navier-Stokes pour obtenir une prédiction des propriétés de base de l'écoulement. La résolution des équations de Navier-Stokes pour des applications pratiques est extrêmement difficile et demande des ordinateurs de très grande capacité. Même en utilisant ces ordinateurs, le temps de calcul est beaucoup trop long pour que la résolution des équations de Navier-Stokes soit intéressante.

Une autre méthode pour obtenir une prédiction des propriétés de l'écoulement est celle des essais en soufflerie. La difficulté de cette méthode est qu'elle est très onéreuse puisque qu'elle demande de grandes installations.

Nous nous proposons de tester une méthode appelée VII ou Viscous-Inviscid Interaction qui nous permettrait de calculer la distribution de pression et autres paramètres aérodynamique pour différentes ailes tri-dimensionnelles. Cette méthode est basée sur l'hypothèse suivante, l'écoulement peut être divisé en deux parties, une partie externe où les effets visqueux sont négligés et une partie proche de la surface de l'aile où il faudra tenir compte de la viscosité. Cette hypothèse est certainement valide puisque

dans beaucoup d'applications de l'aérodynamique, les effets de la viscosité et de la turbulence sont limités à une très mince région près de la surface de l'aile, région qui est appelée la couche limite, et au sillage. Dans cette région, nous devrons résoudre les équations de la couche limite. A l'extérieur de cette région, les équations non-visqueuses d'Euler ou toute autre approximation appropriée sera résolue. Les deux régions seront résolues séparément et les deux solutions obtenues seront combinées de façon interactive pour obtenir la solution au problème. Cette méthode est beaucoup plus économique que la résolution des équations de Navier-Stokes ou que les essais en soufflerie. De plus, elle donne des résultats très satisfaisants.

Le rapport expose donc la théorie nécessaire à la construction d'un programme en utilisant cette méthode. Pour le calcul non-visqueux, deux méthodes de panneaux sont étudiées. Le chapitre 1 présente la théorie de ces deux méthodes. Le chapitre 2 présente la théorie des différents modèles pour la couche limite utilisés. De plus, ce chapitre présente aussi la modèle pour la combinaison des deux solutions. Le modèle retenu est celui de la vitesse de transpiration. L'effet de la couche limite vient ajouter une composante de vitesse normale. Cette méthode a l'avantage de ne pas changer la géométrie du problème à chaque itération. Le chapitre 3 présente une description des programmes et des instructions afin de les utiliser. Le chapitre 4 présente les résultats pour trois cas qui ont été testés et comparés avec des résultats expérimentaux disponibles ou d'autres résultats présentés dans les références. Finalement, les annexes présentent des informations complémentaires à la théorie présentée dans les chapitres 1 et 2.

ABSTRACT

One must study the flow around a wing and obtain the aerodynamic parameters, for instance the pressure and velocity distributions and the overall forces, to design successfully this wing for a specific application. The aeronautical industry is interested to develop methods that are accurate yet not too costly to calculate these aerodynamic parameters. If one takes into account the viscosity and compressibility of the fluid, one must resolve the Navier-Stokes equations to predict the basic flow properties. The solution of the Navier-Stokes for practical applications is extremely difficult and involves the use of supercomputers. Even then, the computational time involved is prohibitive.

Another method used to obtain the basic flow properties is the use of wind tunnels. The disadvantage of this method is that it is very costly as it requires large installations.

The object of the project is to test a method named VII or Viscous-Inviscid Interaction to calculate the pressure distribution and other aerodynamic parameters. The method is based on the following assumption, that the flow can be divided in two separate regions, an external region where the effects of viscosity can be neglected and an internal region near the surface of the wing where the viscosity is taken into account. This assumption is certainly valid for many practical applications because the effects of viscosity and turbulence are confined to a thin region near the body surface, region named boundary layer, and its wake. In this region, the boundary layer has to be solved. In the external region, the inviscid Euler equations or a suitable

approximation are solved. The two solutions are obtained separately and then are matched in an iterative manner to obtain a composite solution to the problem. This method is less expensive or time-consuming than the solution of the Navier-Stokes equations or the wind tunnel testing. It gives very accurate results.

The report presents the theory necessary to construct a code using this VII method. Two panel methods are studied for the inviscid calculation. Chapter 1 presents these two methods. Chapter 2 presents the different models used for the boundary layer calculation. It also presents the matching technique for the two solutions. The model studied is the transpiration velocity model. It has the distinct advantage that the geometry of the body remains constant during the calculation. Chapter 3 describes the computer codes and gives instructions for the use of these codes. Chapter 4 presents the results for three test cases that have been studied and compared with experimental results when available or other results taken from the references. Finally, the appendices presents additional information to complete the theory presented in chapters 1 and 2.

ACKNOWLEDGEMENTS

RÉSUMÉ

De plus en plus, l'industrie aéronautique utilise des méthodes numériques pour aider dans la conception d'avions. Il est certainement possible d'obtenir des résultats très précis avec plusieurs des méthodes numériques employées. Une de ces méthodes est connue sous le nom de "Viscous-Inviscid Interaction" ou VII. Le but de ce projet est d'adapter des programmes utilisant cette méthode et de les tester.

La méthode de VII peut être séparée en trois parties distinctes. D'abord une méthode numérique pour le calcul de l'écoulement dans la partie où la viscosité est négligée. Deuxièmement, une méthode de calcul pour la couche limite. Et finalement, une méthode de combinaison pour les résultats des deux premières méthodes. Cette méthode est particulièrement efficace pour les cas où la couche limite demeure attachée jusqu'au bord de fuite comme les ailes d'avion en régime de croisière. Dans ce projet, tous les cas étudiés tombent dans cette catégorie.

L'hypothèse de base pour le calcul potentiel est que l'écoulement est non-visqueux et irrotationel donc incompressible. Dans ce cas, la vitesse V peut être dérivée d'un potentiel Φ par la relation suivante

$$\overline{V} = \nabla\Phi \tag{1}$$

L'écoulement est donc régi par l'équation suivante

$$\nabla^2 \Phi = 0 \tag{2}$$

Cette équation est une des plus étudiée et est appelée

l'équation de Laplace. Toutes les solutions de l'équation de Laplace sont des fonctions harmoniques.

Les méthodes numériques les plus souvent utilisées pour résoudre ce type de problème sont les méthodes de panneaux. Le principe de superposition peut donc être appliqué à cause de la linéarité de l'équation. Ce principe spécifie que la somme de différentes solutions de l'équation aux dérivées partielles est aussi une solution de l'équation. Ainsi, l'écoulement irrotationel et incompressible autour d'une aile peut-être représenté par la somme de différents écoulements irrotationels et incompressibles élémentaires. Ces écoulements sont appelés des singularités comme les sources, tourbillons et doublets. Les méthodes de panneaux distribuent des singularités sur la surface de l'aile ou sur la surface de cambrure moyenne et obtiennent les paramètres de l'écoulement en résolvant le système d'équations linéaires résultant. La formulation mathématique de ces méthodes de panneaux nous vient du théorème de Green. Dans le projet, deux méthodes de panneaux sont étudiées, la méthode de la distribution des singularités internes comme décrite par Singh[8] et la méthode des singularités égales de Newling[9]. Ces deux méthodes sont décrites ci-après.

Méthode des singularités internes

Cette méthode distribue des sources et des tourbillons sur la surface de cambrure moyenne de l'aile. Elle résout cette distribution de singularités en appliquant la condition frontière de vitesse normale. Cette vitesse normale est égale à zéro pour la première itération et est non-nulle pour les autres itérations. La vitesse normale est calculée à certains points choisis sur la surface de l'aile. Ces points sont

appelés points de collocation. Le calcul de la couche limite vient modifier cette vitesse normale pour les autres itérations suivant la première. Les Figures 3 à 7 montrent la géométrie de l'aile et sa discrétisation.

Des sources et des tourbillons sont distribués sur la surface de cambrure moyenne, en laissant un espace près du bord d'attaque. De plus, la distribution de tourbillons est appliquée sur la surface du sillage aussi. Deux sources linéaires sont placées sur des lignes L_1 et L_2 près du bord d'attaque dans la direction de l'envergure. Finalement, un tourbillon en fer à cheval est placé sur la ligne L_3 qui est à mi-distance entre L_1 et L_2. Les deux sources linéaires et le tourbillon en fer à cheval sont placés pour mieux simuler la rondeur du bord d'attaque. Venant du théorème de Green, l'équation à résoudre est la suivante

$$-4\pi \overline{V}_\omega \overline{n}_p = \iint_{S_c} \sigma_s (\overline{K}_s \overline{n}_p)\, dS + \int_{S_c+S_v} (\overline{\gamma} \times \overline{K}_v)\, \overline{n}_p dS$$
$$+ \sum_{L_3} (\overline{K}_{HV} \overline{n}_p)\, \Gamma_h + \int_{L_1+L_2} (\sigma_1 + \sigma_2)\, (\overline{K}_{LS} \overline{n}_p)\, dl \qquad (3)$$

La composante normale de V_p est zéro à tous les points de collocation à la première itération et non-nulle pour toutes les autres.

Pour obtenir la solution pour l'écoulement non-visqueux, on doit résoudre l'équation (3) simultanément avec la condition de Kutta. Pour ce faire, on doit discrétiser l'équation intégrale pour obtenir un système d'équations algébriques linéaires. L'aile est discrétisée en petits éléments appelés panneaux, d'où le nom de la méthode. La formation de ces panneaux est décrite en plus de détail en annexe A. La Figure

3 montre la discrétisation de la surface. On voit que ces panneaux sont formés par deux séries de lignes qui sont approximativement parallèles, une dans le sens de la corde et l'autre dans le sens de l'envergure. Les centroïdes de ces panneaux sont choisis comme points de collocation où est appliquée la condition frontière. Des points de collocation sont ajoutés près du bord d'attaque. Pour calculer la surface de cambrure moyenne, le programme fait la moyenne entre les coordonnées z des panneaux correspondants sur l'intrados et l'extrados. La discrétisation de cette surface est montrée à la Figure 4.

La force de la distribution de sources est constante sur un élément mais varie d'élément en élément. La force de la distribution de tourbillons reste constante dans la direction de l'envergure mais varie linéairement dans l'autre direction. Pour obtenir un résultat, nous devons satisfaire la condition de Kutta. Cette condition sera satisfaite en maintenant la valeur des tourbillons au bord de fuite à zéro. L'équation intégrale (3) peut être approximée par le système d'équations algébriques linéaires suivant:

$$\sum_{k+1}^{(I-1)(M-1)} A_{jk}\sigma_{sk} + \sum_{k=1}^{(I-1)(M-1)} B_{jk}\gamma_k + \sum_{k=1}^{M-1} C_{jk}(\sigma_{L1k}+\sigma_{L2k})$$
$$+\sum_{k=1}^{M-1} D_{jk}\Gamma_{hk} = -\overline{n}_p\overline{V}_\infty \tag{4}$$

A_{jk}, B_{jk}, C_{jk} et D_{jk} sont les composantes normales de la vitesse induite au jième point de collocation par la kième source, tourbillon, source linéaire et tourbillon en fer à cheval respectivement. Les équations nécessaires pour calculer ces vitesses induites sont données dans les annexes B et C. Ce système d'équations est écrit sous forme matricielle et est

résolu par un technique d'orthogonalisation pour obtenir les valeurs des singularités. On peut alors calculer la vitesse à tout point de collocation par

$$\overline{V}_j = \sum_{k=1}^{N_T} \overline{V}_{jk} \Pi_k + \overline{V}_\infty \qquad (5)$$

où V_{jk} représente la vitesse induite au jième point de collocation par la kième singularité Π_k. N_T représente le nombre de singularités. Une fois les vitesses connues, le coefficient de pression est calculé comme suit

$$C_{pj} = 1 - \frac{\overline{V}_j \overline{V}_j}{V_\infty^2} \qquad (6)$$

Les forces sur l'aile sont calculées par une intégration numérique en supposant que la pression est constante sur chaque panneau.

Méthode des singularités égales

Cette méthode distribue des singularités sur la surface de l'aile. L'aile est discrétisée de la même façon que dans le cas de la méthode des singularités internes. Une distribution de sources et de tourbillons est placée sur la surface. La valeur des tourbillons est constante sur chaque panneau mais varie de panneau en panneau. La vorticité reste constante dans la direction de l'envergure mais varie linéairement dans l'autre direction. Pour réduire le nombre d'inconnues, la valeur des singularités est supposée égale sur des panneaux correspondants sur l'intrados et l'extrados. Nous avons une équation intégrale à résoudre que nous transformons en

système linéaire par la discrétisation de la surface. Le système est le suivant

$$\sum_{k=1}^{\frac{MxN}{2}} A_{jk}\sigma_k + \sum_{k=1}^{\frac{MxN}{2}} B_{jk}\gamma_k = -\overline{n}_k\overline{V}_\infty \qquad (7)$$

A_{jk} et B_{jk} représentent les vitesses induites par la kième source et tourbillon respectivement sur le jième point de collocation. Les valeurs des singularités sont obtenues par une technique d'orthogonalisation. Ensuite, la distribution de pression et de vitesse sont obtenues de la même façon que dans le cas de la méthode des singularités internes.

Calcul de la couche limite

La deuxième partie de la technique VII est le calcul de la couche limite. Une hypothèse est formulée, que le gradient de pression à travers la couche limite est négligeable et que seulement les dérivées normales des contraintes en cisaillement sont importantes pour le calcul. Le calcul de la couche limite se divise en trois parties: un calcul laminaire, une prédiction de la transition et un calcul turbulent.

Dans le projet, la méthode utilisée pour le calcul de l'écoulement laminaire est la méthode de Thwaites[10]. La transition de l'écoulement laminaire à turbulent est calculer grâce au critère de Mitchel. Cette transition est supposée soudaine. Cette hypothèse nous permet d'obtenir les valeurs de départ pour le calcul de l'écoulement turbulent en supposant qu'elles sont égales à celles de l'écoulement laminaire.

La méthode intégrale décrite par P.D. Smith[11] est utilisée pour le calcul de la couche limite turbulente en trois dimensions. Trois équations sont primordiales à ce calcul: les deux équations de la quantité de mouvement et l'équation de la continuité. Un système de coordonnées curvilignes non-orthogonales est nécessaire à la résolution du problème. La surface de l'aile est divisée en une série d'éléments quadrilatéraux.

Les trois équations fondamentales sont écrites pour le nouveau système de coordonnées. Pour réduire le nombre d'inconnues, des profils de vitesse sont supposés dans la direction de l'écoulement et la direction de l'envergure. De plus, des relations empiriques sont utilisées pour les coefficients de friction et le coefficient d'entraînement. Avec toutes ces simplifications, le nombre d'inconnues est réduit à trois, l'épaisseur dans la direction de l'écoulement θ_{11}, le paramètre de forme H et β, l'angle entre la ligne de courant extérieure et là ligne de courant correspondante sur la surface de l'aile. Le système d'équations aux dérivées partielles du premier ordre en fonction de ces trois inconnues est écrit comme suit

$$F_{11}\frac{\partial\theta_{11}}{\partial x}+\theta_{11}F_{11H}\frac{\partial H}{\partial x}+\theta_{11}F_{11\beta}\frac{\partial\beta}{\partial x}=S_1$$
$$F_{21}\frac{\partial\theta_{11}}{\partial x}+\theta_{11}F_{21H}\frac{\partial H}{\partial x}+\theta_{11}F_{21\beta}\frac{\partial\beta}{\partial x}=S_2 \qquad (8)$$
$$J_1\frac{\partial\theta_{11}}{\partial x}+\theta_{11}J_{1H}\frac{\partial H}{\partial x}+\theta_{11}J_{1\beta}\frac{\partial\beta}{\partial x}=S_3$$

Les expressions pour les différents F, J et S sont donnés en annexe D. Ces équations sont hyperboliques. Les équations hyperboliques ont deux directions caractéristiques réelles. Une méthode de différences finies est utilisée pour les

résoudre. Le plan x-y est divisé pour former une grille
rectangulaire comme montré à la Figure 9. Parce que les
équations sont hyperboliques, il y a le concept d'un front
qui avance. Au point (i,j), tous les termes du membre de
droite sont connus, alors on peut calculer les dérivées.
Ensuite, les dérivées au point (i+1,j) sont trouvées par
extrapolation. La sous-routine effectuant le calcul de la
couche limite reçoit de l'information du calcul potentiel.
Ces données sont interpolées par une technique de spline
bicubique.

Vitesse de transpiration

Une fois le calcul de la couche limite complété, nous devons
calculer la vitesse de transpiration qui vient modifier la
vitesse normale pour un autre calcul non-visqueux équivalent.
Cette vitesse de transpiration est donnée par l'équation
suivante:

$$W_{iw} = \frac{1}{q}\left[\frac{\partial}{\partial x}\left(\frac{u_e \Delta_1 q}{h_1} \right) + \frac{\partial}{\partial y}\left(\frac{u_e \Delta_2 q}{h_2} \right) \right] \qquad (9)$$

Cette vitesse modifie les conditions aux limites pour le
calcul potentiel et la distribution de vitesse et de pression
sont recalculées pour le prochain calcul de la couche limite.
Ces vitesses de transpiration sont calculées après chaque
cinq itérations du calcul de la couche limite. Le procédé
itératif arrête quand la différence entre les coefficients de
portance obtenus entre deux itérations est plus petite qu'une
certaine valeur pré-déterminée.

Modifications aux programmes

Les programmes étaient originalement destinés à être utilisés aur un mini-ordinateur Horizon III et ont été modifiés pour être utilisés sur le système MUSIC. Il y a plusieurs différences entre les deux compilateurs FORTRAN. D'abord toute la structure d'entrée et de sortie de données a été changée. Les programmes doivent être exécutés en lot puisque la demande de mémoire était trop grande. Originalement, il y avait trois programmes, un pour chacune des deux méthodes de panneaux et un pour le calcul de la couche limite. Chacun de deux programmes pour les méthodes de panneaux a été regroupé avec le programme pour le calcul de la couche limite pour ne former que deux programmes.

Pour combiner les programmes, il faut passer les variables en paramètres. Pour ce faire, les programmes ont dûs être dissectés pour bien comprendre leur structure. Le compilateur sur le Horizon III est moins strict que celui sur MUSIC. Cela nous a obligé à apporter des modifications de quelques fonctions et quelques boucles. Pour utiliser ces programmes, des batchfiles ont été écrits et l'usager n'a qu'à exécuter ces batchfiles. La description complète des programmes et de leur utilisation est décrite au chapitre 3.
Trois cas ont été étudiés à l'aide des programmes. Le cas d'une aile polygonale avec profil NACA 0005. Ce cas teste bien les limites de la méthode. Les résultats obtenus sont comparés avec la solution de Roberts[14]. La comparaison est montrée par les Figures 10 à 13. Les résultats sont satisfaisants excepté près de la base de l'aile. Quand on s'éloigne de la base de l'aile, les résultats sont très satisfaisants. Le deuxième cas étudié est celui d'une aile quasi-rectangulaire avec profil NACA 64A410, donc un profil cambré. Les résultats sont obtenus pour les deux méthodes de panneaux et sont montrés aux Figures 14 à 16. Les résultats

concordent très bien. Finalement, le troisième cas est celui d'une aile avec un angle de flèche de 45° et profil NACA 64A010. Les résultats obtenus sont comparés avec des résultats expérimentaux. La comparaison est montrée aux Figures 17 à 21. La différence est de l'ordre de 1.11%. On peut donc voir que les résultats obtenus par une technique VII sont très satisfaisants. De plus, nos tests numériques ont démontré que la méthode des singularités internes est environ deux fois plus rapide que l'autre méthode étudiée.

L'application bidimensionnelle de la couche limite donne de très bons résultats pour des cas où l'angle de flèche et l'allongement ont des valeurs raisonnables. Pour des cas où la couche limite ne demeure pas attachée jusqu'au bord de fuite, une méthode tridimensionnelle de la couche limite devra être appliquée.

Nous n'avons pu obtenir de bons résultats avec des ailes très minces, de profil NACA 0002. De plus, pour des angles d'attaque supérieurs à 9°, les résultats ne sont pas très satisfaisants.

Pour améliorer les résultats obtenus, une méthode tridimensionnelle complète pourrait remplacer la méthode quasi-tridimensionnelle utilisée dans ce projet. De plus, d'autres méthodes de panneaux pourraient être essayées pour le calcul potentiel combiné avec une correction pour la couche limite.

La technique VII est très certainement une alternative de choix aux méthodes d'essais en soufflerie ou à la résolution des équations de Navier-Stokes car elle donne de très bons résultats et elle est très économique d'utilisation. Elle

peut même être étendue au calcul d'autres cas intéressants comme en régime transsonique par exemple, où une modélisation pertinente de la couche limite au pied des ondes de choc sera nécessaire.

Contents

List of Figures

Notation

A_{jk}	normal velocity induced at the j-th collocation point by a unit value of source density on the k-th element
B_{jk}	normal velocity induced at the j-th collocation point by a unit value of vorticity on the k-th element
C_f	skin friction coefficient
C_{f1}	skin friction coefficient in the streamwise direction
C_{f2}	skin friction coefficient in the normal direction
C_{jk}	normal velocity induced at the j-th collocation point by a unit strength line source
C_p	pressure coefficient
C_L	total lift coefficient
D_{jk}	normal velocity induced at the j-th collocation point by a unit strength k-th horseshoe vortex
F	total force on the wing surface
H	shape parameter
H	transformed shape parameter
H_1	entrainment shape parameter
Ki	kernel functions (i=1,4)
l	Thwaites non-dimensional parameter
m	Thwaites non-dimensional parameter
M	Mach number
n	index of the power law velocity profile
n_p	outward normal vector
R_N	Reynolds number
R_x	local Reynolds number

R_θ	Reynolds number based on momentum thickness
s	streamwise coordinate
u	velocity in the x direction
u_e	resultant velocity at the edge of a three dimensional boundary layer
U	velocity in the streamwise direction
v	velocity in the y direction
V	velocity in the normal direction in boundary layer calculation and total velocity in inviscid flow calculation
V_{iw}	transpiration velocity
w	velocity in the z direction
α	angle of attack; angle between the x axis and the external streamline in boundary layer calculation
β	angle between the external streamline and corresponding limiting streamline on the surface of the wing
ρ	density
γ	vorticity strength
Γ_h	horseshoe vortex strength
σ	source strength
σ_L	line source strength
μ	doublet strength
Π	generalised singularity strength
Φ	velocity potential function
Ω_{LE}	leading edge sweepback
τ	shear stress
δ	boundary layer thickness
δ^*	boundary layer displacement thickness
θ	boundary layer momentum thickness

Δ_1, Δ_2 streamwise and crossflow displacement thicknesses in   the non-orthogonal coordinate system

θ_{11}, θ_{12} streamwise and crossflow momentum integral thicknesses

θ_{21}, θ_{22} in the non-orthogonal coordinate system

δ_1, δ_2 streamwise and crossflow displacement thicknesses in   the streamline coordinate system

θ_{11}, θ_{12} streamwise and crossflow momentum integral thicknesses

θ_{21}, θ_{22} in the streamline coordinate system

τ_w shear stress at the wall

Subscripts

c   camber surface

e   at the edge of the boundary layer

w   on the wall; on the wake surface

P   general field point

∞ freestream values

iw   on the wall in the equivalent inviscid flow

s   source

v   vorticity

LS   line source

HV   horseshoe vortex

OBJECTIVE

The objective of the project has been to adapt existing codes and have them working for the calculation of various problems associated with low speed flow past clean wings using a viscous-inviscid interaction technique. The external inviscid flow calculation is done using a panel method whereas an integral method is used for the calculation of the boundary layer correction. Two different panel techniques are explored and used throughout the project. These are the internal singularity distribution method in which a distribution of singularities is placed on the mean camber surface and the equal singularity method in which a distribution of singularities is placed on the body surface with the assumption that the strength of the singularities on two corresponding panels on the lower and upper surfaces are equal. The two potential flow solutions are then matched by using a surface transpiration model in an iterative manner.

INTRODUCTION

The design of a wing for a specific application involves
satisfying several specifications and to realize this
objective, an appropriate planform geometry and airfoil must
be chosen. To successfully develop a satisfying wing, one
must understand the physics of the flows. The calculations
for the design and development of wings involves prediction,
as accurately and as quickly as possible, of the basic flow
properties: pressure, velocity and the overall forces on and
near the system. Because of the fact that air is a viscous
and compressible fluid, the equations of Navier-Stokes have
to be solved to realize this prediction while some form of
turbulence modelling is necessary for the large regions of
turbulent flow occurring at the high Reynolds number involved
in aviation. The computational efforts and problems involved
with the solution of the Navier-Stokes equations, even with
the simplification for steady flows, are formidable. For
practical applications, the computational time involved in
the solution of these equations is prohibitive.

Fortunately, in many practical applications of aerodynamic
interest, the effects of viscosity and turbulence are
confined to relatively thin shear layers near the body
surface and its wake. Outside this region one can obtain
highly accurate results by solving the inviscid Euler
equations or a suitable approximation to them. The solution
of the inviscid Euler equations involves much less effort and
computational time than the solution of the time-averaged
Navier-Stokes equations. We can take advantage of this fact
by calculating separately the external inviscid flow and the
viscous boundary layer and then combine the results
interatively to provide a composite solution to the problem.

This technique is known as "viscous-inviscid interaction"(VII).

Most of the viscous-inviscid interaction methods use some form of panel methods for the calculation of the external inviscid flow and momentum integral equation for solving the boundary layer. Finally, the results obtained from these two calculation methods are combined iteratively, with an appropriate matching condition.

The use of the viscous-inviscid technique should reduce the need for wind tunnels which are much more expensive. This technique enables us to obtain the basic flow properties, the pressure and velocity distributions and overall forces for an arbitrarily shaped body by specifying the complete geometry of the body involved and the freestream flow conditions.

For many problems of great practical importance, the separate potential flow and boundary layer solutions are relevant and provide high overall accuracy. They must be combined with sufficient attention to the mathematical modelling of the interaction between the two solutions. By arranging the calculation in an iterative manner, each successive inviscid solution provides the pressure distribution necessary for the next boundary layer correction solution, the displacement effect of which is then used to modify the inner boundary conditions for a near inviscid calculation. This loop must be repeated until the necessary precision is attained. This precision is measured by calculating the difference between the calculated total lift coefficients between two successive iterations. The viscous-inviscid interaction approach is most successful in the cases where the boundary layer remains attached up to the trailing edge of the wing, as would

normally be the case for a transport aircraft under cruising conditions. In the project, all cases examined fall in this category. It is however possible to apply the VII technique to applications where there is a significant amount of boundary layer separation near the trailing edge, or at the foot of a shock wave in transonic flow, or in the case of multi-element aerofoils. These cases have been examined in the Sinhamapatra thesis[1].

The effect of the boundary layer on the external inviscid flow is simulated by means of an inviscid calculation of the flow over a solid displacement surface. The boundary layer correction changes the geometry of the surface. A different approach called the transpiration model was proposed originally by Lighthill[2], in which the displacement effect is simulated by means of a distribution of sources on the true surface of the wing, leading to a non-zero component of the normal velocity there. So for the first calculation of the potential flow, the normal velocity is equal to zero at the body surface. For the subsequent calculations, the boundary conditions of normal velocity at the body surface are modified to obtain a non-zero component. This apporach is the one chosen for the project.

In a viscous-inviscid interaction scheme, a fundamental assumption is made, the overall flow can be divided into separate regions, the inner region where the Navier-Stokes equations or a suitable approximation to them must be solved, and the outer region where a potential flow calculation is accurate enough. This assumption is valid for flows at high Reynolds number which constitute the most interesting cases of external aerodynamics. To match the two solutions, we must insure that the composite flow field is continuous at the

interface between the inner and outer regions with respect to the magnitude and direction of the velocity.

It is more convenient to use the second of the two models of displacement effect mentioned earlier. The transpiration model has the advantage that, if a panel method is used, the matrix of influence coefficients does not change from iteration to iteration and can be inverted and stored once and for all. This is due to the fact that the geometry of the body remains constant during the scheme and the influence coefficients depend only on the geometry. Only the right-hand side vector of normal velocities changes at every iteration. Whereas the solid displacement model changes the geometry of the body at every iteration so the matrix of influence coefficients has to be recalculated. In a panel method, the most time-consuming step is certainly the calculation of the influence coefficients. For this particular advantage, the transpiration velocity model has been used throughout this project.

The precision of a VII scheme depends mostly on the inviscid calculation. The governing equations for inviscid flow are the Euler equations which can be approximated for low speed flows by the Laplace's equation. It is then known as potential flow. As exact analytic solutions to the potential flow is known only for two-dimensional bodies with specific geometry, it is necessary to use numerical methods that approximate the solution. The accuracy of these methods can be made as great as possible by sufficiently refining the numerical solutions. Analytical methods for the resolution of the potential flow problem exist and they work by introducing approximations into the analytic formulation itself and thus limit the overall accuracy.

One class of numerical methods used for the resolution of the potential flow is known as the panel method, which are nominally exact for the hypothetical case of zero Mach number and infinite Reynolds number. Two of these panel methods for three-dimensional wings are examined in this project, equal singularity model which distributes sources and vortices on the body surface, and the internal singularity model which distributes sources and vortices on the mean camber surface of the wing. In both cases, the boundary conditions are satisfied on the body surface. Comparisons have been made between these two methods and results are compared with available experimental or numerical solutions. It has been found that the equal singularity method takes about twice as much time as the mean camber method for comparable accuracy. The major part of the theory necessary for this project has been taken out of the thesis "Viscous-inviscid matching on aerofoils and wings at low speed" by K.P. Sinhamapatra[1]. This reference has been essential to this work.

CHAPTER I   INVISCID CALCULATION METHODS

1.1 The potential flow

The theory presented in this chapter is taken from the following references: Sinhamapatra[1], Kuethe and Chow[3], Milne-Thomson[4], Masson and Paraschivoiu[5], Paraschivoiu[6] and Gerhart and Gross[7].

The basic hypothesis of the potential flow calculation is that the flow is inviscid and irrotational and therefore incompressible. The inviscid formulation of the continuity equation and the linear momentum theorem are respectively:

$$\nabla \cdot \overline{V} + \frac{\overline{V}}{\rho} \cdot \nabla \rho = 0 \tag{1.1}$$

$$\overline{V} \cdot \nabla \overline{V} = -\frac{\nabla p}{\rho} \tag{1.2}$$

In equations (1.1) and (1.2), ρ is the density of the fluid, p its pressure and V its velocity.

The condition of incompressibility means that the density ρ is constant. Also, we have that

$$\overline{V} \cdot \nabla \overline{V} = \nabla \left(\frac{|\overline{V}|^2}{2} \right) + \overline{V} \times \nabla \times \overline{V} = \nabla \left(\frac{|\overline{V}|}{2} \right) \tag{1.3}$$

because the flow is irrotational and therefore

$$\nabla \times \overline{V} = 0 \tag{1.4}$$

Equations (1.1) and (1.2) for irrotational and incompressible

flows are

$$\nabla \cdot \overline{V} = 0 \qquad (1.5)$$

$$\nabla \left(\frac{|\overline{V}|}{2} \right) = -\frac{\nabla p}{\rho} \qquad (1.6)$$

Because the flow is irrotational, the velocity V can be derived from a potential Φ by the following relation

$$\overline{V} = \nabla \Phi \qquad (1.7)$$

By replacing equation (1.7) in the continuity equation, the following equation is obtained

$$\nabla^2 \Phi = 0 \qquad (1.8)$$

Equation (1.8) is one of the most studied equation and is named the Laplace's equation. All solutions of the Laplace's equation are harmonic functions. The velocity potential Φ of a irrotational and incompressible flow is governed by the Laplace's equation. To solve the problem of a potential flow, the Laplace's equation has to be solved. Then the linear momentum theorem gives the pressure.

The numerical methods most often used to solve the potential flow calculation are based on panel techniques. These methods take advantage of the uniqueness theorem for the Laplace's equation and solve unknowns only on the body surface. Laplace's equation is a linear partial differential equation of the second order. Because of the linearity of the equation, the superposition principle can be applied. This principle states that the sum of different solutions of the linear partial differential equation is also a solution of

the equation. The irrotational and incompressible flow past a wing can be represented by the sum of different elementary irrotational and incompressible flows. The potential of the more complex flow Φ can be expressed as the sum of a series of potentials Φ_e of elementary flows as follows

$$\Phi = \sum_{i=1}^{N} a_e \Phi_e \qquad (1.9)$$

where a_e is a constant. These elementary flows are due to singularities such as sources, vortices and doublets. The panel methods distribute singularities on the body surface or the mean camber surface and then obtain the flow parameters by solving the resulting system of linear equations. The mathematical formulation underlying the panel techniques follows from Green's theorem.

Green's theorem states that for any domain Ω, if F_1 and F_2 are two arbitrary scalar fields and they are second order continuous throughout Ω then,

$$\iiint_{\Omega} (F_1 \nabla^2 F_2 - F_2 \nabla^2 F_1)\, d\Omega = \iint_{S} (F_2 \overline{n} \cdot \nabla F_1 - F_1 \overline{n} \cdot \nabla F_2)\, dS \qquad (1.10)$$

Where n is the local normal to the surface S enclosing the domain and is defined as pointing into Ω (Figure 1). For the three dimensional potential flow, F_1 may be replaced by total potential Φ satisfying the Laplace's equation throughout the domain Ω and F_2 may be replaced by $1/r$ where for any source point Q inside Ω, r is defined as the length of the vector r from Q to a fixed observer point P. The derivatives in the Nabla vector operator ∇ are taken with respect to the

coordinates of the source point Q. Equation (1.11) gives the potential at point P, Φ_p:

$$4\pi T\phi_p = \iint\limits_S \frac{-1}{r}\overline{n}\cdot\nabla\phi\, \mathrm{d}S + \iint\limits_S \phi\overline{n}\cdot\nabla(\frac{1}{r})\, \mathrm{d}S \qquad (1.11)$$

These integrals exclude the singular point at which P and Q coincide and r = 0. In particular cases

$$T = 1 \qquad \text{when P lies inside}$$
$$T = 0 \qquad \text{when P lies outside}$$
$$T = 1/2 \qquad \text{when P lies on a smooth part of S.}$$

Equation can be extended to the multi-domain problem (Fig.2). For a point P in any of the domains, each domain having a closed boundary consisting of a number of connected portions of which a portion interfacing two domains A and B being denoted as S_{AB}, if Φ_A and Φ_B denote the single-valued local potentials on the two chosen sides A and B of any one of these surfaces and $\overline{n}_A$ denotes the local outward normal vector corresponding to side A, then potential at point P can be obtained by integrating over all such surfaces:

$$4\pi T\phi_p = \sum \iint\limits_{S_{AB}} \left[-\frac{1}{r}\overline{n}_A\cdot(\nabla\phi_A - \nabla\phi_B) + (\phi_A - \phi_B)\overline{n}_A\cdot\nabla(\frac{1}{r}) \right]\mathrm{d}S \qquad (1.12)$$
$$+ \iint\limits_{S_o} \left[-\frac{1}{r}\overline{n}_1\cdot\nabla\phi_1 + \phi_1\overline{n}_1\cdot\nabla(\frac{1}{r}) \right]\mathrm{d}S$$

In the case where the boundary S_o lies at a finite distance from the inner boundaries, a fictitious region Ω_o may be considered to lie outside S_o, extending to infinity. The contribution to the total potential Φ_p from the boundary S_o may be grouped with those from the number of surfaces S_{AB}.

In the external aerodynamic problem, S_o is assumed to lie indefinitely far from all the inner boundaries. For a point P lying close to S_o the contribution to $4\pi\Phi_p$ from all the inner boundaries S_{AB} becomes indefinitely small. The potential and velocity at all points on this boundary S_o are unperturbed values which would exist if no other boundaries S_{AB} were present. For any point P lying inside S_o, the last integral in equation (1.12) may be replaced by the local value of the function $4\pi\Phi_p$ corresponding to the unperturbed field at this point and this fixes the additive constant for Φ as governed by the uniqueness theorem, for formulation which directly employs the unknown values of total potential on the wetted surface. Equation (1.12) can then be rewritten for any point P lying off or on any of the various boundaries as equation (1.13):

$$4\pi T\phi_p = 4\pi\phi_{\infty_p} + \sum \int\int_{S_{A_B}}\left[-\frac{1}{r}\overline{n_A}\cdot(\nabla\phi_A - \nabla\phi_B) + (\phi_A - \phi_B)\overline{n_A}\cdot\nabla(\frac{1}{r})\right]dS \quad (1.13)$$

T is defined as in equation (1.11). The integral excludes the singular point when P and Q coincide and where r = 0. Each of the terms under the integral in the right hand side of equation (1.13) can be interpreted in terms of singularities. The first term may be interpreted as the perturbation potential induced at an external point P by a source distribution of density $\sigma = n_A\cdot(\nabla\Phi_A - \nabla\Phi_B)/4\pi$ on each surface portion S_{AB} and the second term can be interpreted as the perturbation potential induced at an external point P by a normal doublet distribution of density $\mu = (\Phi_A - \Phi_B)/4\pi$ on the same surface, the doublet axis being along $\overline{n_A}$. We can then rewrite equation (1.13) for any point P not lying on any of the surfaces S_{AB} as:

$$\phi_p = \phi_{\infty_p} + \sum \iint_{S_{A_B}} (\sigma K_1 - \mu K_2)\, dS \qquad (1.14)$$

K_1 and K_2 are scalar kernel functions depending only on the geometry of the wing. $K_1 = -(1/r)$ and $K_2 = \bar{n}_A \cdot (1/r) = (\bar{n}_A \cdot r)/r^3$.

For points P lying on one of the boundaries, a limiting analysis is required as P tends to Q on the boundary. Integral equation (1.14) must be defined to include the local singular contribution $-2\pi\mu_p \bar{n}_A \cdot \bar{n}$ on side A of S due to the local doublet density μ_p.

Applying the operator ∇_p, the derivatives are calculated with respect to the point P, to the equation (1.14), we obtain an equation in terms of velocity:

$$\overline{V}_p = \overline{V}_{\infty_p} + \sum \iint_{S_{A_B}} (\sigma \overline{K}_3 - \mu \overline{K}_4)\, dS \qquad (1.15)$$

K_3 and K_4 are vector kernel functions depending only on the geometry of the wing. $K_3 = -\nabla_p(1/r) = r/r^3$ and $K_4 = \nabla_p(\bar{n}_A \cdot \nabla(1/r)) = (\bar{n}_A \cdot \nabla_p) r/r^3$.

For points P lying on one of the surfaces S_{AB}, the integral is defined to include the local singular contribution $2\pi\sigma_p \bar{n}_A$ on side A or $-2\pi\sigma_p \bar{n}_A$ on side B.

Instead of using source and doublet distributions, we can use

other combinations of singularity distributions with or without vorticity distribution.

Equation (1.15) can be rewritten in terms of the surface source and vorticity distribution.

$$\overline{V_p} = \overline{V_{\infty_p}} + \sum \iint\limits_{S_{A_B}} (\sigma \overline{K_3} + \overline{\gamma} \times \overline{K_3})\, dS \qquad (1.16)$$

The vorticity distribution must satisfy the Helmholtz theorem. Helmholtz second theorem states that "A vortex filament cannot end in a fluid; it must extend to the boundaries of the fluid or form a closed path.". In the present method, two panel techniques are used. Both of them uses a source and vorticity distribution.

The configurations producing circulation generate wakes that carry away the vorticity generated in the boundary layer on the wing surface. These wakes can spring either from sharp edges or smooth surfaces. There is a difference between the potentials in the regions lying on each side of the wake. The contribution to the total integral in equation (1.15) from the wake surface is

$$\iint\limits_{S_w} \nabla \phi_w K_4\, dS \qquad (1.17)$$

S_w is the upper wake surface and Φ_w is the difference between the potentials in the regions on each side of the wake surface.

In the panel technique, discretisation is applied at three different levels: the satisfaction of the boundary conditions, the approximation of the geometry and the approximation of the distribution of singularities.

The present calculation scheme makes use of two different panel methods, the internal singularity distribution technique due to Singh[8] and the equal singularity model by Newling[9]. These two methods will be the subject of this chapter. Their working principles will be exposed.

1.2 Internal Singularity Method

The method is used to calculate the incompressible and inviscid flow around a clean wing. It distributes source and vorticity singularities on the mean camber surface of the body. It then solves this distribution of singularities by satisfying the boundary condition of normal velocity. The normal velocity is zero for the first iteration and non-zero for the subsequent calculations at selected points on the body surface. These points are called collocation points. Figures 3 to 7 illustrates the wing geometry and its discretisation. Figure 5 represents the vorticity distribution on the mean camber surface.

Source and vorticity singularities are distributed on the mean camber surface, leaving a small gap near the leading edge. The choice of the size of that gap near the leading edge and the element adjacent to it on the mean camber surface is very important and has to be carefully determined. The criterion used was developed in the Sinhamapatra thesis[1]. The determination of the size of the gap was realized by studying extensively, numerically, various wings with

different aerofoil sections and planforms. The most accurate
criterion is that the point on the wing surface corresponding
to the end of the mean camber line near the leading edge,
I=1, shall have a slope of about $2.5\cos\Omega_{LE}$, Ω_{LE} being the
leading edge sweepback angle. The next spanwise line, I=2,
should be placed such that the slope is not less than
$0.7\cos\Omega_{LE}$. Once these sizes are determined, the remaining
elements distribution can be fairly arbitrary.

In the present calculation scheme, the mean camber surface is
designated as S_c and the wake surface as S_w. The vorticity
distribution γ_s is placed on S_c and S_w whereas the source
distribution is placed on S_c. In addition to those, two
discrete line source σ_{L1} and σ_{L2} are placed on two lines near
the leading edge in the spanwise direction. These two lines
are designated as L_1 and L_2. To complete the singularity
model, a set of horseshoe vortices are placed with the bound
vortices on a line L_3 halfway between L_1 and L_2, and the
trailing vortices lie in the streamwise direction along the
mean camber surface past the trailing edge and extending into
the wake to infinity downstream. The line sources L_1 and L_2
and the bound vortices on L_3 are placed to simulate the
rounded shape of the leading edge of a subsonic airfoil.

For this singularity model, the total velocity at any point
P, not lying on the mean camber surface, can be written as:

$$4\pi\overline{V_p}=4\pi\overline{V_\infty}\iint\limits_{S_c}\sigma_s\overline{K_s}dS+\int\limits_{S_c+S_w}\int\overline{\gamma}\times\overline{K_v}dS$$

$$+\int\limits_{L_1+L_2}(\sigma_{L1}+\sigma_{L2})\,\overline{K_{LS}}dl+\sum_{L_3}\overline{K_{HV}}\Gamma_h$$

$$(1.18)$$

This equation is designated as equation (1.18). In this equation, the various vectors K represent the appropriate induced field.

The equation for the normal velocity of the point P is obtained by taking the outward normal component of the various induced velocities.

$$-4\pi \overline{V_\infty} \cdot \overline{n_p} = \iint_{S_c} \sigma_s (\overline{K_s} \cdot \overline{n_p})\, dS + \int_{S_c + S_w} (\overline{\gamma} \times \overline{K_v}) \cdot \overline{n_p}\, dS$$
$$+ \sum_{L_3} (\overline{K_{HV}} \cdot \overline{n_p})\, \Gamma_h + \int_{L_1 + L_2} (\sigma_1 + \sigma_2)\, (\overline{K_{LS}} \cdot \overline{n_p})\, dl \qquad (1.19)$$

The outward normal component of the velocity V_p, $V_p \cdot n_p$ is zero at the collocation point on the wing surface for the first iteration but is non-zero for the subsequent equivalent inviscid flow calculations.

To obtain the solution for the present inviscid flow calculation, we have to solve equation (1.19) simultaneously with the Kutta condition. To achieve this objective, we have to discretise this integral equation to obtain a set of linear algebraic equations. The wing surface is discretised into a number of small elements, known as panels hence the name of the numerical method. The formation of these elements from the input points is described in detail in the Appendix A. The points defining the wing are input in such an order that they define a family of approximately parallel curves lying on the wing surface. The figure 3 illustrates this. These approximately parallel curves are designated as N-

lines. On a lifting wing, they are oriented in the freestream direction. On each of the N-line, the points are input beginning at the trailing edge, around the section curve of the wing and back to the trailing edge. Each N-line contains the same number of input points. Points from adjacent N-lines are linked to form surface elements. The set of elements formed from two adjacent N-lines is designated as a strip of elements.

The order in which the points are input is very important because it determines the direction of the outward surface normal vector. The normal vector must point into the flow field. The elements are approximated as plane trapezoids. The centroids of the elements are selected as control points where the boundary condition is applied. They are known as collocation points. An extra set of collocation points along the leading edge are also given as input to the definition of the wing geometry.

To determine the curve on the mean camber surface, the code calculates the z coordinate of any point on the mean camber surface by averaging the z coordinate of the two corresponding point on the lower and upper surface. The curves obtained as such are designated as M-lines. Points on adjacent M-lines are linked to form another family of curves, termed as I-lines. The different curves on the mean camber surface are shown in figure 4. The mean camber surface is divided into a number of small elements by these M-lines and I-lines.

The strength of the uniform surface source distribution varies from surface element to element whereas the strength of the bound vorticity distribution vary linearly in the

chordwise direction but remain constant in the spanwise direction and vary from element to element. The strength of the line source singularities is uniform in each element but vary from element to element.

If we defines Ns the number of spanwise strips and Nc the number of chordwise divisions, so that each strip has Nc elements, it results in $Ns \times Nc$ elements which is denoted as Nt, the number of mean camber surface element. There are two corresponding panels for each mean camber surface element in addition to $2Ns$ elements corresponding to the leading edge gap. So there are $2Nt+2Ns$ elements on the wing surface.

There are Nt unknown values of source strengths and $Nt+Ns$ unknown vorticity strengths. In addition, there are $2Ns$ values of line sources and Ns values of horseshoe vortices so the total number of unknown singularity strengths is $2Nt+4Ns$. Another Ns collocation points are taken at the leading edge in addition to the $2Nt+2Ns$ collocation points corresponding to each panel on the wing surface. The remaining Ns equations are taken from the application of the Kutta condition by setting the bound vorticity at the trailing edge to zero. So we have $2Nt+4Ns$ equations and the same number of unknowns.

To obtain the results for the potential flow calculation, we have to satisfy the Kutta condition. The Kutta condition is satisfied by setting the bound vorticity strength at the trailing edge of the wing at zero.

The integral equation (1.19) can be approximated by a set of linear algebraic equations. These can be written as:

$$\sum_{k=1}^{(I-1)(M-1)} A_{jk}\sigma_{sk} + \sum_{k=1}^{(I-1)(M-1)} B_{jk}\gamma_k + \sum_{k=1}^{M-1} C_{jk}(\sigma_{L1k}+\sigma_{L2k})$$
$$+\sum_{k=1}^{M-1} D_{jk}\Gamma_{hk} = -\overline{n_p}\cdot\overline{V_\infty} \qquad (1.20)$$

$$j=1,2,3,..,2(I-1)(M-1)$$

This set of equation is equation (1.20). A_{jk}, B_{jk}, C_{jk} and D_{jk} are the normal components of the velocities induced at the j-th collocation point by the k-th surface source, bound vorticity, line source and horseshoe vortex respectively. Appendix B contains the equations necessary to calculate the velocity induced by a source distribution whereas Appendix C contains the equations needed to calculate the velocity induced by a vortex segment, a semi-infinite vortex line and a line source.

This set of simultaneous linear equations can be written in matrix form and thus can be solved by an orthogonalisation technique to obtain the unknown singularity strengths.

Once the singularity strengths are known, the total velocity at any j-th collocation point can be calculated with the following equation:

$$\overline{V_j} = \sum_{k=1}^{N_T} \overline{V_{jk}}\, \Pi_k + \overline{V_\infty} \qquad (1.21)$$

V_{jk} represents the total induced velocity at the j-th collocation point by the k-th singularity Π_p. N_T represents the number of singularities.

Once the velocities are known, the pressure coefficients at

the collocation points are calculated from the equation
(1.22):

$$C_{pj}=1-\frac{\overline{V_j}\cdot\overline{V_j}}{V_\infty^2}$$

(1.22)

To obtain the forces on the wing, a numerical integration of
the pressure assuming the pressure to be constant over each
surface element is performed. The force on a particular
element j can be written as

$$\overline{F_j}=-\overline{n_j}C_{pj}S_j$$

(1.23)

$$\overline{F}=\sum\overline{F_j}$$

(1.24)

Equation (1.24) calculates the total force on the wing
surface.

1.3 Equal Singularity Method

This model was developed by Newling[9]. The equal singularity method distributes singularities on the wing surface and the boundary conditions are satisfied on the wing surface also. The organization of input points and surface panels is similar to the internal singularity distribution method. The chosen singularity distribution is composed of sources and vortices. A linearly varying vorticity is superimposed over a uniform source surface distribution on every panel. The vorticity remains constant in the spanwise direction but varies linearly in the chordwise direction. The uniform source strength varies from panel to panel.

For each lifting strip, if N+1 points are used to define the aerofoil geometry, there will be N surface panels. So for each lifting strip, there are N+1 unknown vorticity strengths and N unknown source strengths. To reduce the number of unknowns, it is assumed that the singularity strengths on corresponding panels on the upper and lower surfaces of the wing are equal. With this assumption, it leaves us with (N/2+1) unknown vorticity strengths and N/2 unknown source strengths for each lifting strip. We can further reduce the number of unknowns by the application of the Kutta condition. The bound vorticity strength at the trailing edge is set to zero so that the number of unknown vorticity strengths for each lifting strip is reduced to N/2. The total number of unknowns for M lifting strips is M x N.

$$\iint_S \Pi(\overline{K \cdot n_p}) \, dS = -4\pi \overline{V_\infty \cdot n_p} \qquad (1.25)$$

In equation (1.25), K is the vector kernel and π represents

the unknown generalised singularity strengths distributed on the wing and wake. Equation (1.26) is the governing integral equation and can be used to form a square system of M x N linear equations in unknown singularity strengths. Equation (1.26) can be expressed as:

$$\sum_{k=1}^{\frac{M \times N}{2}} A_{jk} \sigma_k + \sum_{k=1}^{\frac{M \times N}{2}} B_{jk} \gamma_k = - \overline{n_k} \ \overline{V_\infty} \qquad (1.26)$$

$$j = 1, 2, \ldots, M \times N$$

A_{jk} and B_{jk} represent the induced velocities by the k-th source and vorticity element respectively on the j-th collocation point. This set of linear equations is solved with the use of an orthogonalisation method. Once the singularity strengths are known, the velocity and pressure distribution are calculated in the same manner as in the internal singularity method.

CHAPTER II   BOUNDARY LAYER CORRECTION

2.1 Boundary Layer Calculation

The second component of prime importance of any VII scheme is the boundary layer calculation. The calculation of the viscous part of the problem has usually involved the assumptions that the pressure gradient across the boundary layer is negligible and that only the normal derivatives of the shear stresses are important to the calculation. For turbulent flows the Reynolds normal stresses are almost always neglected.

In the aerodynamic range of Reynolds numbers, the flow is predominantly turbulent but it is still necessary to use a method for the laminar boundary layer ahead of the transition and another method for determining the starting conditions for the turbulent boundary layer.

In the present method, the method used for the calculation of the laminar boundary layer calculation is the Thwaites[10] method. The transition from laminar to turbulent flow is calculated using the Mitchel criterion which gives transition in a pressure gradient on the basis of a relation between R_e and R_x given by

$$R_e > 1.174 \left(1 + \frac{22400}{R_x}\right) R_x^{0.46} \qquad (2.1)$$

The transition can be assumed to be sudden. This assumption enables us to obtain the starting values for the turbulent boundary layer calculation by assuming that they are equal to the values for the laminar boundary layer calculation.

For the laminar boundary layer calculation, the Thwaites method is used. A set of transformation formulas are suggested by Stewartson as described in Sinhamapatra[1] to transform the compressible momentum integral equation into the form of incompressible flow. These transformation formulas are:

$$\delta_* = \int_0^\delta (1 - \frac{U_T}{U_{eT}})\, dn \qquad (2.2)$$

$$\theta = \int_0^\delta (1 - \frac{U_T}{U_{eT}})\, \frac{U_T}{U_{eT}}\, dn \qquad (2.3)$$

$$\tau_{wT} = \tau_w (\frac{a_o}{a_e})^{\frac{4\gamma - 2}{\gamma - 1}} \qquad (2.4)$$

where $U_{eT} = (a_o/a_e)U_e$ and $U_T = (a_o/a_e)U$ with a being the speed of sound. Subscript "o" denotes values at stagnation condition, "e" denotes values at the edge of the boundary layer, "w" denotes values at the wall and "τ" stands for transformed parameters.

An integral method for the resolution of the boundary layer calculation solves the Karman momentum equation:

$$\frac{d\theta}{ds} + (H + 2 - M^2)\, \frac{\theta}{U_e}\, \frac{dU_e}{ds} = \frac{1}{2}C_f \qquad (2.5)$$

The shape parameter H is defined as $H = \delta^*/\theta$ and the skin friction coefficient as $C_f = \tau_w/(\frac{1}{2}\rho_e U_e^2)$.

With the modifications to the boundary layer characteristics δ^*, θ and τ_w, equation (2.5) will transform to its incompressible form. To solve this equation, Thwaites introduced two non-dimensional parameters

$$m = \frac{\theta^2}{U_e} \left(\frac{d^2 U}{dn^2} \right)_{n=0} = - \frac{\theta^2}{v} \frac{dU_e}{ds} \qquad (2.6)$$

$$l = \frac{\theta}{U_e} \left(\frac{dU}{dn} \right)_{n=0} \qquad (2.7)$$

With the help of equations (2.6) and (2.7) and known exact results, Thwaites found the solution of equation (2.5) for incompressible flow in the form of a quadrature for the momentum thickness:

$$\frac{\theta^2}{v} = \frac{0.45}{U_e^6} \int_0^s U_e^5 ds \qquad (2.8)$$

The other boundary layer parameters such as δ^* and C_f can be obtained from Thwaites' table of m, l and H, which relates these parameters on the assumption of a one-parameter family for velocity profiles. The calculation necessitates the following empirical relations:

$H = 2.0 + 0.983 (m + 0.25) + 5.83 (m + 0.25)^2$
$l = (0.0484 - 0.818m)^{1/2}$ for $m \leq 0$
$H = 2.0 + 0.61 \, e^{6.283m + 495m^3}$
$l = (0.0729 - 0.773m)^{1/2}$ for $m \geq 0$

and l = 0 for m ≥ 0.089 and then $\delta^* = H\theta$ and $C_f = 2\nu l U_e/\theta$ where δ^* and θ are defined as follows:

$$\delta^* = \int_0^\delta (1 - \frac{\rho U}{\rho_e U_e})\,dn \qquad (2.9)$$

$$\theta = \frac{1}{\rho_e U_e^2} \int_0^\delta \rho U (U_e - U)\,dn \qquad (2.10)$$

The integral method for the calculation of the three dimensional turbulent boundary layer is due to P.D. Smith[11]. Three equations are of prime importance to the calculation of the turbulent boundary layer characteristics: the two momentum integral equations and the continuity integral equation also known as the entrainment equation. A non-orthogonal curvilinear coordinate system is necessary in the present method for the calculation procedure. The surface of the wing is divided into a set of quadrilateral elements. The non-orthogonal coordinates lines and the grid system is used to solve the three governing partial differential equations. A finite difference technique is used for the calculation procedure.

In the axes system used in the present method, x and y form a non-orthogonal curvilinear grid on the wing surface, the z-axis is normal to the wing surface. The figure 8 shows the axes system. This axes system was introduced by Myring[12]. U, v and w represent the velocity components in the x,y and z directions respectively.

An element of length ds on the body surface is given by

$$ds^2 = h_1{}^2 \, dx^2 + h_2{}^2 \, dy^2 + 2g\,dx\,dy \qquad (2.11)$$

In equation (2.11), h_1, h_2 and g are the metrics of the surface coordinate system.

Myring[12] and Smith[11] have developed the three governing integral equations in the non-orthogonal curvilinear coordinate system. The momentum integral equations are:

$$
\begin{aligned}
&\frac{1}{h_1}\frac{\partial \Theta_{11}}{\partial x} + \Theta_{11}\left[\frac{\partial u_e}{\partial x}\frac{(2-M^2)}{h_1 u_e} + \frac{1}{q}\frac{\partial}{\partial x}\left(\frac{q}{h_1}\right) + k_1\right] \\
&+ \frac{1}{h_2}\frac{\partial \Theta_{12}}{\partial y} + \Theta_{12}\left[\frac{\partial u_e}{\partial y}\frac{(2-M^2)}{h_2 u_e} + \frac{1}{q}\frac{\partial}{\partial y}\left(\frac{q}{h_2}\right) + k_3\right] \\
&+ \Delta_1\left[\frac{1}{h_1 u_e}\frac{\partial u_1}{\partial x} + k_1\frac{u_1}{u_e}\right] \\
&+ \Delta_2\left[\frac{1}{h_2 u_e}\frac{\partial u_1}{\partial y} + k_2\frac{v_1}{u_e} + k_3\frac{u_1}{u_e}\right] + \Theta_{22}k_2 = \frac{C_{f1}}{2}
\end{aligned}
\qquad (2.12)
$$

$$
\begin{aligned}
&\frac{1}{h_1}\frac{\partial \Theta_{21}}{\partial x} + \Theta_{21}\left[\frac{\partial u_e}{\partial x}\frac{(2-M^2)}{h_1 u_e} + \frac{1}{q}\frac{\partial}{\partial x}\left(\frac{q}{h_1}\right) + l_3\right] \\
&+ \frac{1}{h_2}\frac{\partial \Theta_{22}}{\partial y} + \Theta_{22}\left[\frac{\partial u_e}{\partial y}\frac{(2-M^2)}{h_2 u_e} + \frac{1}{q}\frac{\partial}{\partial y}\left(\frac{q}{h_2}\right) + l_2\right] \\
&+ \Delta_1\left[\frac{1}{h_1 u_e}\frac{\partial v_1}{\partial x} + l_1\frac{u_1}{u_e} + l_3\frac{v_1}{u_e}\right] \\
&+ \Delta_2\left[\frac{1}{h_2 u_e}\frac{\partial v_1}{\partial y} + l_2\frac{v_1}{u_e}\right] + \Theta_{11}l_1 = \frac{C_{f2}}{2}
\end{aligned}
\qquad (2.13)
$$

The continuity integral equation is given by:

$$\frac{1}{\rho_e u_e q}\left[\frac{\partial}{\partial x}\left(\frac{\rho_e q}{h_1}(u_1\delta - u_e\Delta_1)\right)+\frac{\partial}{\partial y}\left(\frac{\rho_e q}{h_2}(v_1\delta - u_e\Delta_2)\right)\right]$$
$$=\frac{1}{u_e}\left[\frac{u_1}{h_1}\frac{\partial\delta}{\partial x}+\frac{v_1}{h_2}\frac{\partial\delta}{\partial y}+w_1\right]=F \qquad (2.14)$$

M is the Mach number and ρ_e is the density at the edge of the
boundary layer, at $z = \delta$. C_{f1} and C_{f2} are the skin friction
coefficients in the x and y directions respectively. F is the
entrainment coefficient. The velocity components at the edge
of the boundary layer in the x and y directions are denoted
by u_1 and v_1 respectively. The resultant velocity is denoted
by u_e and given by

$$u_e^2 = u_1^2 + v_1^2 + \frac{2g}{h_1 h_2} \qquad (2.15)$$

The parameters k_1, k_2, k_3, l_1, l_2, l_3 and q are function of the
metrics of the surface coordinate system and are developed in
the appendix D. Appendix D also gives the various integral
thicknesses.

Equations (2.12) to (2.14) are the governing equations and
form the basis of the present calculation method. There are
too many unknowns and we have to reduce this number. To
accomplish this and reduce the number of unknowns to three,
Myring[12] and Smith[11] have assumed specified forms of the
velocity profiles along the streamwise and spanwise
directions. This is done by making use of the observed
similarities between the characteristics of the boundary
layer in two and three dimensions. They have further made use
of the empirical relations for the skin friction coefficients
C_{f1} and C_{f1} and the entrainment coefficient F. Empirical
knowledge of these parameters is restricted to the streamline

coordinate system; s, n and z directions, and so all the integral thichnesses are expressed in terms of the velocity components along and normal to the external stream direction.

Appendix D gives the expressions relating θ_{11}, θ_{12}, θ_{21}, θ_{22}, Δ_1 and Δ_2 in terms of θ_{11}, θ_{12}, θ_{21}, θ_{22}, δ_1, δ_2, and α. The θ s and δ s represent the integral thicknesses in the stream line coordinate system. α denotes the angle between the x-axis and the external stream line and λ is the angle between the x-axis and the y-axis. The velocity components in the s and n directions are represented by U and V respectively.

There are three different shape parameters. They are denoted as H, $\overline{H}$, H_1 and they are defined as:

$$H = \frac{\delta_1}{\theta_{11}} \tag{2.16}$$

$$\overline{H} = \frac{1}{\theta_{11}} \int_0^{\delta} \frac{\rho}{\rho_e} \left(1 - \frac{U}{u_e}\right) dz \tag{2.17}$$

$$H_1 = \frac{\delta - \delta_1}{\theta_{11}} \tag{2.18}$$

$$H + 1 = (\overline{H}+1)(1+0.2M^2) \tag{2.19}$$

The streamwise velocity profile has been assumed to be of the form:

$$\frac{U}{u_e} = \left(\frac{z}{\delta}\right)^n \tag{2.20}$$

which gives $\quad H = 1 + 2n$ $\hfill$ (2.21)

The crossflow velocity profile has been assumed by Mager as described in Sinhamapatra[1] to be of the form:

$$\frac{V}{U} = (1-\frac{z}{\delta})^2\tan\beta \qquad (2.22)$$

where ß represents the angle between the external stream line and the corresponding limiting stream line on the surface of the wing.

By using these assumed velocity profiles, the crossflow thicknesses may be related to the streamwise momentum thickness θ_{11} by the expressions given by the equations (D-23) to (D-26) in appendix D. The skin friction coefficient in external flow direction C_f and the two components C_{f1} and C_{f2} in the direction of the x and y axes may be written in terms of ß and C_f. These expressions are given by the equations (D-27) and (D-28) in appendix D.

The entrainment coefficient is given by the expression (2.23)

$$F = 0.025H - 0.022 \qquad (2.23)$$

The number of unknowns in the equations (2.12) to (2.14) can be reduced to three by using the empirical expressions. These three unknowns are the streamwise momentum thickness θ_{11}, the shape parameter H and the angle between the external stream line and the corresponding limiting stream line on the surface of the wing ß. The system of first order partial differential equations in terms of these three unknowns may be written in the form:

$$F_{11}\frac{\partial\theta_{11}}{\partial x}+\theta_{11}F_{11H}\frac{\partial H}{\partial x}+\theta_{11}F_{11\beta}\frac{\partial\beta}{\partial x}=S_1$$

$$F_{21}\frac{\partial\theta_{11}}{\partial x}+\theta_{11}F_{21H}\frac{\partial H}{\partial x}+\theta_{11}F_{21\beta}\frac{\partial\beta}{\partial x}=S_2 \qquad (2.24)$$

$$J_1\frac{\partial\theta_{11}}{\partial x}+\theta_{11}F_{1H}\frac{\partial H}{\partial x}+\theta_{11}J_{1\beta}\frac{\partial\beta}{\partial x}=S_3$$

The expressions for the different Fs, Js and Ss are given by equations (D-31) to (D-42) in appendix D.

The form of these equations may be shown to be hyperbolic. The physical sense of an hyperbolic equation is a propagation phenomenon. Hyperbolic equations have two real characteristic directions. These characteristic directions define zones of influence and zones of dependence. The zone of influence is the region affected by the flow perturbations generated at a particular point P. The zone of dependence is the region where perturbations generated within influence the flow at the particular point P.

The numerical method used to solve these equations must take into account these characteristic directions. If fluid is entering the region of integration across any boundary, then boundary conditions must be specified along that boundary. Also the forward stepsize x is limited by the condition that the downstream point must lie in the zone of influence of the upstream point and its immediate neighbours. The x-y plane is divided to form a rectangular grid as shown in figure 9. Because the equations are hyperbolic, there is the concept of a front proceeding forward. So at the point (i,j) all the coefficients and quantities on the right hand side of the equations are known, the derivatives $(\delta\theta_{11}/\delta x)_{i,j}$, $(\delta H/\delta x)_{i,j}$, $(\delta\beta/\delta x)_{i,j}$ can be calculated. Then we can extrapolate the values to the point (i+1,j) by using equations of the form

$$(\theta_{11})_{I+1,J} = (\theta_{11})_{I,J} + \Delta x \left(\frac{\partial \theta_{11}}{\partial x}\right)_{I,J} \qquad (2.25)$$

The forward stepsize is governed either as specified before so that the downstream point must lie in the zone of influence of the upstream point and its immediate neighbours, or if it less, x is taken to be $10\theta_{11}$, $x \approx \delta$.

The numerical method used must take note of the characteristic directions. We assume that the angles between the characteristic directions and the x-axis are α and $\alpha+\beta$. If both α and $\alpha+\beta$ are positive, a backward difference scheme is used. If both α and $\alpha+\beta$ are negative, a forward difference scheme is used. If α and $\alpha+\beta$ are of opposite signs, a central difference scheme is used instead. The use of these equations means that if fluid is entering the computational region through either side boundaries, then boundary conditions must be specified along that boundary.

The subroutine executing the boundary layer correction receives input data from the potential flow calculation. The input velocity distribution and geometry are interpolated by using bicubic spline interpolation technique. The metrics of the surface coordinate system and their derivatives are also interpolated by bicubic spline interpolation by using the cartesian coordinates of the surface of the wing. Streamwise and crossflow displacement thicknesses δ_1 and δ_2 are re-interpolated by a spline to obtain their values at the collocation points of the equivalent potential flow.

2.2 Transpiration Velocity

Once the boundary layer calculation is finished, we have to calculate the surface transpiration velocity to modify the boundary conditions for the equivalent potential flow calculation. The surface transpiration velocity is defined using the continuity equation:

$$\frac{\partial}{\partial x}\left(\frac{\rho q u}{h_1}\right) + \frac{\partial}{\partial y}\left(\frac{\rho q v}{h_2}\right) + \frac{\partial}{\partial z}(\rho w) = 0 \qquad (2.26)$$

The transpiration velocity W_{iw} is obtained by integrating this equation with respect to z from 0 to δ. For incompressible flow, we obtain the following equation:

$$W_{iw} = \frac{1}{q}\left[\frac{\partial}{\partial x}\left(\frac{u_e \Delta_1 q}{h_1}\right) + \frac{\partial}{\partial y}\left(\frac{u_e \Delta_2 q}{h_2}\right)\right] \qquad (2.27)$$

The transpiration velocities change the boundary conditions for the equivalent inviscid flow and the velocity and pressure distributions are recalculated for the next boundary layer calculation. These transpiration velocites are calculated after each five iterations of boundary layer calculation. The whole calculation technique stops when the difference in the values of the sectional lift coefficients of the wing in subsequent iterations is small enough.

CHAPTER III   THE PROGRAM

3.1 Description of the codes

This section presents the general description of the codes.
First, the internal singularity code will be described. The
code is divided into two major parts, the subroutine PANEL
which does the inviscid calculation and the subroutine BLAYER
which calculates the boundary layer correction. The MAIN
program first calls PANEL then reads the input file
ANSWER.DAT. If ANSWER.DAT contains 1 then the MAIN program
calls BLAYER, or else it stops.

The subroutine PANEL does all the inviscid calculation
without calling any other subroutine. Its different
calculation steps are described in the following algorithm:

1. Read input data of geometric parameters.
2. Calculate wing surface geometry.
3. Calculate camber surface geometry.
4. Calculate panel geometry (sides, diagonals, control
points,   normal vectors).
5. Form the influence coefficients matrix.
6. Solve the singularity strengths by successive
         orthogonalisation.
7. Solve the aerodynamic quantities (velocity, pressure,
forces).
8. Write the results in an output file.

After the inviscid calculation, the necessary parameters are
passed on to the BLAYER subroutine which applies the boundary
layer correction. First BLAYER calls the INTER subroutine
which interpolates the pressure and velocity distribution for

the calculation of the boundary layer growth. Then INTER calls the TRANSP subroutine which calculates all the boundary layer parameters and corrects the right-hand side normal velocity terms. Then BLAYER calls FIRSTI, which for the first iteration, assigns the correct values of influence coefficients to the appropriate variables. This FIRSTI subroutine is necessary to match correctly the original inviscid calculation and viscous calculation codes, so it was added. Then BLAYER solves the singularity strengths by successive orthogonalisation and obtains the aerodynamic quantities. It then writes the results in different output files.

The subroutine TRANSP calculates the laminar boundary layer and then the turbulent boundary layer. Finally, it calculates the transpiration velocity. It calls upon three small subroutines INTP, DERIV, INTR several times during its execution. The subroutine INTP executes a linear interpolation in two dimensions. The subroutine DERIV computes the derivatives. Finally, the subroutine INTR solves the differential equation by a fourth order Runge-Kutta method. This completes the description of the internal singularity code.

The equal singularity code works in a similar manner. The MAIN program calls the subroutine PANEL which does the inviscid calculation and depending on the value of ANSWER.DAT, calls upon the subroutine BLAYER to calculate the boundary layer correction. In this case, the subroutine BLAYER is exactly the same as in the internal singularity code, only the PANEL subroutine differs.

First, PANEL calls the subroutine PLAN which reads the

various input geometric parameters. Then it calls the subroutine GEOINFL which calculates the influence coefficients matrix. In turn, GEOINFL calls the subroutine FLAT which calculates the panel geometry (sides, diagonals, control points, normal vectors). Then GEOINFL calls DLAT which calculates the induced velocity due to a unit source distribution. Finally, GEOINFL does the calculations necessary to obtain the influence coefficients matrix. PANEL then calls the subroutine SOLVE which obtains the singularity strengths. It calls upon the subroutine MATINV which inverts a matrix. Then PANEL calls the subroutine RESULT which computes the pressure and velocity distributions and the overall forces on the wing. Finally, PANEL calls the subroutine SWITCH which, as its name indicates, switches the various parameters needed in the boundary layer calculation in order to match them. This concludes the description of the two codes.

3.2 Modifications to the codes

The codes were originally designed to run on a Horizon III minicomputer and they had to be modified considerably and adapted to run on the Music system which is installed on an IBM 7171 mainframe computer. The original Fortran compiler has many differences with the compiler used on the Music system. These differences has forced us to make changes in the codes.

First, the input and output structures had to be completely changed. The codes were modified as to be executed in batch form so all the input and output files were to be defined in the batchfile. It was not possible to execute the codes in interactive mode because of the large memory requirements and

the computational time involved.

Originally, there were three codes: a code for the inviscid calculation using the equal singularity method, one for the internal singularity method and finally, one that performed the boundary layer correction. To run on the Music system, the codes were combined as to obtain only two codes. Both codes performing the inviscid calculation were combined with the boundary correction code. In the input file, the user has to specify whether the boundary correction is to be applied or not.

To combine the codes, the parameters have to be matched so that when they are passed from one subroutine to another, they have to be consistent. So in order to combine the codes, one had to dissect and come to know the internal working of the codes as to make sure to combine them properly. There were several small changes to be made because of the differences between the two compilers. Several functions had to be changed to the proper type, for example, SQRT had to be changed to DSQRT because the compiler on the mainframe is more strict. Furthermore, the Music compiler does not accept the DO WHILE loop so all these loops in the codes had to be transformed to DO loop. To achieve this, one has to carefully work out all of the possibilities of a loop in order to make sure that the transformation does not change the loop in any case.

3.3 Using the codes

To codes have been modified to be executed in batch using a batchfile. Appendix E lists the batchfiles used to execute respectively the program using the equal singularity method and the internal singularity method. In the batchfile, the user has to specify a number of parameters, such as the memory space needed, the approximate time needed to do the calculations and the various input and output files.

In the first batchfile, VIIE.JCL, we can see the main code is VII.EQU. To execute this code, three input files have been defined, EQUAL1.DAT, ANSWER1.DAT AND STRIP.DAT, which are associated respectively with i/o unit 5, 3 and 12. In addition, there are four unnamed output files. Examples of the three input files are included in Appendix F. EQUAL1.DAT lists the parameters used to define the geometry of the wing, which are the coordinates defining the airfoil shape, the general planform shape, sweepback angle, aspect ratio and the taper ratio. The angle of attack must also be specified. ANSWER1.DAT is either one or zero. If the user wants to use the boundary layer correction, ANSWER1.DAT must be set to one and in the other case to zero. STRIP.DAT lists parameters pertaining to the boundary layer calculation such as the maximum number of iterations, the tolerance which is the maximal value of the difference between the calculated values of succeeding iterations, dx, ds and the Reynolds number.

In the batchfile, VIII.JCL, used to execute the internal singularity method, the central file is VII.INT. The user must again supply three input files, namely SWING5.DAT, ANSWER1.DAT and STRIP.DAT. ANSWER1.DAT and STRIP.DAT are the same input files as in the case of the equal singularity

method. SWING5.DAT is the equivalent of EQUAL1.DAT. The code writes the results in four unnamed output files. The user then has to name the output files himself.

The first input file listed in Appendix F is the case of a wing with a cross section airfoil NACA 64A410 with an aspect ratio of 4.9 and a taper ratio of 0.85. The code reads on the first line IPL, M and NSYM. IPL is assigned a value between 1 and 6 to describe the general geometry of the planform of the wing. IPL is equal to 1 for a rectangular wing, 2 for a tapered wing, 3 for a tapered wing with both edges oblique, 4 for a swept wing, 5 for a strake wing and 6 is for the special case when all the corner points are input. M represents the number of spanwise division and NSYM is either 0 or 1. If the user wants the code to take into account the symmetry of the wing, NSYM must be put to 1. The second input line lists the spanwise divisions position in y/s. The third line lists respectively, the aspect ratio, the taper ratio and the sweepback angle. Then, the code reads NALPHA which is the number of angle of attacks to be calculated and the different alphas. The fifth line lists the number of panels on a given section and then the coordinates of the airfoil are given in table form for x/c and z/c.

The input file for the internal singularity code is a little bit different. Parameters are input in a different order. First, the code reads the number of panels and the number of spanwise division. Then, it reads NPLAN which is similar to IPL in the case of the equal singularity code, NALPHA and NSYM. The third line lists the aspect ratio, the taper ratio and the sweepback angle. Then the different alphas are read. The fifth line lists the different position of the spanwise stations. Again, the coordinates of the airfoil are listed in

tabular form. Finally, the code reads the direction cosines of the normal at the leading edge point and the leading edge coordinates.

In the case of a strake wing, some additional information must be input, namely the semi-span, the root chord, the strake sweep, the leading edge sweep, the trailing edge sweep and the strake width.

In the two batchfile, if one wants to run another case, one has to replace EQUAL1.DAT or SWING5.DAT by the name of the input file containing the pertinent data.

To retrieve the results, the user has to use the OSJR command. When OSJR is typed, the screen shows the various jobs that have been executed. They are assigned a four-digit number. To visualize the results, the user must type OUT j=xxxx where xxxx represents the number of the job. Then the screen shows different files from d=1 to d=n. These files hold all the information about the compilation and execution of the codes along with the results. d=1 and d=2 lists several statistics about the compilation and execution. d=3 lists the time and CPU necessary to execute the code. d=4 lists all the code lines and d=5 lists all the subroutines. When debugging a program, it is these two files that hold precious information. All the files after d=5, from d=6 and up, are the output files. To copy these files to the library, the user must type OUT j=xxxx, d=n, file=name, where xxxx is the job number, n is the file number and name is the name given to the file, for example RESULTS.DAT. Then the job must be either deleted or routed to MUSIC or a printer.

CHAPTER IV   RESULTS AND DISCUSSION

Three cases were examined in the project. The first one is the case of a slender strake wing with a cross section airfoil NACA 0005 having the following characteristics: a semi-span of 1, a root chord of 1.5, a strake sweep of 75°, a leading edge sweep of 35°, a trailing edge sweep angle of 9° and a strake width of 0.25 at an attack angle of 5°. Experimental results were not available, so the results are compared with Roberts[14] datum Solution. Roberts solution divides the wing into 12 spanwise divisions and 42 chordwise divisions whereas the present method divides the wing into 11 spanwise divisions and 31 chordwise divisions. The figures 10 to 13 show the comparison of pressure distribution. One can see that at the root of the wing, at $y/s=0.035$, the results do not coincide very satisfactorily but going outboard, the results coincide almost exactly for the stations at $y/s=0.28$ and $y/s=0.9$ for a lesser number of panels. The agreement is quite good.

The second compares the results obtained with the two different potential flow calculation methods. The two methods were used to calculate the pressure distribution and the load distribution on a wing having the following characteristics: aspect ratio of 4.9, taper ratio of 0.85 and no sweepback. The cross section airfoil of the wing is a 7.6% thick NACA 64A410, so it is a cambered wing. The wing is set at an angle of attack of 6 degrees. The results were also compared with the potential flow results obtained by Sinhamapatra[1]. Figures 14 and 15 show the pressure distributions calculated at two different spanwise stations: $y/s=0.1$ and $y/s=0.9$. One can see that the two curves obtained with the equal singularity and internal singularity methods coincide very well. They agree

also very much with the potential flow results obtained by Sinhamapatra[1]. Figure 16 shows the load distribution calculated in the three cases. Again, one can see that the results obtained agree satisfactorily with the results of ref.1.

The third involves the comparison between the three different methods discussed in the present report, namely, the inviscid calculation using the internal singularity method and the equal singularity method, and the iterative VII technique using the equal singularity method for the potential flow calculation. They are applied to a swept wing of aspect ratio of 3, taper ratio of 0.5 and a sweepback angle of 45°. The cross section of the wing is an airfoil 7.6% thick NACA 64A010. Figures 17 to 19 show the comparison of pressure distribution between the three. Then the lift distribution obtained by the two potential flow calculation methods are shown in Figure 20. The results obtained by the VII technique are then compared with experimental results taken from Kolbe and Boltz[15] in Figure 21. It is found that the strip theory application of the boundary layer correction to the inviscid solution gives reasonably accurate results. There is a difference of 1.11% between the values of lift obtained with the VII technique and the experimental results as seen in Figure 21. The results obtained with the inviscid calculation only and the VII technique differ by 4.12%. The difference between the results obtained with the two different panel methods differ by about 1.5% with the equal singularity method being the more accurate as shown in Figure 20.

The strip theory approach to the boundary layer correction gives fairly good results for wings having simple planform with moderate values of aspect ratio, taper ratio and

sweepback angle. In cases with a large crossflow, or cases where the boundary layer does not remain attached until the trailing edge, a fully three dimensional boundary layer scheme is necessary. Developing a fully three dimensional boundary layer correction scheme involves much more time and considering this fact, the strip theory approach is very useful in the first stages of the design of a three dimensional wing. One can obtain very rapidly rough values of the various aerodynamic parameters needed, and if need be, one can then modify the code to accomodate a fully three dimensional boundary layer correction. On the MUSIC system, the time needed to execute the inviscid calculation with the internal singularity method is about 10 seconds of real computational time and 18 seconds for the equal singularity method. Depending on the number of users actually logged on the network, it takes from 5 to 20 minutes of real time. We can see that the internal singularity is about twice as fast as the other method studied.

CHAPTER V   CONCLUSION

The objective of the present project was to test a method
that would predict the basic flow parameters with reasonable
accuracy, and would be less time-consuming than the other
methods used at present, such as wind tunnel testing or
Navier-Stokes solvers. The viscous-inviscid interaction
method has been applied to the case of three-dimensional
clean wings or wings with all the control surfaces in initial
position. This represents the case of an aircraft in cruising
condition. Two different panel methods have been used for the
potential flow calculation and an integral method has been
used for the boundary layer calculation. The two solutions
are then matched by the transpiration velocity model in an
iterative manner. The transpiration velocity model was used
because it has the distinct advantage that the geometry of
the wing surface remains constant during the calculation and
therefore the influence coefficients matrix remains constant
and can be stored and inverted once and for all. In
comparison with the displacement thickness model, where the
body surface is modified with each iteration, and therefore
the influence coefficients have to be recalculated each time,
a considerable amount of computational time has been saved.

Even if the method is strictly first-order with the three-
dimensional boundary layer simplified by a strip theory
approach, the results obtained are sufficiently accurate for
the cases studied for the preliminary design stages of an
aircraft. However, there are restrictions to the method. It
has been found that for a very thin wing, NACA 0002, both
potential flow calculation methods failed to provide
reasonable results for unknown reasons. It has been
established that both methods are able to provide such

results. Sinhamapatra[1] shows some results for the case of a very thin wing with cross-section airfoil NACA 0002. Also for high angles of attack, for alpha higher than 9 degrees, again the method failed to provide accurate results.

Because the equal singularity method code and the boundary layer correction code were not designed to be matched and the various variables are calculated in different order, we had to write subroutines to arrange the parameters in the right order so that the boundary layer code would receive the transferred data correctly. Unfortunately, all the various parameters are organized correctly except for the influence coefficients. So because of time constraints, the two codes are not quite matched but it would not be arduous work to finish the matching and obtain results of VII method using the equal singularity method. The results provided in the report for VII are for the boundary layer correction code matched with the internal singularity code. The results obtained could be compared with those using VII with internal singularity method.

To improve the present method, one could finish the matching of boundary layer and equal singularity model. Also, a fully three-dimensional boundary layer calculation method could be used to replace the strip theory approach used in the present method. This would certainly improve the accuracy of the results in the cases where the crossflow is considerably large. Finally, the method could be extended to multi-aerofoil sections. The basic flow properties could be calculated for wings with deflected flaps in any position. In these cases, there is a significant amount of boundary layer separation, either at the trailing edge, or at the cavities beneath the slats and shrouds of multi-element airfoils.

Also, in high lift condition, additional viscous effect occur, namely the wake-boundary layer intercation. To obtain satisfactory results, the method would have to include wake-boundary layer interaction and higher order boundary layer correction terms.

Finally, the viscous-inviscid interaction method could be applied using other panel methods, especially those using a doublet distribution. Also, triangular panels could be tried because they are more flexible and represent more accurately any complex surfaces. Normandin[16] uses a potential flow calculation method based on a doublet distribution and triangular panels and the results obtained are very satisfactory. This method could be tried using the method described in Normandin[16] and matching it with a boundary layer correction by the transpiration velocity model.

The viscous-inviscid interaction technique is certainly a very attractive alternative to the traditional method of wind tunnel testing because of the high cost involved, or to the Navier-Stokes solvers because of the enormous computational resources needed. The VII technique can be used to obtain satisfactory results and the present method can be extended to a number of interesting cases as described earlier, even to transonic flows with an appropriate modelling of the boundary layer separation at the foot of shock waves.

REFERENCES

[1]   SINHAMAPATRA, K.P., "Viscous-Inviscid Matching on Wings at Low Speeds", Department of Aeronautical Engineering, IIT Kharagpur, India, 1988.

[2]   LIGHTHILL, M.J., "On Displacement Thickness", JFM. Vol.4, 1958.

[3]   CHOW, C.Y. and KUETHE, A.M., "Foundations of Aerodynamics", Fourth Edition, John Wiley & Sons, 1986.

[4]   MILNE-THOMSON, L.M., "Theoretical Aerodynamics", Fourth Edition, MacMillan, 1966.

[5]   MASSON, C. and PARASCHIVOIU, I., "Description et comparaison de cinq méthodes de panneaux en deux dimensions", Département de Génie Mécanique, Ecole Polytechnique de Montréal, Canada, 1990.

[6]   PARASCHIVOIU, I., "Aérodynamique", Notes de cours 2.410, Ecole Polytechnique de Montréal, 1990.

[7]   GERHART, P.M. and GROSS, R.J., "Fundamentals of Fluid Mechanics", Addison-Wesley Publishing Company, 1985.

[8]   SINGH, N., BANDYOPADHYAY, G. and BASU, B.C., "Calculation of Potential Flow about Arbitrary Three Dimensional Wings Using Internal Singularities Distribution", Aero. Quarterly, August 1983.

[9]   NEWLING, J.C., "An Improved Two-Dimensional Multi-Aerofoil Program", HSM-MAE-R-FDM-0007, 1977.

[10]   THWAITES, B., "Incompressible Aerodynamics", Clarendon Press, Oxford, 1960.

[11]   SMITH, P.D., "An Integral Prediction Method for Three-Dimensional Compressible Turbulent Boundary Layers", ARC R & M 3739, 1974.

[12]   MYRING, D.F., "An Integral Prediction Method for Three-Dimensional Turbulent Boundary Layers in Incompressible Flow", RAE TR 70147, 1970.

[13]   MAGER, A., "Generalisation of Boundary Layer Momentum Integral Equations to Three Dimensional Flows, Including Those of Rotating Systems", NACA Report 1067, 1952.

[14]   ROBERTS, A. and RUNDLE, K., "Comparison of Incompressible Flow about and Thick Wings using the Spline Mode System", BAC(CAD) Report Aero MA19, 1972.

[15]   BOLTZ, W.F. and KOLBE, C.D., "The Forces and Pressure Distributions at Subsonic Speeds on a Plane Wing having 45° Sweepback, an Aspect Ratio of 3 and a Taper Ratio of 0.5", NACA RMA51G31, 1951.

[16]   NORMANDIN, F., "Etude d'une aile d'avion et de son sillage en régime subsonique", Département de Génie Mécanique, Ecole Polytechnique de Montréal, Canada, 1990.

APPENDIX A   FORMATION OF ELEMENTS FROM INPUT POINTS

Appendix A gives an outline of the method used to calculate the different geometric parameters necessary to define the geometry of the wing. The coordinates of the input points are $(X_k^i, Y_k^i, Z_k^i, k=1,2,3,4)$ for a particular element in the reference system. The four different subscripts k are used to list the coordinates of the four corners of the quadrilateral element in a condensed manner. In vector form,

$$\overline{X_k^i} = X_k^i \overline{i} + Y_k^i \overline{j} + Z_k^i \overline{k} \tag{A.1}$$

$\overline{i}$, $\overline{j}$, $\overline{k}$ are the unit vectors along the axes of the reference coordinate system. The corner points k=1 and k=2 are placed on the first n-line and the corner points k=3 and k=4 are on the second n-line. This is shown in figure YY. Quantities associated with the first n-line are denoted by the subscript F and quantities associated with the second are denoted by S. The n-line vectors can be expressed as:

$$\overline{P_F} = \overline{X_1^i} - \overline{X_2^i}$$
$$\overline{P_S} = \overline{X_3^i} - \overline{X_4^i} \tag{A.2}$$

Two parallel sides of the trapezoidal element are supposed to be parallel to the weighted average of the two n-line vectors. The unit vector $\overline{i}_E$ parallel to the two parallel sides of the trapezoid is expressed as:

$$\overline{I_E} = \frac{\overline{P_F} + \overline{P_S}}{|\overline{P_F} + \overline{P_S}|} \tag{A.3}$$

It is also the unit vector the axis of the element coordinate system. Examining equation (A.3), we can see that each parallel side has the same midpoint and the same length as the segment of n-line from which it was formed. The side lengths d_F and d_S and the midpoints in vector form X_F and X_S are:

$$
\begin{aligned}
d_F &= |\overline{P_F}| \\
d_S &= |\overline{P_S}|
\end{aligned}
\tag{A.4}
$$

$$
\begin{aligned}
\overline{X_F} &= \frac{1}{2}\,(\overline{X_1^i} + \overline{X_2^i}) \\
\overline{X_S} &= \frac{1}{2}\,(\overline{X_3^i} + \overline{X_4^i})
\end{aligned}
\tag{A.5}
$$

The corner of the trapezoidal elements are the endpoints of the parallel sides. They can be expressed in vector form,

$$
\begin{aligned}
\overline{X_1} &= \overline{X_F} - \frac{1}{2} d_F \overline{I_E} \\
\overline{X_2} &= \overline{X_F} + \frac{1}{2} d_F \overline{I_E} \\
\overline{X_3} &= \overline{X_S} + \frac{1}{2} d_S \overline{I_E} \\
\overline{X_4} &= \overline{X_S} - \frac{1}{2} d_S \overline{I_E}
\end{aligned}
\tag{A.6}
$$

Now the normal vector to the plane of the element and its corresponding unit vector can be calculated and are expressed

as,

$$\overline{N}=(\overline{X_4} - \overline{X_2}) \times (\overline{X_3} - \overline{X_1}) \tag{A.7}$$

$$\overline{n}=\frac{\overline{N}}{|\overline{N}|} \tag{A.8}$$

n is also the unit vector along the ξ-axis of the element coordinate system. The unit vector along the η-axis of the element coordinate system can be calculated by taking the cross product of the other two unit vectors:

$$\overline{J_E}=\overline{n} \times \overline{I_E} \tag{A.9}$$

The three unit vectors expressed in equations (A.3), (A.8) and (A.9) can be written in the component form as,

$$\overline{I_E}=a_{11}\overline{i}+a_{12}\overline{j}+a_{13}\overline{k}$$
$$\overline{J_E}=a_{21}\overline{i}+a_{22}\overline{j}+a_{23}\overline{k}$$
$$\overline{n}=\overline{K_E}=a_{31}\overline{i}+a_{32}\overline{j}+a_{33}\overline{k}$$

or

$$\begin{bmatrix} \overline{I_E} \\ \overline{J_E} \\ \overline{K_E} \end{bmatrix} = \begin{bmatrix} a_{11} & a_{12} & a_{13} \\ a_{21} & a_{22} & a_{23} \\ a_{31} & a_{32} & a_{33} \end{bmatrix} \begin{bmatrix} \overline{i} \\ \overline{j} \\ \overline{k} \end{bmatrix} \tag{A.10}$$

This 3 x 3 matrix of components a_{ij} enables us to transform the coordinates of the points and the components of vectors between the reference and the element coordinate systems.

The origin of the element coordinate system is taken as the point whose coordinates are the averages of the those of the input corner points. The average point is denoted as X_{av} and can be expressed as,

$$\overline{X_{av}} = \frac{1}{2} \ (\overline{X_F} + \overline{X_S}) \tag{A.11}$$

The element coordinates of the corner points can expressed using this new origin. The equations are,

$$\begin{aligned}
\xi_k^* &= a_{11}(X_k - X_{av}) + a_{12}(Y_k - Y_{av}) + a_{13}(Z_k - Z_{av}) \\
\eta_k^* &= a_{21}(X_k - X_{av}) + a_{22}(Y_k - Y_{av}) + a_{23}(Z_k - Z_{av})
\end{aligned} \tag{A.12}$$
$$(k = 1, 2, 3, 4)$$

$(X_k,\ Y_k,\ Z_k)$ are the coordinates of $\vec{X_k}$ from equation (A.6). Figures 18 and 19 illustrates the various geometric parameters to be calculated to completely define the geometry of each wing element. We can see that

$$\begin{aligned}
\eta_1^* &= \eta_2^* \\
\eta_3^* &= \eta_4^* = -\eta_1^*
\end{aligned} \tag{A.13}$$

The width of the element w is

$$w = \eta_1^* - \eta_3^* = 2 \ \eta_1^* \tag{A.14}$$

The slopes of the non-vertical sides of the element (Fig. 19) are

$$m_{32} = \frac{(\xi_2^* - \xi_3^*)}{w}$$
$$m_{41} = \frac{(\xi_1^* - \xi_4^*)}{w}$$

(A.15)

The coordinates of the centroid of the element can be calculated in the element coordinate system and are expressed as

$$\eta_o = \frac{w^2}{2} \frac{m_{32} - m_{41}}{\xi_3^* + \xi_2^* - \xi_1^* - \xi_4^*}$$
$$\xi_o = \frac{m_{32} + m_{41}}{2} \eta_o$$

(A.16)

Now the reference coordinates of the centroid can be expressed as

$$X_o = X_{av} + a_{11}\xi_o + a_{21}\eta_o$$
$$Y_o = Y_{av} + a_{12}\xi_o + a_{22}\eta_o$$
$$Z_o = Z_{av} + a_{13}\xi_o + a_{23}\eta_o$$

(A.17)

The centroid calculated in equation (A.17) is now taken as the origin of the element coordinate system and replaces the average point. With this new origin, the element coordinates of the corner points can be expressed as

$$\xi_k = \xi_k^* - \xi_o$$
$$\eta_k = \eta_k^* - \eta_o$$
$$(k=1,2,3,4)$$

(A.18)

Other geometric parameters can be calculated. They are the points where the sides intercept the x-axis (Fig.19) b_{32} and b_{41} and the lengths of the sides d_{12}, d_{32}, d_{34} and d_{41}.

$$b_{32} = \frac{\xi_3 \eta_2 - \xi_2 \eta_3}{w}$$
$$b_{41} = \frac{\xi_4 \eta_1 - \xi_1 \eta_4}{w}$$

(A.19)

$$d_{12} = d_F$$
$$d_{34} = d_S$$
$$d_{32} = w(1+m_{32}^2)^{\frac{1}{2}}$$
$$d_{41} = w(1+m_{41}^2)^{\frac{1}{2}}$$

(A.20)

APPENDIX B VELOCITY INDUCED BY A SOURCE DISTRIBUTION

Appendix B presents the near-field or exact formulas which are used in the present method to calculate the induced velocity due to a source distribution. The calculation starts with the various geometric parameters calculated in Appendix A. We need the coordinates of the corner points ξ_k, η_k, k=1,2,3,4, the width w from equation (A.14), the slopes m_{32} and m_{41} from (A.15), the intercepts b_{32} and b_{41} from equation (A.19) and the side lengths d_{12}, d_{32}, d_{34} and d_{41} from equation (A.20). Figure 19 illustrates all these geometric parameters.

The equation giving the potential due to a source distribution of unit density at a particular point P with coordinates x, y, z is

$$\phi = \frac{1}{4\pi}\iint_A \frac{1}{r}\,dA = -\frac{1}{4\pi}\iint_A \frac{1}{((x-\xi)^2+(y-\eta)^2+z^2)^{\frac{1}{2}}}\,d\xi\,d\eta \quad (B.1)$$

The distance between point P and a point on the panel with coordinates (ξ, η, 0) is denoted r in equation (B.1). The range of integration is the area A of the panel. The components of the induced velocity in the element coordinates system are

$$V_x^s = \frac{\partial\phi}{\partial x} = \frac{1}{4\pi}\iint_A \frac{(x-\xi)}{r^3}\,d\xi\,d\eta$$

$$V_y^s = \frac{\partial\phi}{\partial y} = \frac{1}{4\pi}\iint_A \frac{(y-\eta)}{r^3}\,d\xi\,d\eta \quad (B.2)$$

$$V_z^s = \frac{\partial\phi}{\partial z} = \frac{1}{4\pi}\iint_A \frac{z}{r^3}\,d\xi\,d\eta$$

To simplify the calculation of equation (B.2), the integrals

are expressed as the sum of four terms. Each of these four terms depends only on one side of the quadrilateral panel.

The following preliminary quantities are to be calculated:

$$r_k = \sqrt{(x-\xi_k)^2 + (y-\eta_k)^2 + z^2} \qquad \text{(B.3)}$$
$$k = 1, 2, 3, 4$$

$$\alpha_k = \frac{x-\xi_k}{r_k}$$
$$\beta_k = \frac{y-\eta_k}{r_k} \qquad \text{(B.4)}$$
$$\gamma_k = \frac{z}{r_k}$$
$$k = 1, 2, 3, 4$$

$$p_k^{(32)} = m_{32}(z^2 + (y-\eta_k)^2) - (x-\xi_k)(y-\eta_k)$$
$$k = 3, 2 \qquad \text{(B.5)}$$
$$p_k^{(41)} = m_{41}(z^2 + (y-\eta_k)^2 - (x-\xi_k)(y-\eta_k)$$
$$k = 4, 1$$

The basic functions are

$$L^{(mn)} = \log \frac{r_m + r_n - d_{mn}}{r_m + r_n + d_{mn}} \qquad \text{(B.6)}$$

m, n consecutive i.e. mn=12, 23, 34 or 41

$$T_k^{(32)} = \tan^{-1}\left(\frac{p_k^{(32)}}{(z r_k)}\right)$$
$$k = 3, 2 \qquad \text{(B.7)}$$
$$T_k^{(41)} = \tan^{-1}\left(\frac{p_k^{(41)}}{(z r_k)}\right)$$
$$k = 4, 1$$

Using the above preliminary functions, the components of the induced velocity due to a trapezoidal source element of unit density may be written as

$$4\pi V_x^s = -\frac{1}{(1+m_{32}^2)^{\frac{1}{2}}} L^{(32)} + \frac{1}{(1+m_{41}^2)^{\frac{1}{2}}} L^{(41)}$$

$$4\pi V_y^s = -L^{(12)} + L^{(34)} + \frac{m_{32}}{(1+m_{32}^2)^{\frac{1}{2}}} L^{(32)} - \frac{m_{41}}{(1+m_{41}^2)^{\frac{1}{2}}} L^{(41)} \qquad (B.8)$$

$$4\pi V_z^s = -T_2^{(32)} + T_3^{(32)} + T_1^{(41)} - T_4^{(41)}$$

The velocity induced at the i-th control point by the j-th panel can be written in vector form as,

$$\overline{V_{ij}^s} = V_x^s \, \overline{i_{Ej}} + V_y^s \, \overline{j_{Ej}} + V_z^s \, \overline{k_{Ej}} \qquad (B.9)$$

$\vec{i}_{Ej}$, $\vec{j}_{Ej}$, $\vec{k}_{Ej}$ are the unit vectors along the axes of the element coordinate system given by equation (A.10).

APPENDIX C   VELOCITY INDUCED BY HORSESHOE VORTEX
AND A UNIFORM LINE SOURCE

C.1 Velocity Induced by a Vortex Segment of Unit Strength

In the reference coordinate system which is rectangular, the induced velocity at any point (X, Y, Z) by a vortex segment extending from (X_1, Y_1, Z_1) to (X_2, Y_2, Z_2) and having vorticity directed from (X_1, Y_1, Z_1) to (X_2, Y_2, Z_2) according to the right hand rule as shown in Figure 20, can be found by application of Biot-Savart's law. The components u_1, v_1 and w_1 of this velocity along the X, Y and Z directions respectively can be expressed as follows,

$$u_1 = \frac{a_1}{(a_1^2 + b_1^2 + c_1^2)^{\frac{1}{2}}} \frac{1}{4\pi d} (\cos\theta_1 - \cos\theta_2)$$

$$v_1 = \frac{b_1}{(a_1^2 + b_1^2 + c_1^2)^{\frac{1}{2}}} \frac{1}{4\pi d} (\cos\theta_1 - \cos\theta_2) \qquad (C.1)$$

$$w_1 = \frac{c_1}{(a_1^2 + b_1^2 + c_1^2)^{\frac{1}{2}}} \frac{1}{4\pi d} (\cos\theta_1 - \cos\theta_2)$$

In equation (C.2),

$$\begin{aligned}
a_1 &= (Y_2 - Y_1)(Z - Z_1) - (Y - Y_1)(Z_2 - Z_1) \\
b_1 &= (Z_2 - Z_1)(X - X_1) - (Z - Z_1)(X_2 - X_1) \\
c_1 &= (X_2 - X_1)(Y - Y_1) - (X - X_1)(Y_2 - Y_1)
\end{aligned} \qquad (C.2)$$

and

$$\cos\theta_1 = \frac{R_1^2 - R_2^2 + L_{12}^2}{2L_{12}R_1}$$

$$\cos\theta_2 = \frac{R_1^2 - R_2^2 - L_{12}^2}{2L_{12}R_2}$$

(C.3)

$$d = R_2 (1 - \cos\theta_2)^{\frac{1}{2}}$$

(C.4)

where

$$L_{12} = \sqrt{(X_2 - X_1)^2 + (Y_2 - Y_1)^2 + (Z_2 - Z_1)^2}$$

(C.5)

$$R_k = \sqrt{(X - X_k)^2 + (Y - Y_k)^2 + (Z - Z_k)^2}$$
$$k = 1, 2$$

(C.6)

C.2 Velocity Induced by a Semi-Infinite Vortex Line of Unit Strength

The velocity induced at any point (X, Y, Z) by a vortex line extending from infinity to a point (X^*, Y^*, Z^*), and having a vorticity defined as positive in the vector direction of the vorticity points toward the point (X, Y, Z) as shown in Figure 21, can be expressed in terms of its components u_2, v_2 and w_2 along the X, Y and Z directions respectively as,

$$u_2 = -\frac{a^*}{\sqrt{a^{*2} + b^{*2} + c^{*2}}} \frac{1}{4\pi d_1} (1 - \cos\theta^*)$$

$$v_2 = -\frac{b^*}{\sqrt{a^{*2} + b^{*2} + c^{*2}}} \frac{1}{4\pi d_1} (1 - \cos\theta^*)$$

$$w_2 = -\frac{c^*}{\sqrt{a^{*2} + b^{*2} + c^{*2}}} \frac{1}{4\pi d_1} (1 - \cos\theta^*)$$

(C.7)

where in equation (C.7),

$$a^* = A_y(Z-Z^*) - A_z(Y-Y^*)$$
$$b^* = A_z(X-X^*) - A_x(Z-Z^*) \qquad (C.8)$$
$$c^* = A_x(Y-Y^*) - A_y(X-X^*)$$

where A_x, A_y and A_z are the direction cosines of the vortex line in a direction from point (X^*, Y^*, Z^*) to infinity along the vortex line. These direction cosines are independant of the sign of the vorticity.

$$\cos\theta^* = -\frac{A_x(X-X^*) + A_y(Y-Y^*) + A_z(Z-Z^*)}{R^*} \qquad (C.9)$$

$$d_1 = R^*(1-\cos^2\theta^*)^{\frac{1}{2}} \qquad (C.10)$$

$$R^* = \sqrt{(X-X^*)^2 + (Y-Y^*)^2 + (Z-Z^*)^2} \qquad (C.11)$$

C.3 Velocity Induced by a Line Source of Unit Strength

The velocity induced by a line source between point $A(X_1, Y_1, Z_1)$ and point $B(X_2, Y_2, Z_2)$ with line source of unit density as shown in Figure 22 can be expressed as,

$$\overline{V^{(LS)}} = \overline{E}\,\overline{e} + \overline{D}\,\overline{d} \qquad (C.12)$$

where

$$\overline{E} = \frac{1}{4\pi}\left(\frac{1}{R_2} - \frac{1}{R_1}\right) \qquad (C.13)$$

$$\overline{D} = \frac{1}{4\pi d}\left[\frac{\overline{r_1}\cdot\overline{e}}{R_1} - \frac{\overline{r_2}\cdot\overline{e}}{R_2}\right] \tag{C.14}$$

$$= \frac{1}{4\pi d}(\cos\theta_1 - \cos\theta_2)$$

where

$$\cos\theta_1 = \frac{R_1^2 - R_2^2 + L_{AB}^2}{2L_{AB}R_1} \tag{C.15}$$

$$\cos\theta_2 = \frac{R_1^2 - R_2^2 - L_{AB}^2}{2L_{AB}R_2}$$

$$d = R_2(1-\cos^2\theta_2)^{\frac{1}{2}} \tag{C.16}$$

R_1 and R_2 are the lengths of the vectors to the point (X, Y, Z) from the ends of the line between (X_1, Y_1, Z_1) and (X_2, Y_2, Z_2). These vectors are

$$\overline{r_k} = (X-X_k)\,\overline{i} + (Y-Y_k)\,\overline{j} + (Z-Z_k)\,\overline{k} \tag{C.17}$$

$$R_k = |\,\overline{r_k}\,| = \sqrt{(X-X_k)^2 + (Y-Y_k)^2 + (Z-Z_k)^2} \tag{C.18}$$

k = 1 or 2

$\overrightarrow{e}$ is the unit vector along the direction $\overrightarrow{AB}$ and is given by,

$$\overline{e} = \frac{\overline{AB}}{|\,\overline{AB}\,|} = \frac{(X_2-X_1)}{L_{AB}}\,\overline{i} + \frac{(Y_2-Y_1)}{L_{AB}}\,\overline{j} + \frac{(Z_2-Z_1)}{L_{AB}}\,\overline{k} \tag{C.19}$$

$$L_{AB} = \sqrt{(X_2 - X_1)^2 + (Y_2 - Y_1)^2 + (Z_2 - Z_1)^2} \qquad (C.20)$$

$\overline{d}$ is the vector drawn from AB (or its extension) to the point (X,Y,Z) such that it is perpendicular to AB hence,

$$\overline{d} = (\overline{e} \times \overline{r_1}) \times \overline{e} \qquad (C.21)$$

Using equations (C.17),(C.18) and (C.20), d can be obtained from equation (C.21).

Once E^*, D^*, $\vec{e}$, $\vec{d}$ are known, the induced velocity vector can be obtained from equation (C.12).

APPENDIX D   THREE DIMENSIONAL TURBULENT BOUNDARY LAYER

D.1 The Governing Equations

For the coordinate system described in Chapter II, the boundary layer momentum integral equations are

$$
\frac{\left(\dfrac{\partial \Theta_{11}}{\partial x}\right)}{h_1} + \Theta_{11}\left[\frac{\partial u_e}{\partial x}\frac{(2-M^2)}{h_1 u_e} + \frac{1}{q}\frac{\partial}{\partial x}\left(\frac{q}{h_1}\right) + k_1\right] + \frac{1}{h_2}\frac{\partial \Theta_{12}}{\partial y} +
$$
$$
\Theta_{12}\left[\frac{\partial u_e}{\partial y}\frac{(2-M^2)}{h_2 u_e} + \frac{1}{q}\frac{\partial}{\partial y}\left(\frac{q}{h_2}\right) + k_3\right]
$$
$$
+\Delta_1\left[\frac{1}{h_1 u_e}\frac{\partial u_1}{\partial x} + k_1\frac{u_1}{u_e}\right] + \Delta_2\left[\frac{1}{h_2 u_e}\frac{\partial u_1}{\partial y} + k_2\frac{v_1}{u_e} + k_3\frac{u_1}{u_e} + \Theta_{22}k_2\right] = \frac{C_{f1}}{2} \tag{D.1}
$$

$$
\frac{\left(\dfrac{\partial \Theta_{21}}{\partial x}\right)}{h_1} + \Theta_{21}\left[\frac{\partial u_e}{\partial x}\frac{(2-M^2)}{h_1 u_e} + \frac{1}{q}\frac{\partial}{\partial x}\left(\frac{q}{h_1}\right) + l_3\right] + \frac{1}{h_2}\frac{\partial \Theta_{22}}{\partial y}
$$
$$
+\Theta_{22}\left[\frac{\partial u_e}{\partial y}\frac{(2-M^2)}{h_2 u_e} + \frac{1}{q}\frac{\partial}{\partial y}\left(\frac{q}{h_2}\right) + l_2\right]
$$
$$
+\Delta_1\left[\frac{1}{h_1 u_e}\frac{\partial v_1}{\partial x} + l_1\frac{u_1}{u_e} + l_3\frac{v_1}{u_e}\right] + \Delta_2\left[\frac{1}{h_2 u_e}\frac{\partial v_1}{\partial y} + l_2\frac{v_1}{u_e} + \Theta_{11}l_1\right] = \frac{C_{f2}}{2} \tag{D.2}
$$

M is the Mach number and u_1, v_1 are the velocity components in the x and y directions respectively at the edge of the boundary layer. u_e is the resultant velocity at the edge of the boundary layer and is given by

$$
u_e^2 = u_1^2 + v_1^2 + \frac{2g}{h_1 h_2}u_1 v_1 \tag{D.3}
$$

C_{f1} and C_{f2} are the skin friction coefficients in the x and y directions respectively and k_1, k_2, k_3, l_1, l_2, l_3 and q are the functions of the metrics h_1, h_2 and g and are given as

$$k_1 = \frac{h_1 g}{q^2} \left[\frac{1}{h_1} \frac{\partial h_1}{\partial y} + \frac{g}{h_1^3} \frac{\partial h_1}{\partial x} - \frac{1}{h_1^2} \frac{\partial g}{\partial x} \right]$$

$$k_2 = \frac{h_1}{q^2} \left[\frac{\partial g}{\partial y} + h_2 \frac{\partial h_2}{\partial x} - \frac{g}{h_2} \frac{\partial h_2}{\partial y} \right]$$

$$k_3 = \frac{1}{q^2} \left[h_1 h_2 (1 + (\frac{g}{h_1 h_2})^2) \frac{\partial h_1}{\partial y} - 2g \frac{\partial h_2}{\partial x} \right]$$

$$l_1 = \frac{h_2}{q^2} \left[\frac{\partial g}{\partial x} + h_1 \frac{\partial h_1}{\partial y} - \frac{g}{h_1} \frac{\partial h_1}{\partial x} \right]$$

$$l_2 = \frac{h_2 g}{q^2} \left[\frac{1}{h_2} \frac{\partial h_2}{\partial x} + \frac{g}{h_2^3} \frac{\partial h_2}{\partial y} - \frac{1}{h_2^2} \frac{\partial g}{\partial x} \right]$$

$$l_3 = \frac{1}{q^2} \left[h_1 h_2 (1 + (\frac{g}{h_1 h_2})^2) \frac{\partial h_2}{\partial x} - 2g \frac{\partial h_1}{\partial y} \right]$$

$$q^2 = (h_1 h_2)^2 - g^2$$

$$(\text{D.4})$$

a_1, a_2, b_1 and b_2 are other quantities function of the metrics that are needed. Their expressions are

$$a_1 = -\frac{h_1 h_2^2}{q^2}$$

$$a_2 = \frac{g h_1}{q^2}$$

$$b_1 = \frac{g h_2}{q^2}$$

$$b_2 = -\frac{h_1^2 h_2}{q^2}$$

$$(\text{D.5})$$

The entrainment or continuity integral equation is given as

$$\frac{1}{\rho_e u_e q} \left[\frac{\partial}{\partial x} \left(\frac{\rho_e q}{h_1} (u_1 \delta - u_e \Delta_1) \right) + \frac{\partial}{\partial y} \left(\frac{\rho_e q}{h_2} (v_1 \delta - u_e \Delta_2) \right) \right]$$

$$= \frac{1}{u_e} \left[\frac{u_1}{h_1} \frac{\partial \delta}{\partial x} + \frac{v_1}{h_2} \frac{\partial \delta}{\partial y} - w_1 \right] = F$$

$$(\text{D.6})$$

w_1 is the velocity component in the z direction and F is the

entrainment coefficient. F is given as

$$F = 0.025H - 0.022 \tag{D.7}$$

D.2 Various Integral Parameters and Empirical Relations

In non-orthogonal curvilinear coordinate system, the integral parameters are:

$$\Theta_{11} = \int_0^\delta \frac{\rho u (u_1 - u)}{\rho_e u_e^2} dz$$

$$\Theta_{12} = \int_0^\delta \frac{\rho v (u_1 - u)}{\rho_e u_e^2} dz \tag{D.8}$$

$$\Theta_{21} = \int_0^\delta \frac{\rho u (v_1 - v)}{\rho_e u_e^2} dz$$

$$\Theta_{22} = \int_0^\delta \frac{\rho v (v_1 - v)}{\rho_e u_e^2} dz$$

$$\Delta_1 = \int_0^\delta \frac{\rho_e u_1 - \rho u}{\rho_e u_e} dz \tag{D.9}$$

$$\Delta_2 = \int_0^\delta \frac{\rho_e v_1 - \rho v}{\rho_e u_e} dz$$

In the streamline coordinate system (s, n, z):

66

$$\theta_{11} = \int_0^\delta \frac{\rho U(U_1 - U)}{\rho_e u_e^2} \, dz$$

$$\theta_{12} = \int_0^\delta \frac{\rho V(U_1 - U)}{\rho_e u_e^2} \, dz$$

$$\theta_{21} = \int_0^\delta -\frac{\rho UV}{\rho_e u_e^2} \, dz$$

$$\theta_{22} = \int_0^\delta -\frac{\rho V^2}{\rho_e u_e^2} \, dz$$

(D.10)

$$\delta_1 = \int_0^\delta \frac{\rho_e U_1 - \rho U}{\rho_e u_e} \, dz$$

$$\delta_2 = \int_0^\delta -\frac{\rho V}{\rho_e u_e} \, dz$$

(D.11)

In this coordinate system $u_e = U_1$.

The different shape parameters are defined as

$$H = \frac{\delta_1}{\theta_{11}}$$

$$H_1 = \frac{\delta - \delta_1}{\theta_{11}}$$

$$\bar{H} = \frac{1}{\theta_{11}} \int_0^\delta \frac{\rho}{\rho_e} \left(1 - \frac{U}{U_e}\right) dz$$

$$H + 1 = (\bar{H} + 1)(1 + 0.2M^2)$$

(D.12)

For incompressible flow, the two shape parameters H and $\bar{H}$ are

identical in value. The various integral thickness parameters
of the two axes systems are related as

$$\Theta_{11} = [\theta_{11}\sin^2(\lambda-\alpha) - (\theta_{12}+\theta_{21})\sin(\lambda-\alpha)\cos(\lambda-\alpha) \quad (D.13)$$
$$+\theta_{22}\cos^2(\lambda-\alpha)]/\sin^2\lambda$$

$$\Theta_{12} = [\theta_{11}\sin\alpha\sin(\lambda-\alpha) + \theta_{12}\sin(\lambda-\alpha)\cos\alpha - \theta_{21}\sin\alpha\cos(\lambda-\alpha) \quad (D.14)$$
$$-\theta_{22}\cos\alpha\cos(\lambda-\alpha)]/\sin^2\lambda$$

$$\Theta_{21} = [\theta_{11}\sin\alpha\sin(\lambda-\alpha) - \theta_{12}\sin\alpha\cos(\lambda-\alpha) + \theta_{21}\sin(\lambda-\alpha)\cos\alpha \quad (D.15)$$
$$-\theta_{22}\cos\alpha\cos(\lambda-\alpha)]/\sin^2\lambda$$

$$\Theta_{22} = \frac{\theta_{11}\sin^2\alpha - (\theta_{12}+\theta_{21})\sin\alpha\cos\alpha + \theta_{22}\cos^2\alpha}{\sin^2\lambda} \quad (D.16)$$

$$\Delta_1 = \frac{\delta_1\sin(\lambda-\alpha) - \delta_2\cos(\lambda-\alpha)}{\sin\lambda} \quad (D.17)$$

$$\Delta_2 = \frac{\delta_1\sin\alpha + \delta_2\cos\alpha}{\sin\lambda} \quad (D.19)$$

α is the angle between the x-axis and the external streamline
and λ is the angle between the x-axis and the y-axis and can
be obtained from the following relations:

$$\cos\lambda = \frac{g}{h_1 h_2}$$
$$\sin\alpha = \frac{V_1\sin\lambda}{u_e} \quad (D.20)$$

With the assumed velocity profiles, power law for the streamwise component of the velocity and Mager[13] profile for the crossflow component, the following relations are obtained

$$H = 2n + 1 \qquad\qquad (D.21)$$

$$H_1 = \frac{2H}{H-1} \qquad\qquad (D.22)$$

$$\theta_{21} = \theta_{11} \tan\beta \, f_{21}(H) \qquad\qquad (D.23)$$

$$\theta_{12} = \theta_{11} \tan\beta \, f_{12}(H) \qquad\qquad (D.24)$$

$$\delta_2 = \theta_{11} \tan\beta \, f_2(H) \qquad\qquad (D.25)$$

$$\theta_{22} = \theta_{11} \tan^2\beta \, f_{22}(H) \qquad\qquad (D.26)$$

ß is the angle between an external streamline and the corresponding limiting streamline on the surface of the wing. The following relation is used for the skin friction coefficient in the external flow direction. The two components of the skin friction in the x and y directions can be expressed as

$$C_{f1} = C_f \frac{\sin(\lambda-\alpha) - \cos(\lambda-\alpha)\tan\beta}{\sin\lambda} \qquad\qquad (D.27)$$

$$C_{f2} = C_f \frac{\sin\alpha + \cos\alpha\tan\beta}{\sin\lambda} \qquad\qquad (D.28)$$

The various f functions necessary to calculate equations
(D.23) to (D.26) and their derivatives with respect to H for
Mager[13] are given are follows

$$f_{21}=-\frac{2}{(H-1)(H+2)}$$
$$f_{2}=-\frac{16H}{(H-1)(H+3)(H+5)}$$
$$f_{12}=f_{21}-f_{2}$$
$$f_{22}=\frac{12f_{21}}{(H+3)(H+4)}$$
$$f_{21}'=\frac{2(2H+1)}{[(H-1)(H+2)]^2}$$
$$f_{2}'=\frac{f_2 f_{21}'}{f_{21}}+\frac{48f_{21}(H^2+5H+5)}{[(H+3)(H+5)]^2}$$
$$f_{12}'=f_{21}'-f_{2}'$$
$$f_{22}'=\frac{[12f_{21}'-f_{22}(2H+7)]}{(H+3)(H+4)}$$

(D.29)

′ denotes differentiation with respect to H.
The coefficients necessary to calculate equations (2.18),
(2.19) and (2.20) and the complete of required functions are
given as:

defining t = tanß
(D.30)

and tt=$(1+t^2)/\sin^2\lambda$

$$F_{11} = \frac{\sin^2(\lambda-\alpha) - (f_{12}+f_{21})\sin(\lambda-\alpha)\cos(\lambda-\alpha)\,t + f_{22}\cos^2(\lambda-\alpha)\,t^2}{\sin^2\lambda}$$

$$F_{12} = (\sin\alpha\sin(\lambda-\alpha) + [f_{12}\cos\alpha\sin(\lambda-\alpha) - f_{21}\sin\alpha\cos(\lambda-\alpha)]t$$
$$- f_{22}\cos\alpha\cos(\lambda-\alpha)\,t^2)/\sin^2\lambda$$

$$F_{21} = (\sin\alpha\sin(\lambda-\alpha) + [f_{21}\cos\alpha\sin(\lambda-\alpha) - f_{12}\sin\alpha\cos(\lambda-\alpha)]t$$
$$- f_{22}\cos\alpha\cos(\lambda-\alpha)\,t^2)/\sin^2\lambda \qquad \text{(D.32)}$$

$$F_{22} = \frac{\sin^2\alpha + (f_{12}+f_{21})\sin\alpha\cos\alpha\,t + f_{22}\cos^2\alpha\,t^2}{\sin^2\lambda}$$

$$F_1 = \frac{H\sin(\lambda-\alpha) - f_2\cos(\lambda-\alpha)\,t}{\sin\lambda}$$

$$F_2 = \frac{H\sin\alpha + f_2\cos\alpha\,t}{\sin\lambda}$$

$$J_1 = \frac{H_1\sin(\lambda-\alpha) + f_2\cos(\lambda-\alpha)\,t}{\sin\lambda}$$
$$J_2 = \frac{H_1\sin\alpha - f_2\cos\alpha\,t}{\sin\lambda} \qquad \text{(D.31)}$$

$$F_{11H} = \frac{-(f_{12}'+f_{21}')\sin(\lambda-\alpha)\cos(\lambda-\alpha)\,t + f_{22}'\cos^2(\lambda-\alpha)\,t^2}{\sin^2\lambda}$$

$$F_{12H} = ([f_{12}'\cos\alpha\sin(\lambda-\alpha) - f_{21}'\sin\alpha\cos(\lambda-\alpha)]t$$
$$- f_{22}'\cos\alpha\cos(\lambda-\alpha)\,t^2)/\sin^2\lambda$$

$$F_{21H} = ([f_{21}'\cos\alpha\sin(\lambda-\alpha) - f_{12}'\sin\alpha\cos(\lambda-\alpha)]t$$
$$- f_{22}'\cos\alpha\cos(\lambda-\alpha)\,t^2)/\sin^2\lambda \qquad \text{(D.33)}$$

$$F_{22H} = \frac{(f_{12}'+f_{21}')\sin\alpha\cos\alpha\,t + f_{22}'\cos^2\alpha\,t^2}{\sin^2\lambda}$$

$$F_{1H} = \frac{(1+0.2M^2)\sin(\lambda-\alpha) - f_2'\cos(\lambda-\alpha)\,t}{\sin\lambda}$$

$$F_{2H} = \frac{(1+0.2M^2)\sin\alpha + f_2'\cos\alpha\,t}{\sin\lambda}$$

$$J_{1H} = \frac{H_1'\sin(\lambda-\alpha) + f_2'\cos(\lambda-\alpha)\,t}{\sin\lambda}$$
$$J_{2H} = \frac{H_1'\sin\alpha - f_2'\cos(\lambda-\alpha)\,t}{\sin\lambda} \qquad \text{(D.34)}$$

$$F_{11\alpha} = \frac{2\cos(\lambda-\alpha)\sin(\lambda-\alpha)(f_{22}t^2-1)+(f_{21}+f_{12})(2\cos^2(\lambda-\alpha)-1)t}{\sin^2\lambda}$$

$$F_{12\alpha} = ([\cos\alpha\sin(\lambda-\alpha)-\cos(\lambda-\alpha)\sin\alpha](1-f_{22}t^2)$$
$$-(f_{12}+f_{21})(\cos\alpha\cos(\lambda-\alpha)+\sin\alpha\sin(\lambda-\alpha))t)/\sin^2\lambda$$

$$F_{21\alpha} = F_{12\alpha}$$

$$F_{22\alpha} = \frac{2\sin\alpha\cos\alpha(1-f_{22}t^2)+(f_{12}+f_{21})(2\cos^2\alpha-1)t}{\sin^2\lambda}$$

$$F_{1\alpha} = -\frac{H\cos(\lambda-\alpha)+f_2\sin(\lambda-\alpha)t}{\sin\lambda}$$

$$F_{2\alpha} = \frac{H\cos\alpha-f_2\sin\alpha\,t}{\sin\lambda}$$

$$(D.35)$$

$$J_{1\alpha} = \frac{-H_1\cos(\lambda-\alpha)+f_2\sin(\lambda-\alpha)t}{\sin\lambda}$$

$$J_{2\alpha} = \frac{H_1\cos\alpha+f_2\sin\alpha\,t}{\sin\lambda} \qquad (D.36)$$

$$F_{11\beta} = [-(f_{12}+f_{21})\sin(\lambda-\alpha)\cos(\lambda-\alpha)+2f_{22}\cos^2(\lambda-\alpha)t]tt$$

$$F_{12\beta} = [f_{12}\sin(\lambda-\alpha)\cos\alpha-f_{21}\cos(\lambda-\alpha)\sin\alpha$$
$$-2f_{22}\cos\alpha\cos(\lambda-\alpha)t]\,tt$$

$$F_{21\beta} = [f_{21}\sin(\lambda-\alpha)\cos\alpha-f_{12}\cos(\lambda-\alpha)\sin\alpha \qquad (D.37)$$
$$-2f_{22}\cos\alpha\cos(\lambda-\alpha)t]\,tt$$

$$F_{22\beta} = [(f_{12}+f_{21})\sin\alpha\cos\alpha+2f_{22}\cos^2\alpha\,t]tt$$

$$F_{1\beta} = [-f_2\cos(\lambda-\alpha)]tt\sin\lambda$$

$$F_{2\beta} = [f_2\cos\alpha]tt\sin\lambda$$

$$J_{1\beta} = -F_{1\beta}$$
$$J_{2\beta} = -F_{2\beta} \qquad (D.38)$$

$$F_{11\lambda} = -\left[F_{11\alpha} + \frac{2F_{11}\cos\lambda}{\sin\lambda}\right]$$

$$F_{12\lambda} = \frac{\cos(\lambda-\alpha)\left[\sin\alpha + f_{12}\cos\alpha\, t\right] + \sin(\lambda-\alpha)\left[f_{22}\cos\alpha\, t + f_{21}\sin\alpha\right]t - 2F_{12}s}{\sin^2\lambda}$$

$$F_{21\lambda} = \frac{\cos(\lambda-\alpha)\left[\sin\alpha + f_{21}\cos\alpha\, t\right] + \sin(\lambda-\alpha)\left[f_{22}\cos\alpha\, t + f_{12}\sin\alpha\right]t - 2F_{21}s}{\sin^2\lambda}$$

$$F_{22\lambda} = -\frac{2F_{22}\cos\lambda}{\sin\lambda}$$

$$F_{1\lambda} = \frac{H\cos(\lambda-\alpha) + f_2\sin(\lambda-\alpha)\, t - F_1\cos\lambda}{\sin\lambda}$$

$$F_{2\lambda} = -\frac{F_2\cos\lambda}{\sin\lambda}$$

$$(D.40)$$

$$J_{1\lambda} = -J_{1\alpha} - J_1\frac{\cos(\lambda)}{\sin\lambda}$$

$$J_{2\lambda} = -J_2\frac{\cos\lambda}{\sin\lambda}$$

$$(D.39)$$

The S functions are defined as follows

$$S_1 = \frac{C_{f1}}{2}h_1 - \theta_{11}\left[F_{11\alpha}\frac{\partial\alpha}{\partial x} + F_{11\lambda}\frac{\partial\lambda}{\partial x} + F_{11}\left[\frac{(2-M^2)}{u_e}\frac{\partial u_e}{\partial x} + \frac{h_1}{q}\frac{\partial}{\partial x}\left(\frac{q}{h_1}\right) + k_1 h_1\right]\right.$$

$$+\frac{h_1}{h_2}\left(\frac{F_{12}}{\theta_{11}}\frac{\partial\theta_{11}}{\partial y} + F_{12H}\frac{\partial H}{\partial y} + F_{12\beta}\frac{\partial\beta}{\partial y} + F_{12\alpha}\frac{\partial\alpha}{\partial y} + F_{12\lambda}\frac{\partial\lambda}{\partial y}\right.$$ $(D.41)$

$$+F_{12}\left[\frac{(2-M^2)}{u_e}\frac{\partial u_e}{\partial y} + \frac{h_2}{q}\frac{\partial}{\partial y}\left(\frac{q}{h_2}\right) + k_3 h_2\right]\right) + F_1\left(\frac{1}{u_e}\frac{\partial u_1}{\partial x} + \frac{k_1 h_1 u_1}{u_e}\right)$$

$$+F_2\left(\frac{h_1}{h_2 u_e}\frac{\partial u_1}{\partial y} + \frac{k_2 h_1 v_1}{u_e} + \frac{K_3 h_1 u_1}{u_e}\right) + F_{22}k_2 h_1\right]$$

$$S_2 = \frac{C_{f2}}{2} h_2 - \theta_{11} \left[F_{21\alpha} \frac{\partial \alpha}{\partial x} + F_{21\lambda} \frac{\partial \lambda}{\partial x} + F_{21} \left[\frac{(2-M^2)}{u_e} \frac{\partial u_e}{\partial x} + \frac{h_1}{q} \frac{\partial}{\partial x} \left(\frac{q}{h_1} \right) + l_3 h_1 \right] \right.$$

$$+ \frac{h_1}{h_2} \left(\frac{F_{22}}{\theta_{11}} \frac{\partial \theta_{11}}{\partial y} + F_{22H} \frac{\partial H}{\partial y} + F_{22\beta} \frac{\partial \beta}{\partial y} + F_{22\alpha} \frac{\partial \alpha}{\partial y} + F_{22\lambda} \frac{\partial \lambda}{\partial y} \right.$$

$$+ F_{22} \left[\frac{(2-M^2)}{u_e} \frac{\partial u_e}{\partial y} + \frac{h_2}{q} \frac{\partial}{\partial y} \left(\frac{q}{h_2} \right) + l_2 h_2 \right] \right) + F_1 \left(\frac{1}{u_e} \frac{\partial v_1}{\partial x} + \frac{l_1 h_1 u_1}{u_e} \frac{l_3 h_1 v_1}{u_e} \right)$$

$$\left. + F_2 \left(\frac{h_1}{h_2 u_e} \frac{\partial v_1}{\partial y} + \frac{l_2 h_1 v_1}{u_e} \right) + l_1 h_1 \right]$$

$$(D.42)$$

$$S_3 = F h_1 - \theta_{11} \left[J_{1\alpha} \frac{\partial \alpha}{\partial x} + J_{1\lambda} \frac{\partial \lambda}{\partial x} + \frac{h_1}{h_2} \left(\frac{J_2}{\theta_{11}} \frac{\partial \theta_{11}}{\partial y} \right. \right.$$

$$+ J_{2H} \frac{\partial H}{\partial y} + J_{2\beta} \frac{\partial \beta}{\partial y} + J_{2\alpha} \frac{\partial \alpha}{\partial y} + J_{2\lambda} \frac{\partial \lambda}{\partial y} \right) + J_1 \left(\frac{(1-M^2)}{u_e} \frac{\partial u_e}{\partial x} \right.$$

$$\left. + \frac{h_1}{q} \frac{\partial}{\partial x} \left(\frac{q}{h_1} \right) \right) + \frac{h_1}{h_2} J_2 \left(\frac{(1-M^2)}{u_e} \frac{\partial u_e}{\partial y} + \frac{h_2}{q} \frac{\partial}{\partial y} \left(\frac{q}{h_2} \right) \right) \right]$$

$$(D.43)$$

Appendix E   Batchfiles

```
/INCLUDE SOUMET.A.OS
//ME00    JOB (ADMAQN,QVTEME),'PASCAL',
//        MSGLEVEL=(1,1),MSGCLASS=A,
//        CLASS=4,
//        TIME=10,
//        REGION=32000K
/*ROUTE PRINT MUSIC
/*JOBPARM L=10
// EXEC FORTVCLG
//FORT.SYSIN DD *
/INCLUDE ME00:VII.EQU(NEST)
/*
//GO.SYSIN DD *
/INCLUDE ME00:EQUAL1.DAT(NEST)
/*
//GO.FT06F001 DD SYSOUT=A
//TRACEUR DD DSN=&TRILOG,SPACE=(TRK,(1,1)),UNIT=INTRDR
//GO.FT03F001 DD *
/INCLUDE ME00:ANSWER1.DAT(NEST)
/*
//GO.FT04F001 DD SYSOUT=A
//GO.FT12F001 DD *
/INCLUDE ME00:STRIP.DAT(NEST)
/*
//GO.FT14F001 DD SYSOUT=A
//GO.FT16F001 DD SYSOUT=A
/*
```

```
/INCLUDE SOUMET.A.OS
//ME00    JOB (ADMAQN,QVTEME),'VOTRE NOM ICI',
//        MSGLEVEL=(1,1),MSGCLASS=A,
//        CLASS=4,
//        TIME=10,
//        REGION=32000K
/*ROUTE PRINT MUSIC
/*JOBPARM L=10
// EXEC FORTVCLG
//FORT.SYSIN DD *
/INCLUDE ME00:VII.INT(NEST)
/*
//GO.SYSIN DD *
/INCLUDE ME00:SWING5.DAT(NEST)
/*
//GO.FT06F001 DD SYSOUT=A
//TRACEUR DD DSN=&TRILOG,SPACE=(TRK,(1,1)),UNIT=INTRDR
//GO.FT03F001 DD *
/INCLUDE ME00:ANSWER1.DAT(NEST)
/*
//GO.FT04F001 DD SYSOUT=A
//GO.FT11F001 DD SYSOUT=A
//GO.FT12F001 DD *
/INCLUDE ME00:STRIP.DAT(NEST)
/*
//GO.FT14F001 DD SYSOUT=A
/*
```

Appendix F   Input Files

```
3  5  1
0.0  0.2  0.4  0.6  0.8  1.0
4.9 0.85 0.0
1   6.0
31
1.0       -0.00021
0.89896   -0.00076
0.79849   -0.00229
0.64915   -0.01086
0.54975   -0.01736
0.50011   -0.02024
0.45050   -0.02266
0.40090   -0.02436
0.30166   -0.02537
0.25200   -0.02499
0.20230   -0.02406
0.15252   -0.02244
0.07770   -0.01919
0.02724   -0.01251
0.00918   -0.00796
0.0        0.0
0.00582    0.01112
0.02276    0.02095
0.07230    0.03865
0.14748    0.05366
0.19770    0.06126
0.24800    0.06705
0.29834    0.07131
0.39910    0.07552
0.44950    0.07522
0.49989    0.07344
0.55025    0.07040
0.65085    0.06106
0.80151    0.03967
0.90104    0.02038
1.0        0.021
```

```
31 5
3 1 1
4.9 0.85 0.0
6.0
1.0 0.8 0.6 0.4 0.2 0.0
1.0       -0.00021
0.89896   -0.00076
0.79849   -0.00229
0.64915   -0.01086
0.54975   -0.01736
0.50011   -0.02024
0.45050   -0.02266
0.40090   -0.02436
0.30166   -0.02537
0.25200   -0.02499
0.20230   -0.02406
0.15252   -0.02244
0.07770   -0.01919
0.02724   -0.01251
0.00918   -0.00796
0.0        0.0
0.00582    0.01112
0.02276    0.02095
0.07230    0.03865
0.14748    0.05366
0.19770    0.06126
0.24800    0.06705
0.29834    0.07131
0.39910    0.07552
0.44950    0.07522
0.49989    0.07344
0.55025    0.07040
0.65085    0.06106
0.80151    0.03967
0.90104    0.02038
1.0        0.021
0.982424  0.186661  0.0  0.0
```
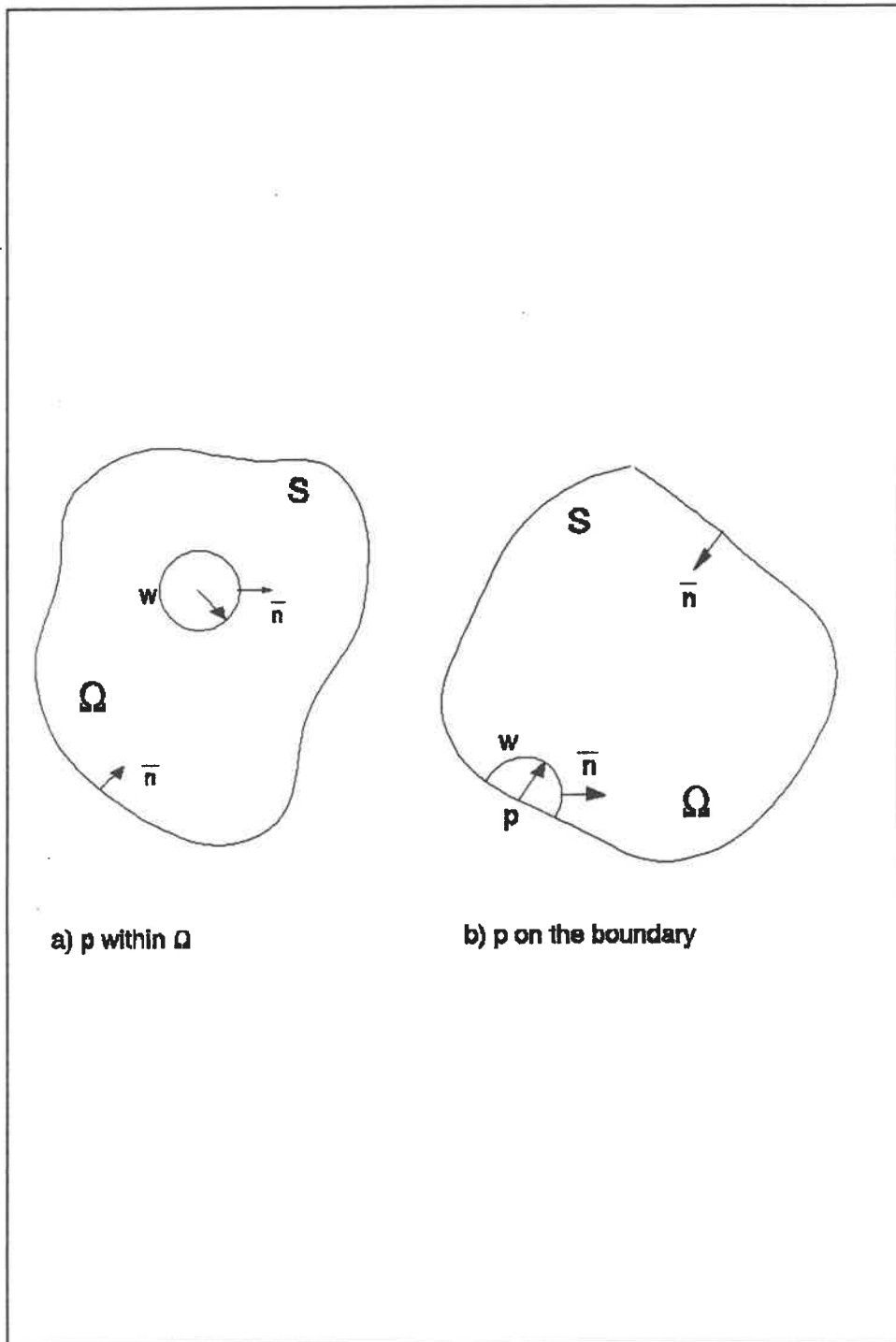
Figure 1   Green's theorem: The Single Domain
Problem
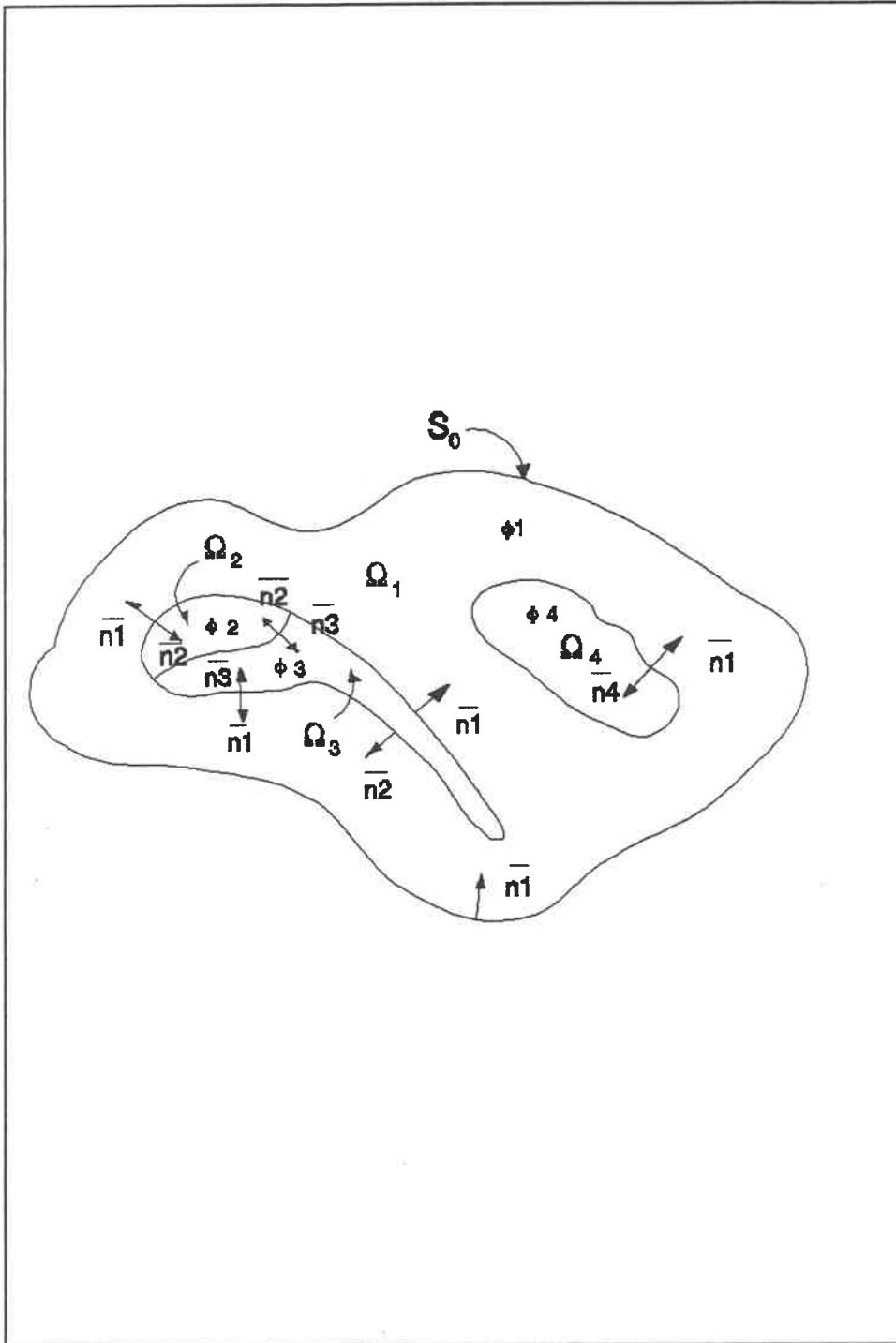
Figure 2 Green's Theorem: The Multi-Domain Problem
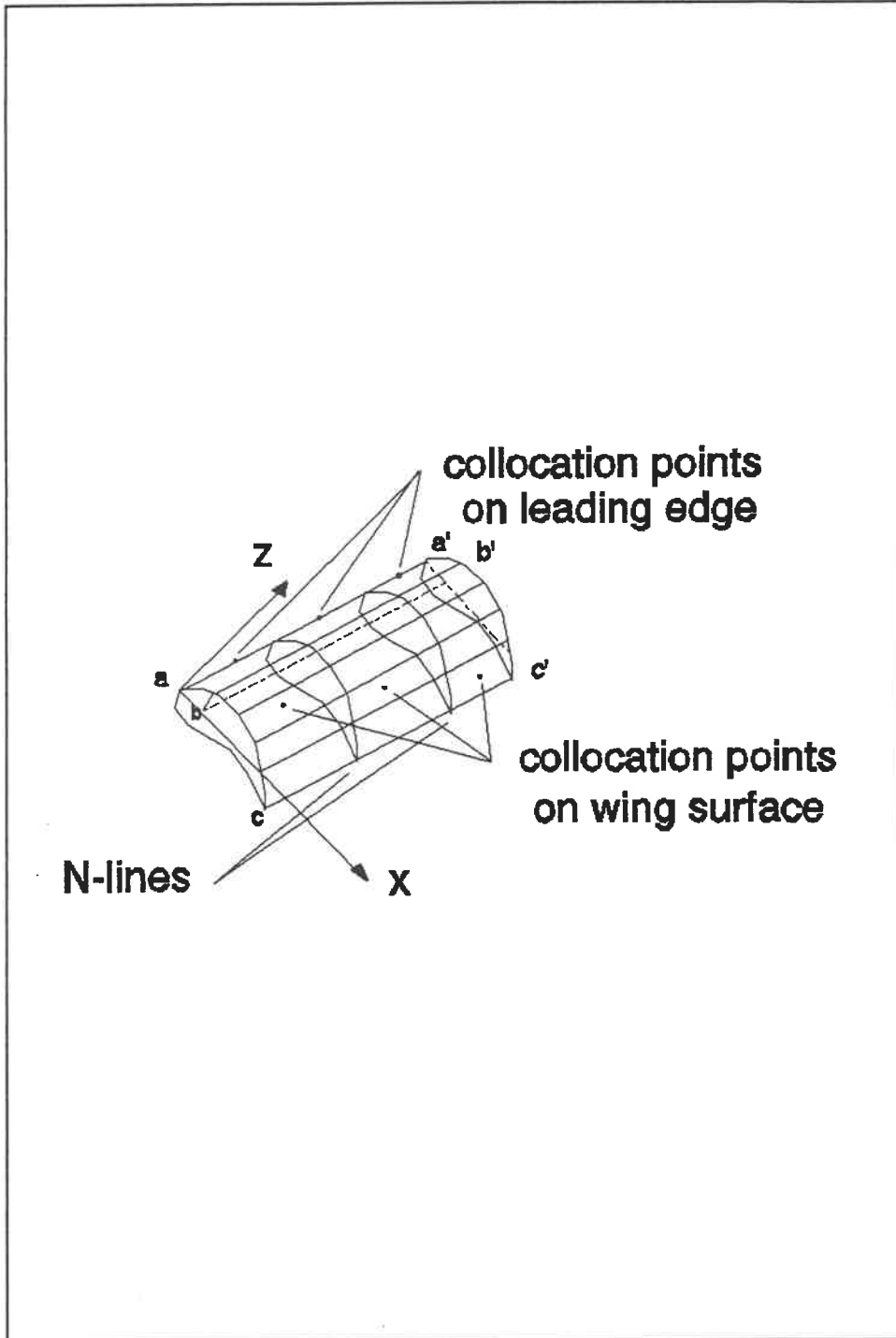
Figure 3 Wing Surface Elements
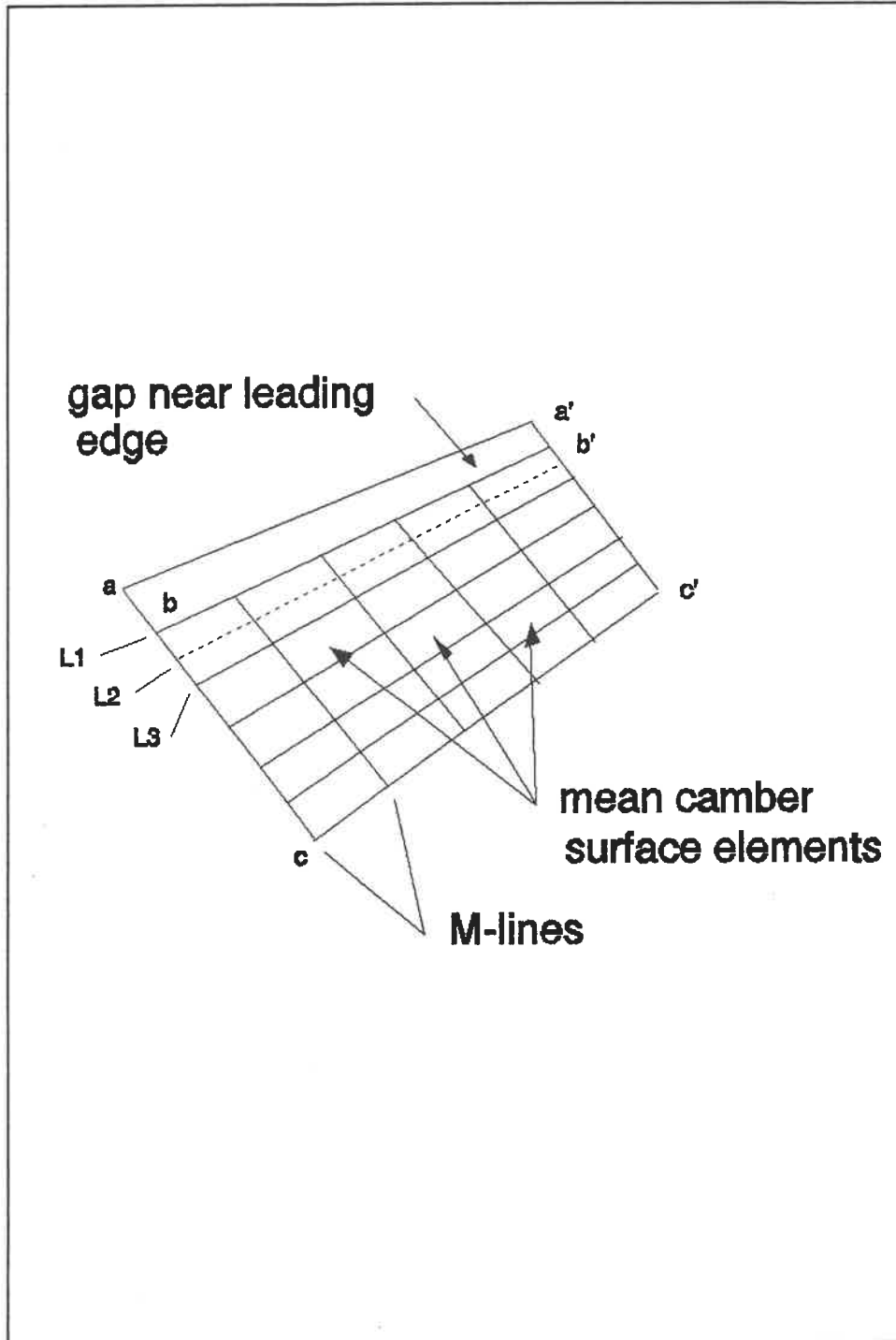
Figure 4 Mean Camber Surface Elements
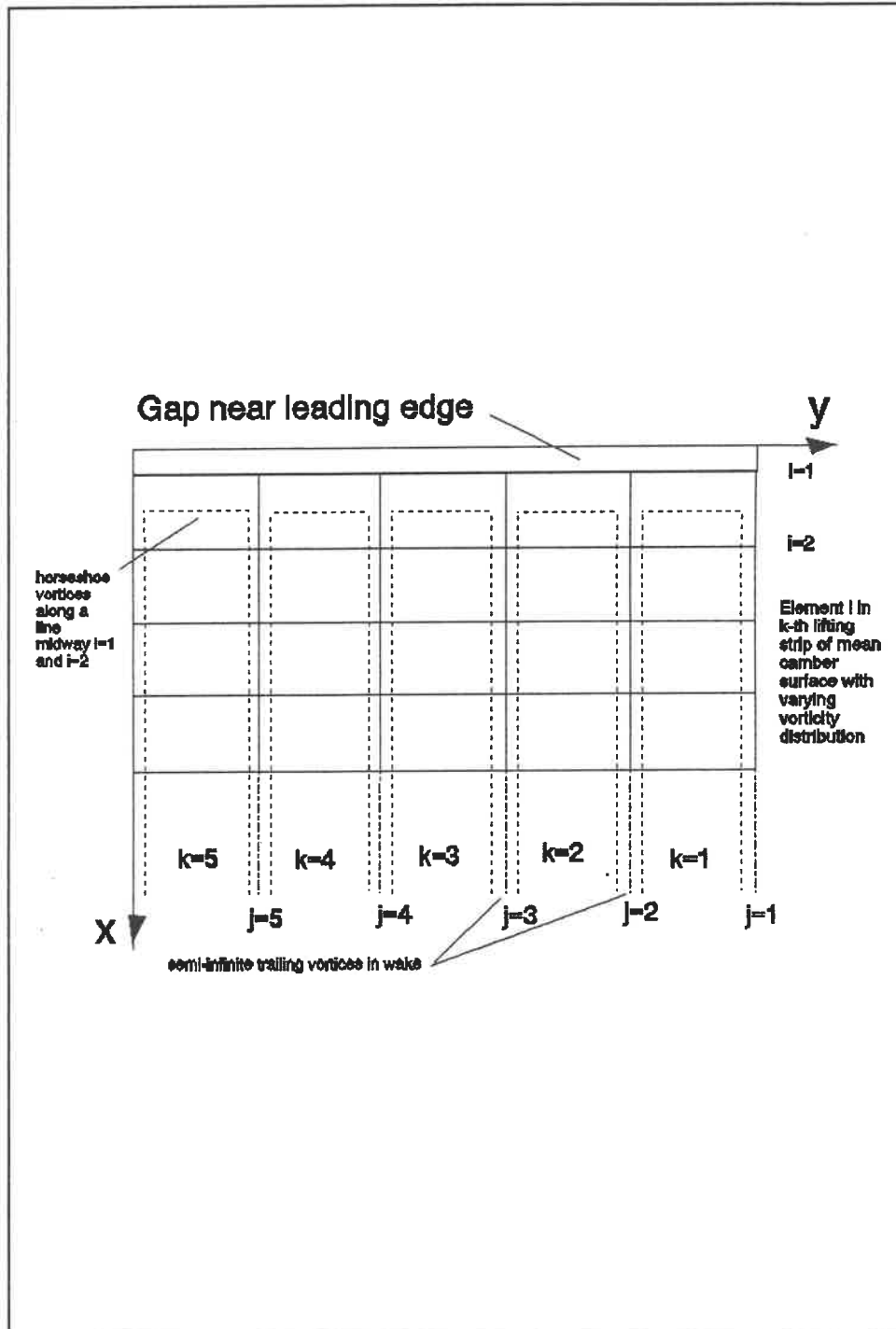
Figure 5 Vorticity Distribution on Mean Camber Surface Elements in Internal Singularity Model
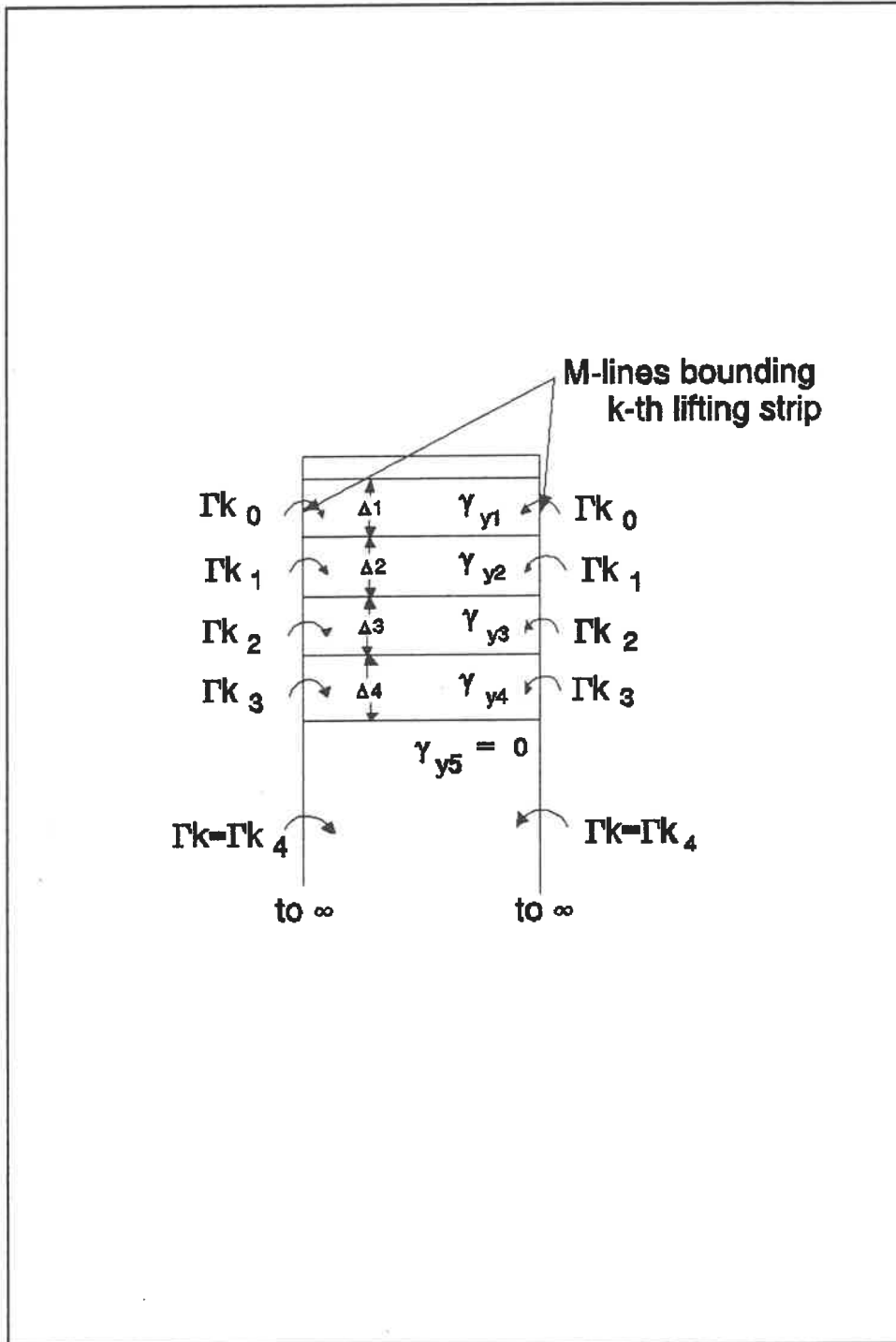
Figure 6   Trailing Vortex Filaments Along M-Lines
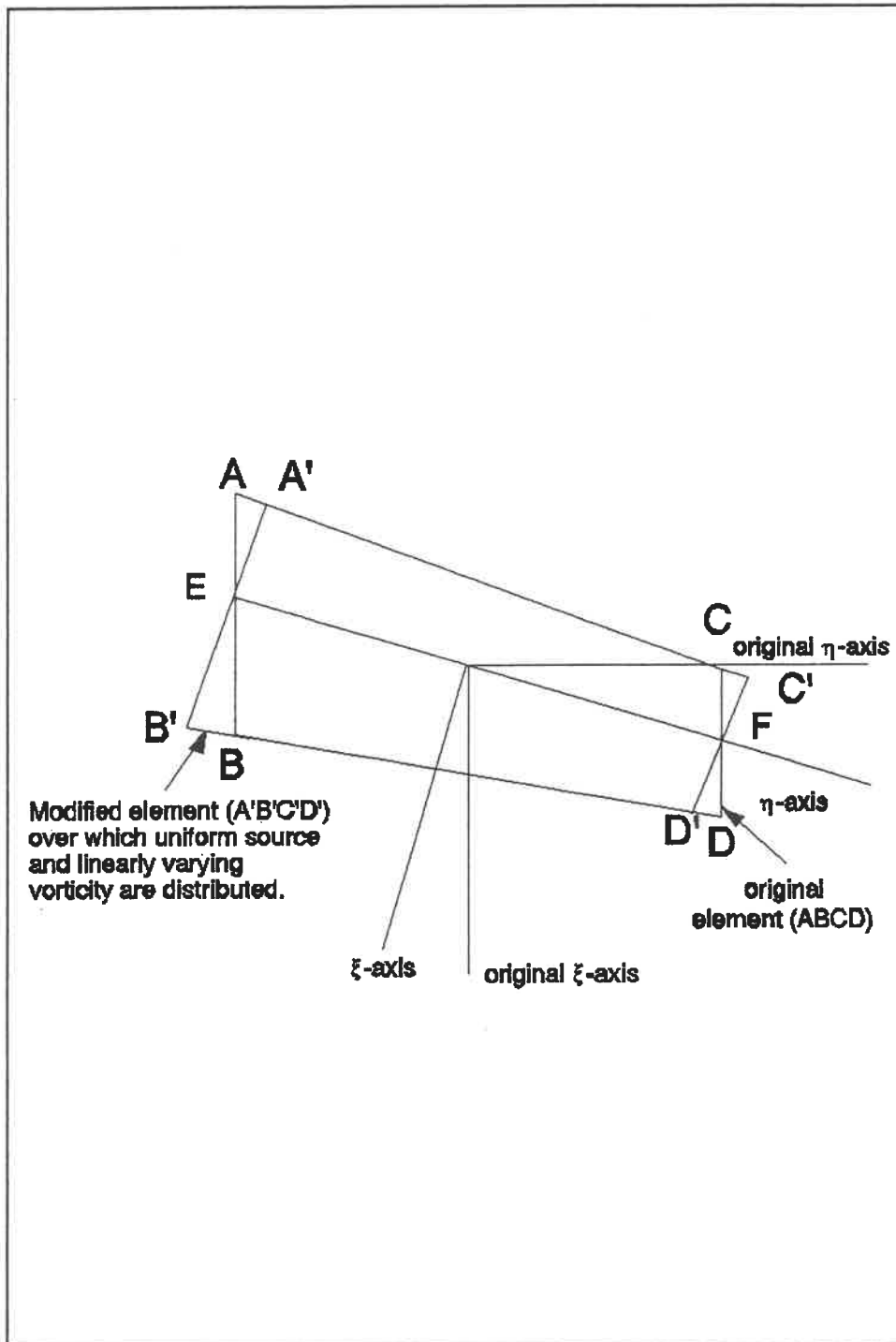
Figure 7 Modification Involved for Trapezoidal Element
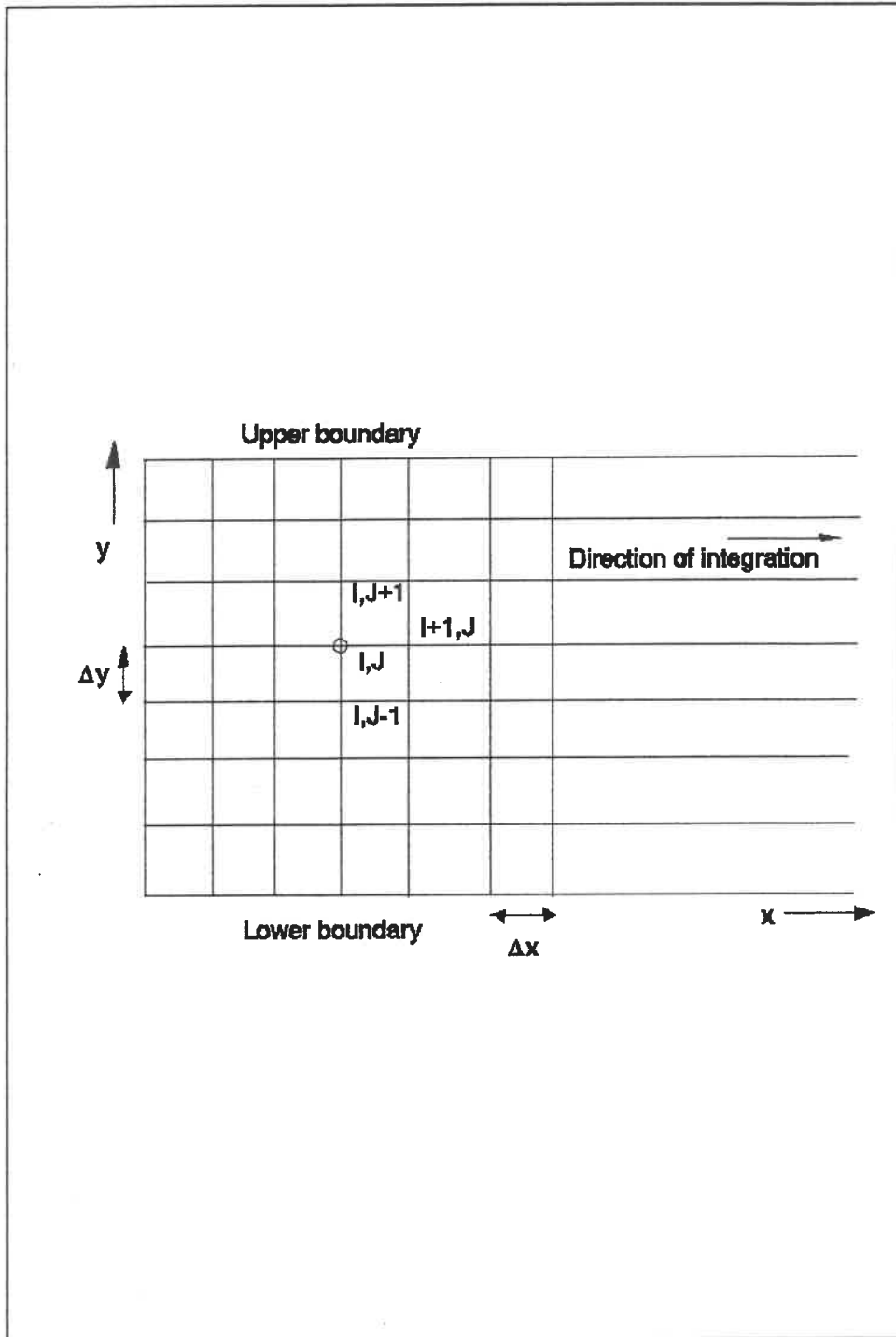
Figure 8 Computational Mesh
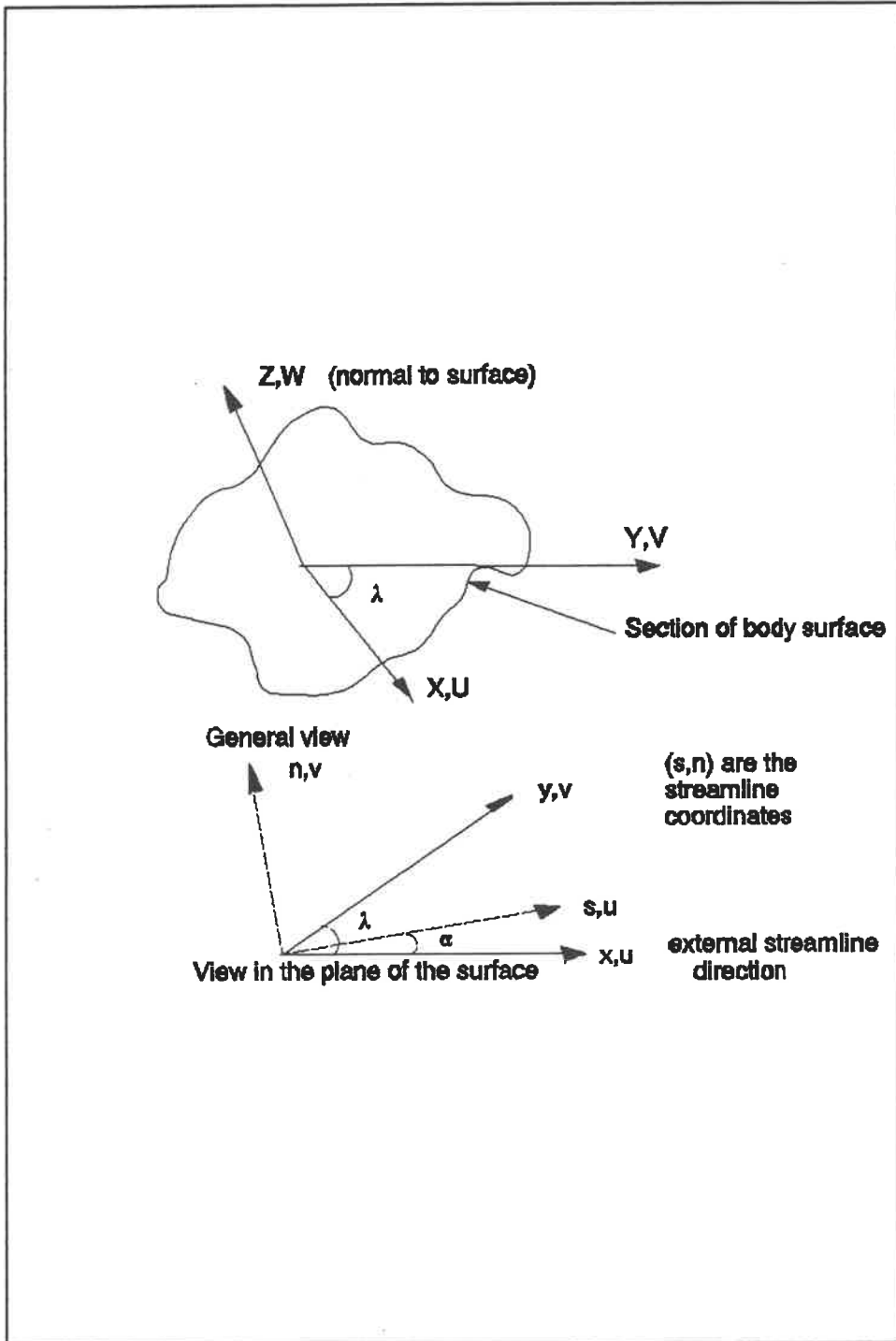
Figure 9   Coordinate System

Pressure Distribution
Strake Wing NACA 0005
alpha=5
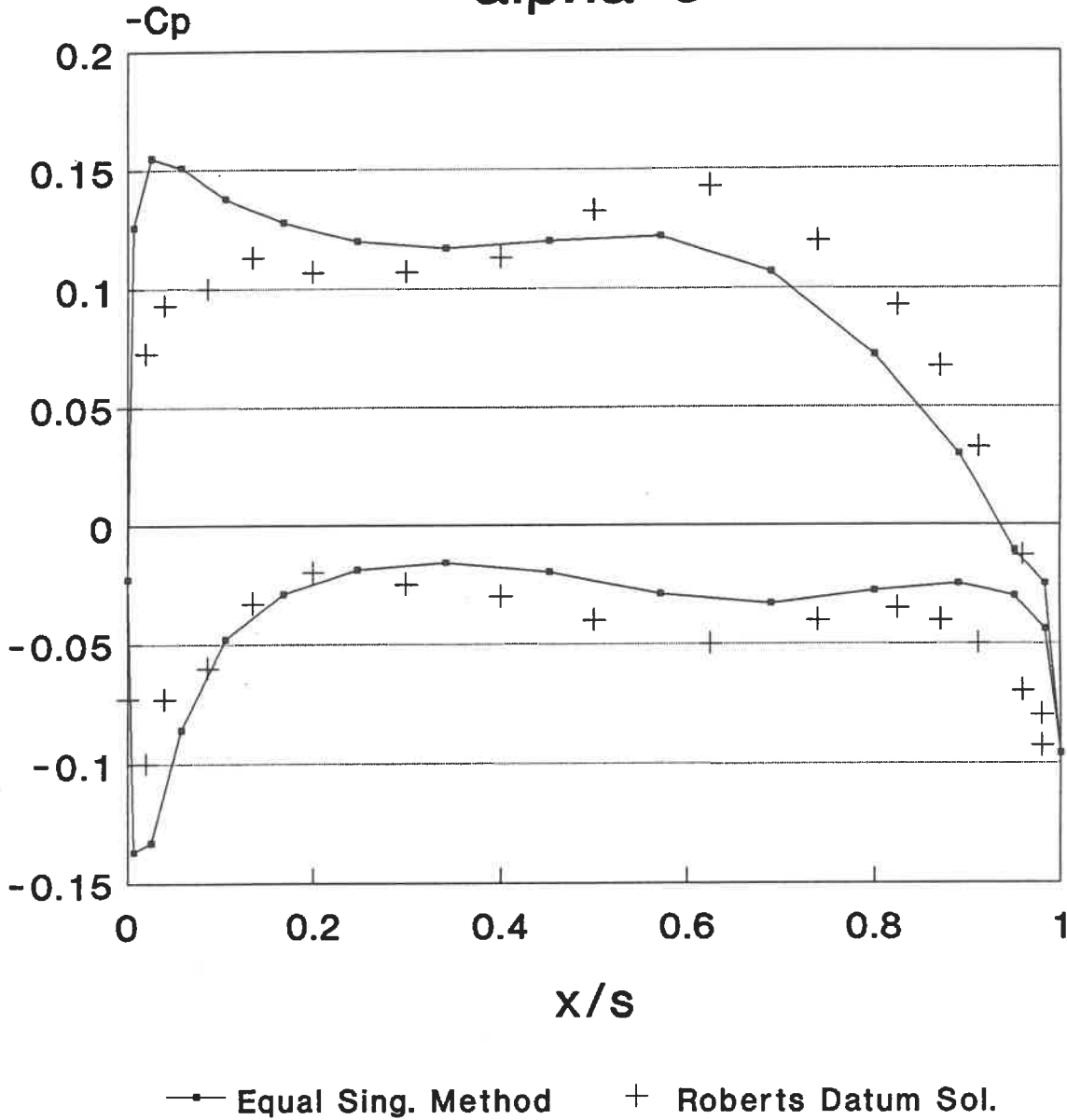
Fig. 10 : Comparison of Pressure Distribution
Strake Wing: y/s=0.035

y/s=0.035
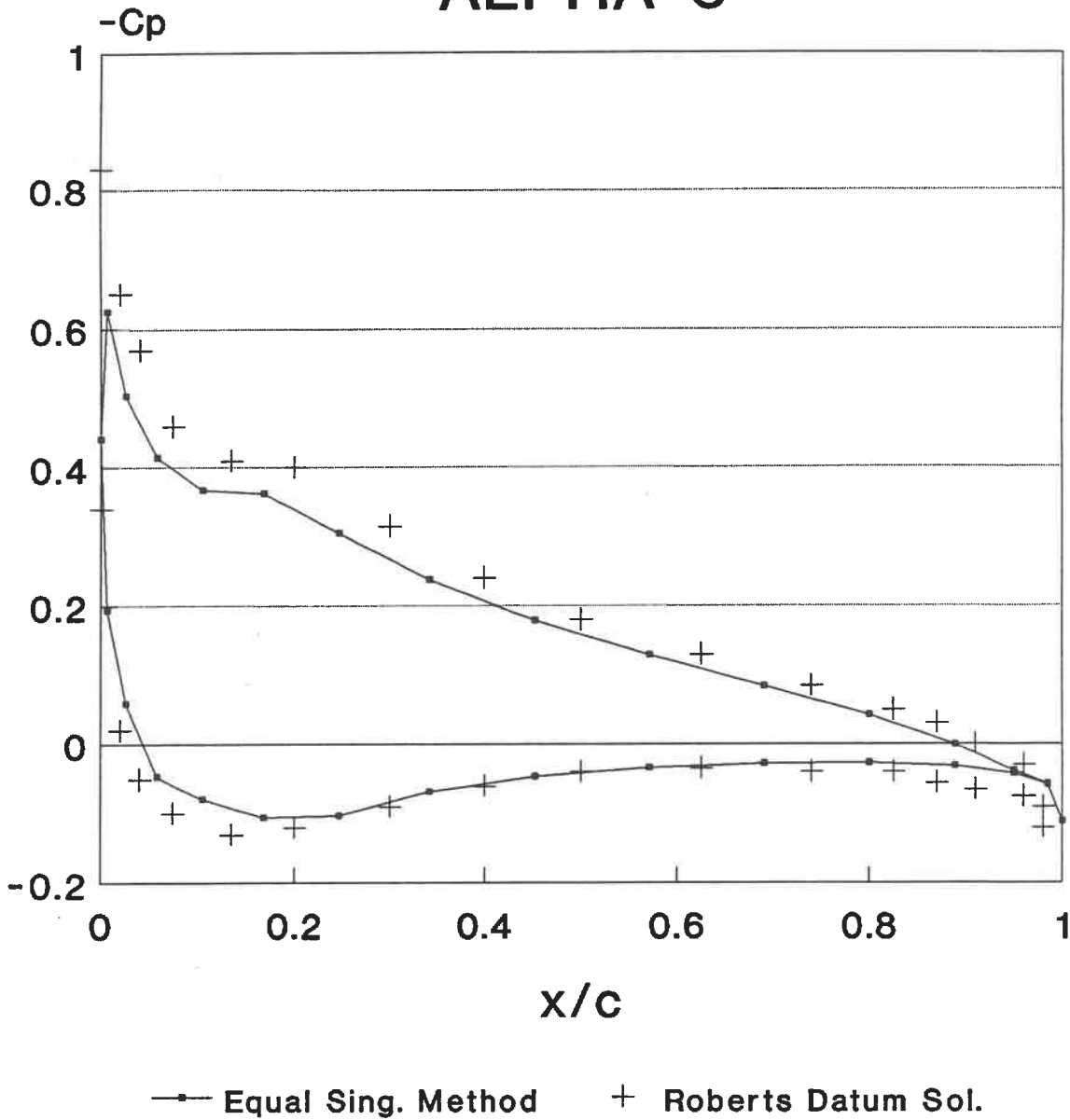
Fig. 11 : Comparison of Pressure Distribution Strake Wing: y/s=0.22

Pressure Distribution
Strake Wing NACA 0005
ALPHA=5

-Cp

x/c
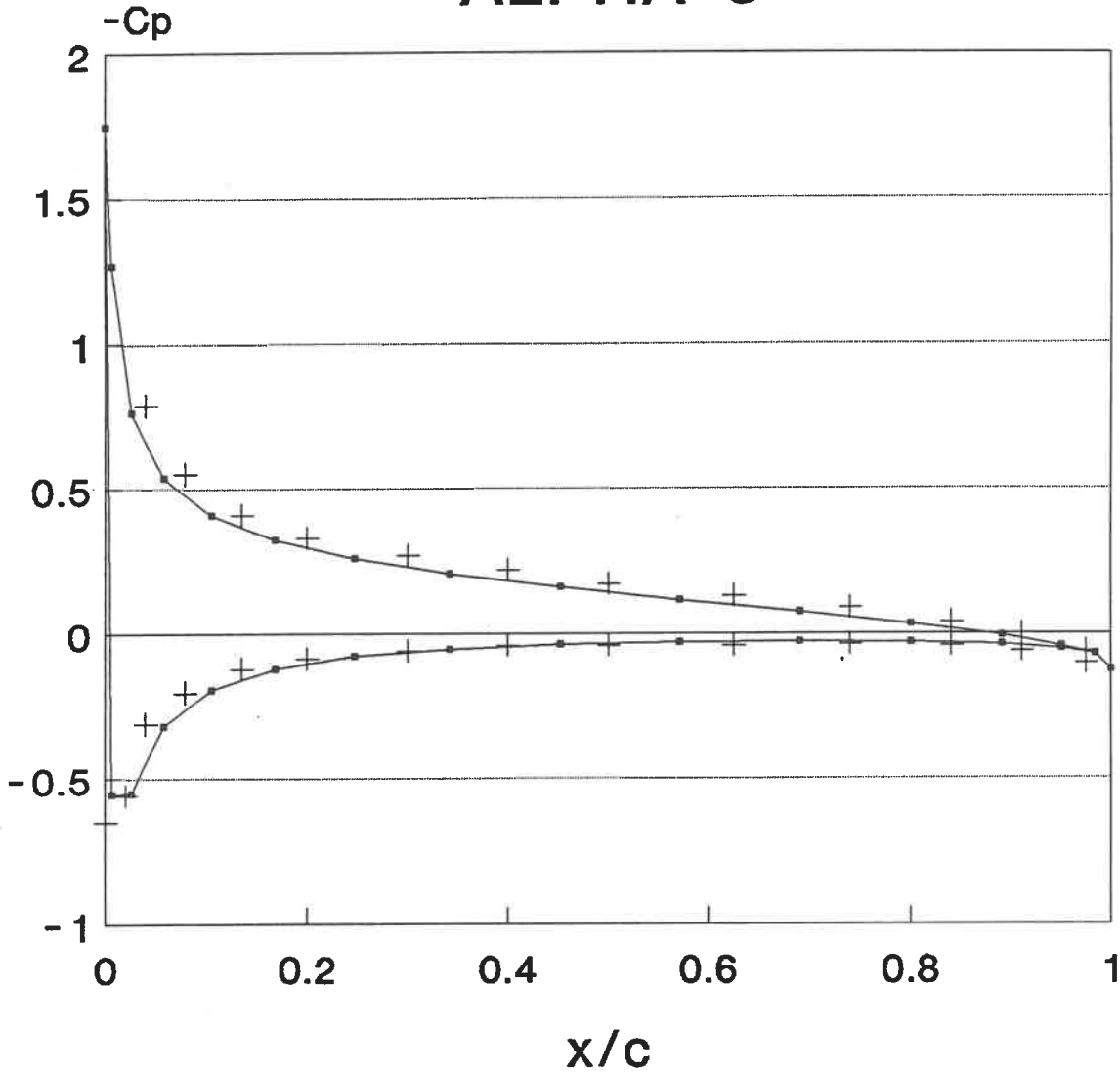
—•— Equal Sing. Method   + Roberts Datum Sol.

Fig. 12 : Comparison of Pressure Distribution
Strake Wing: y/s=0.28

y/s=0.28

Pressure Distribution
Strake Wing NACA 0005
ALPHA=5

-Cp

x/c

⊷ Equal Sing. Method   + Roberts Datum Sol.
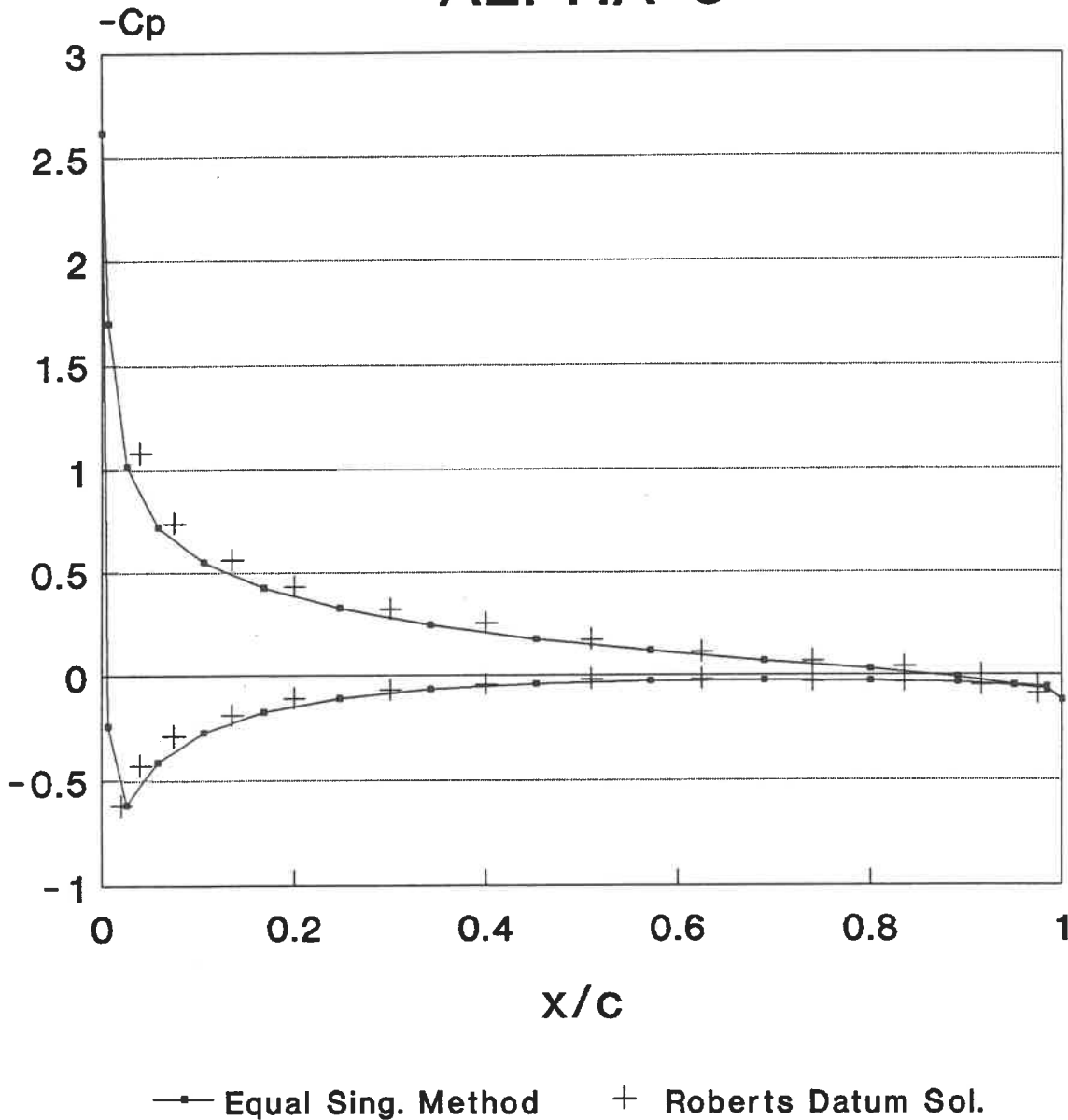
Fig. 13 : Comparison of Pressure Distribution
Strake Wing: y/s=0.9

y/s=0.9

Pressure Coefficient
NACA 64A410 7.6% thick
Alpha=6

Legend:
—*— Inviscid(Eq.)   —+— Inviscid(Ref.1)
—•— Inviscid(In.)
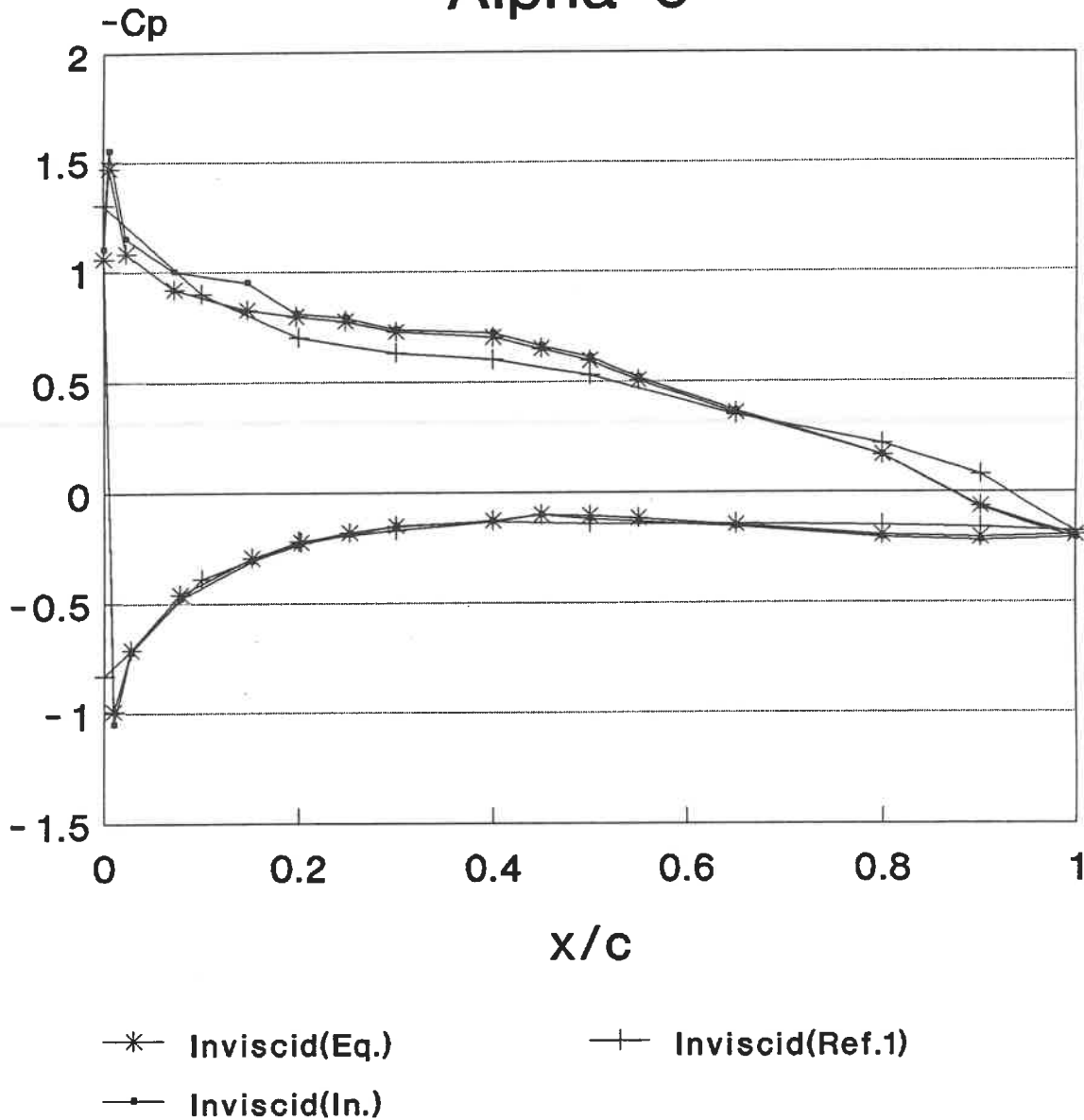
y/s=0.1 A.R.=4.9 T.R.=0.85

Fig. 14 : Comparison of Pressure Distribution Near Rectangular Wing: y/s=0.1

Pressure Coefficient
NACA 64A410 7.6% thick
Alpha=6
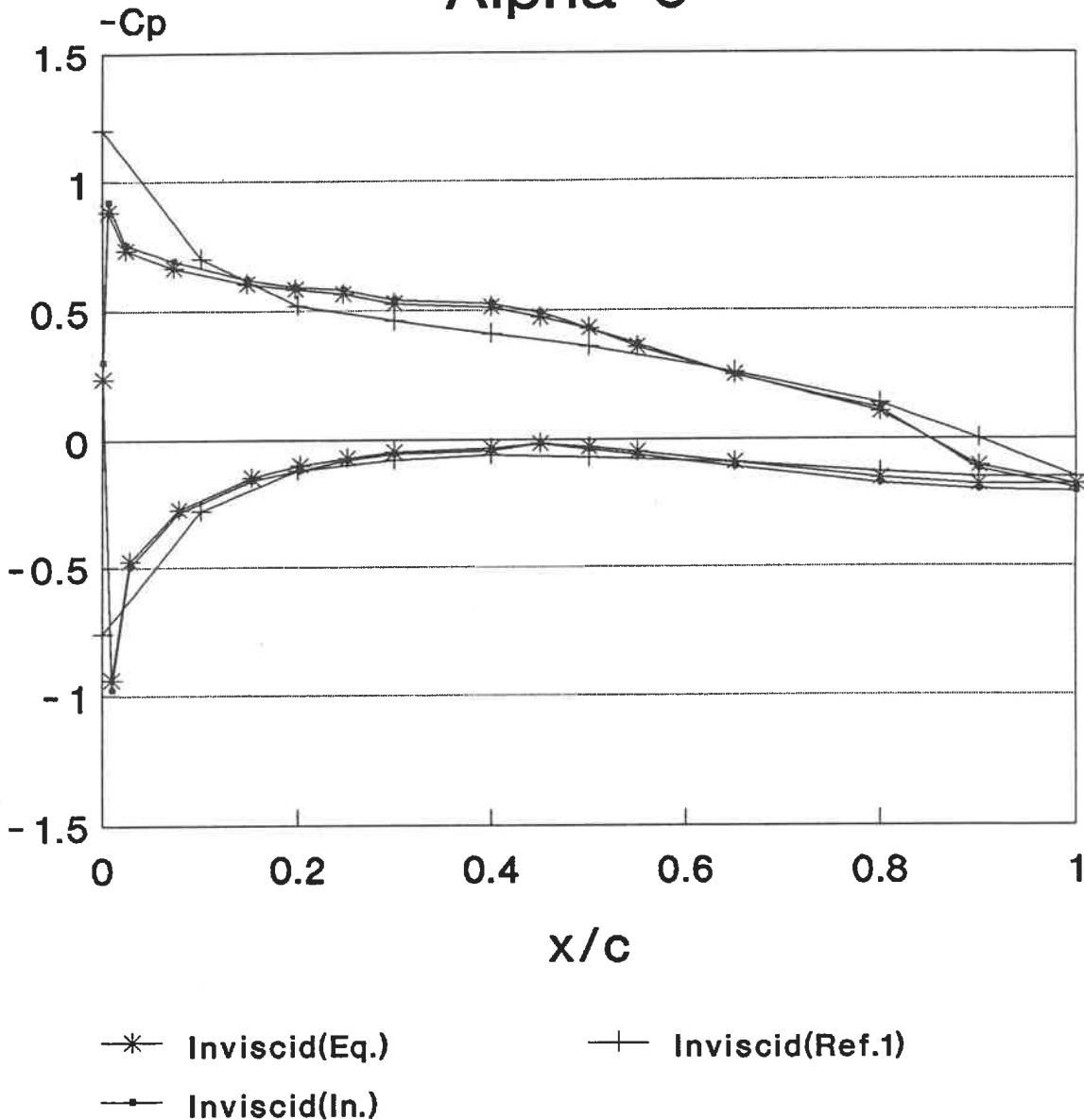
y/s=0.9 A.R.=4.9 T.R.=0.85

Fig. 15:Comparison of Pressure Distribution Near Rectangular Wing: y/s=0.9

Load Distribution
NACA 64A410 7.6% thick

A.R.=4.9 T.R.=0.85

Fig. 16:Comparison of Load
Distribution
Near Rectangular Wing
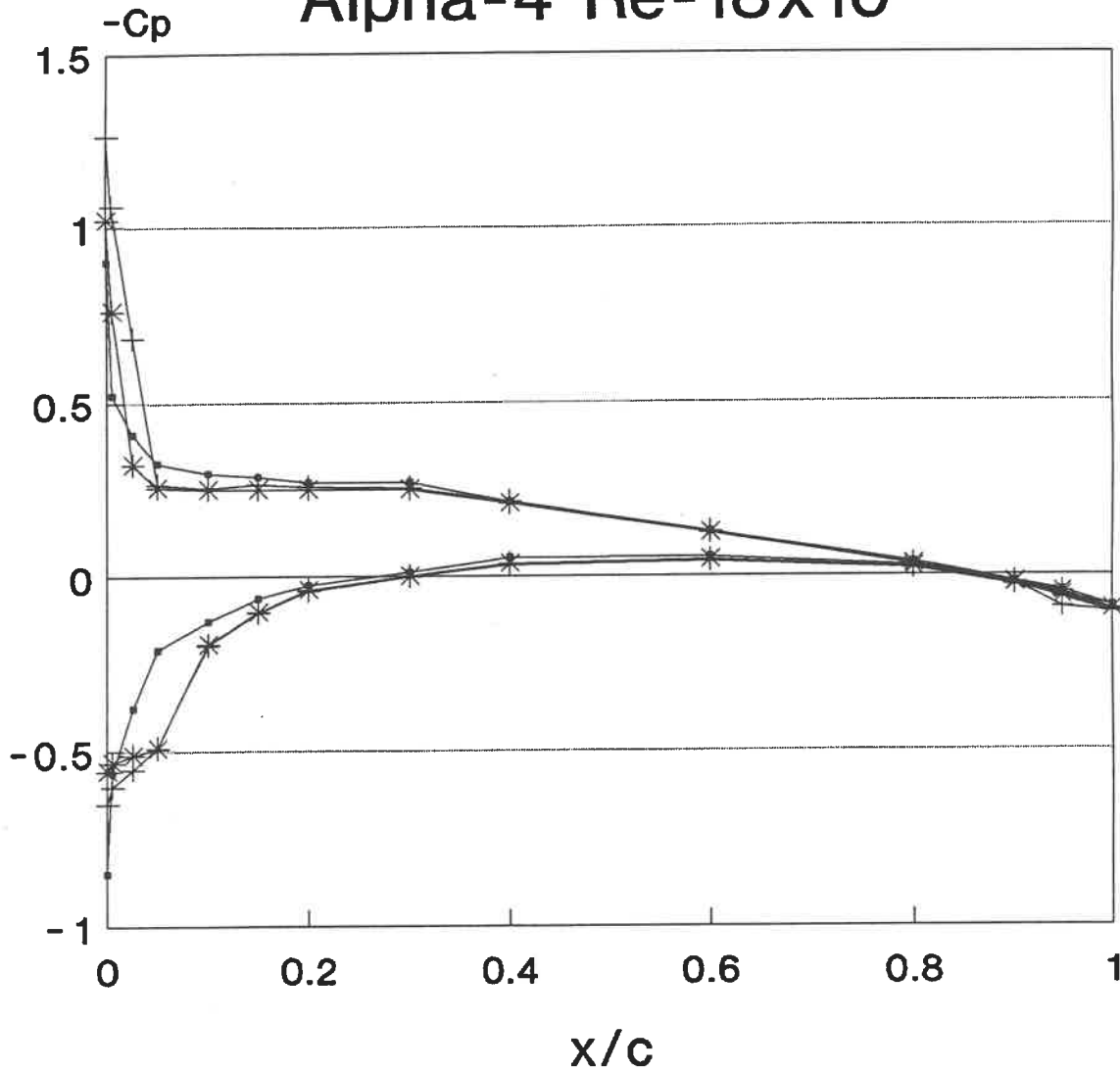
Pressure Distribution
NACA 64A010 7.6% thick
Alpha=4 Re=18x10^6

Fig. 17:Comparison of Pressure Distribution
Swept Wing: y/s=0.1

y/s=0.1 A.R.=3.0 T.R.=0.5 Sw=45.0

Pressure Distribution
NACA 64A010 7.6% thick
Alpha=4 Re=18x10^6
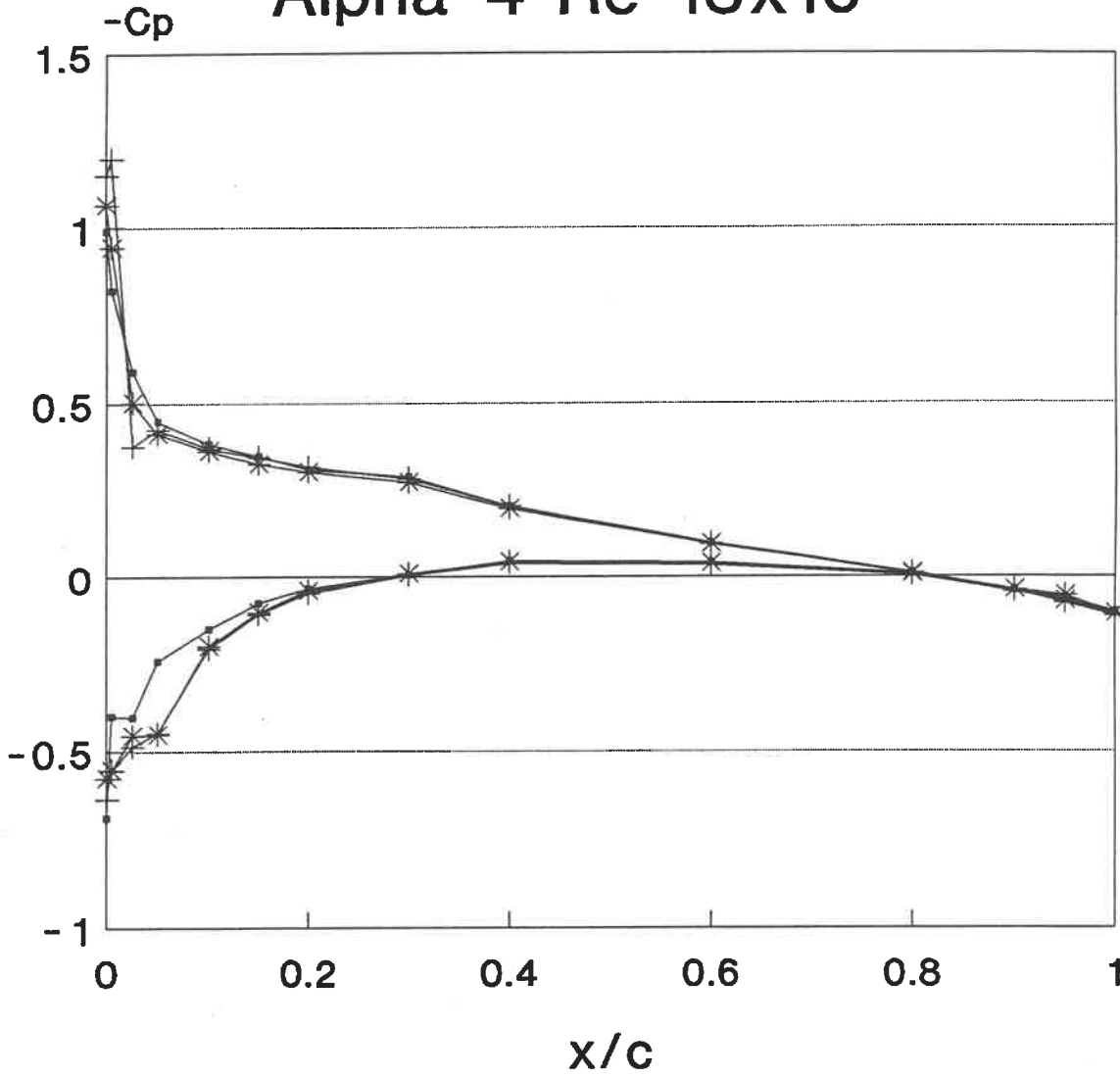
Fig. 18:Comparison of Pressure Distribution
Swept Wing: y/s=0.5

Pressure Distribution
NACA 64A010 7.6% thick
Alpha=4 Re=18x10^6
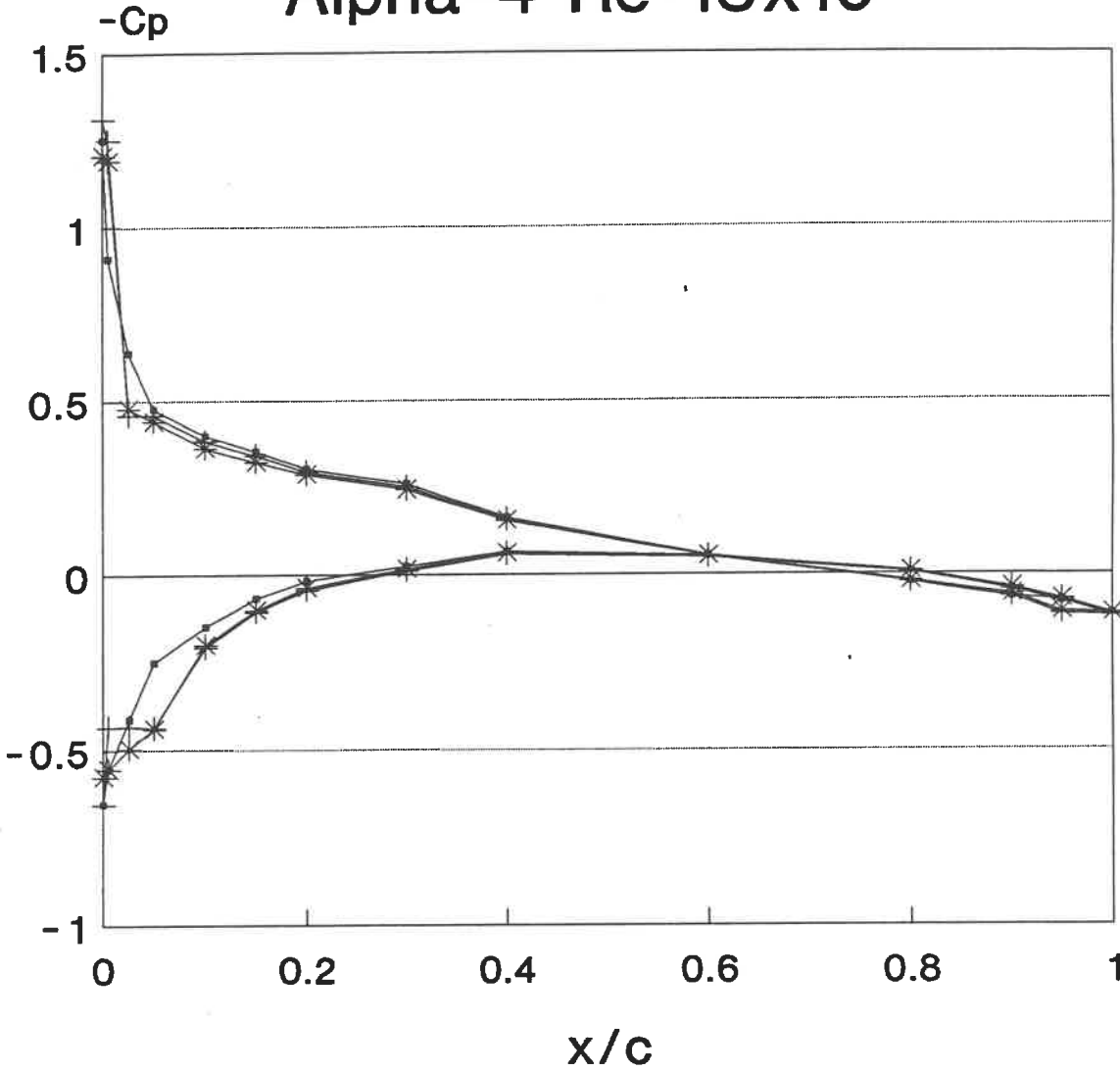
y/s=0.9 A.R.=3.0 T.R.=0.5 Sw=45.0

Fig. 19:Comparison of Pressure
Distribution
Swept Wing: y/s=0.9

Lift Coefficient
NACA 64A010 7.6% thick
Re=18x10^6
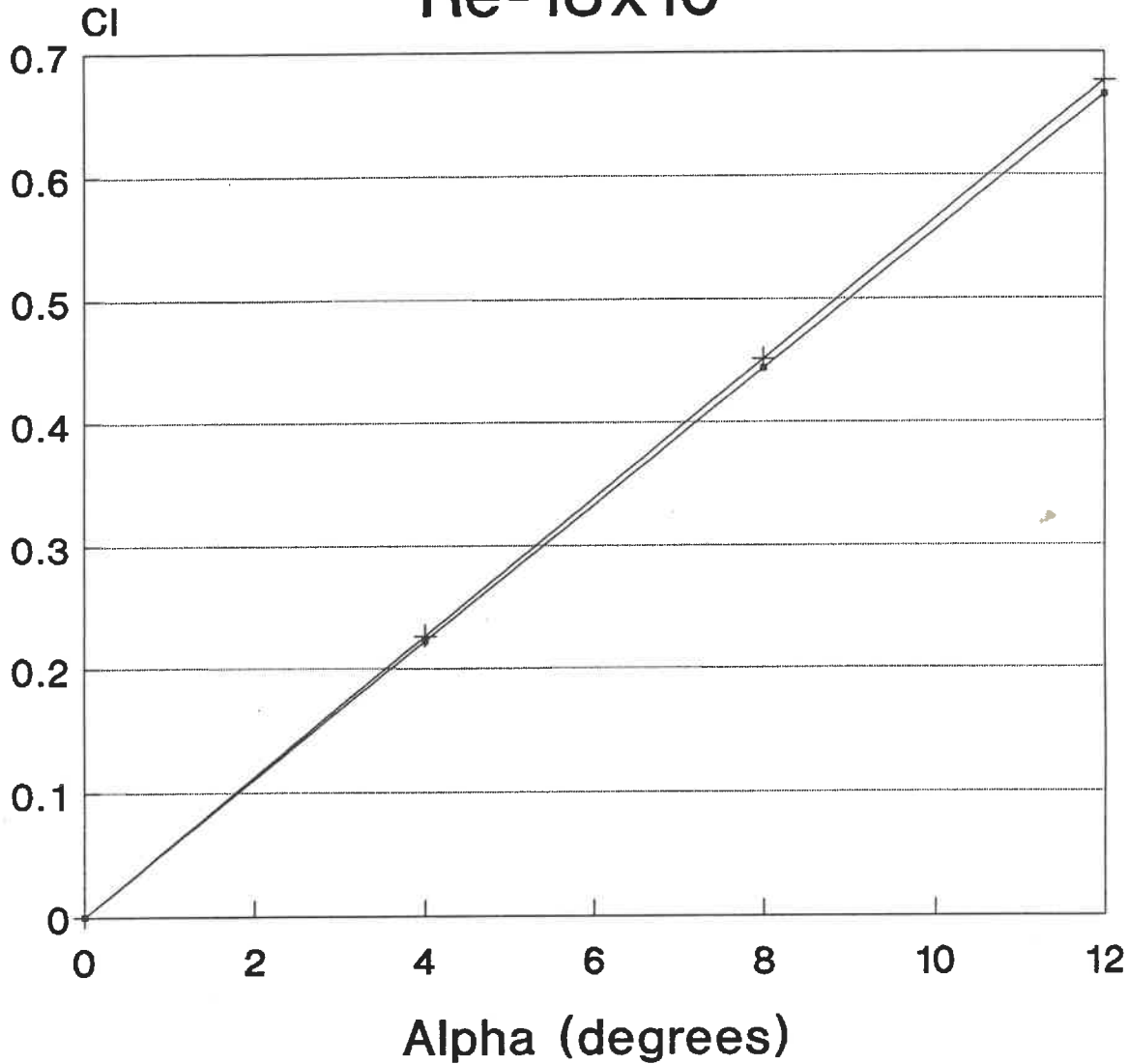
Fig. 20: Comparison of Lift Distribution
Equal Sing. vs Internal. Sing.

A.R.=3.0 T.R.=0.5 Sw=45.0

Lift Coefficient
NACA 64A010 7.6% thick
Re=18x10^6
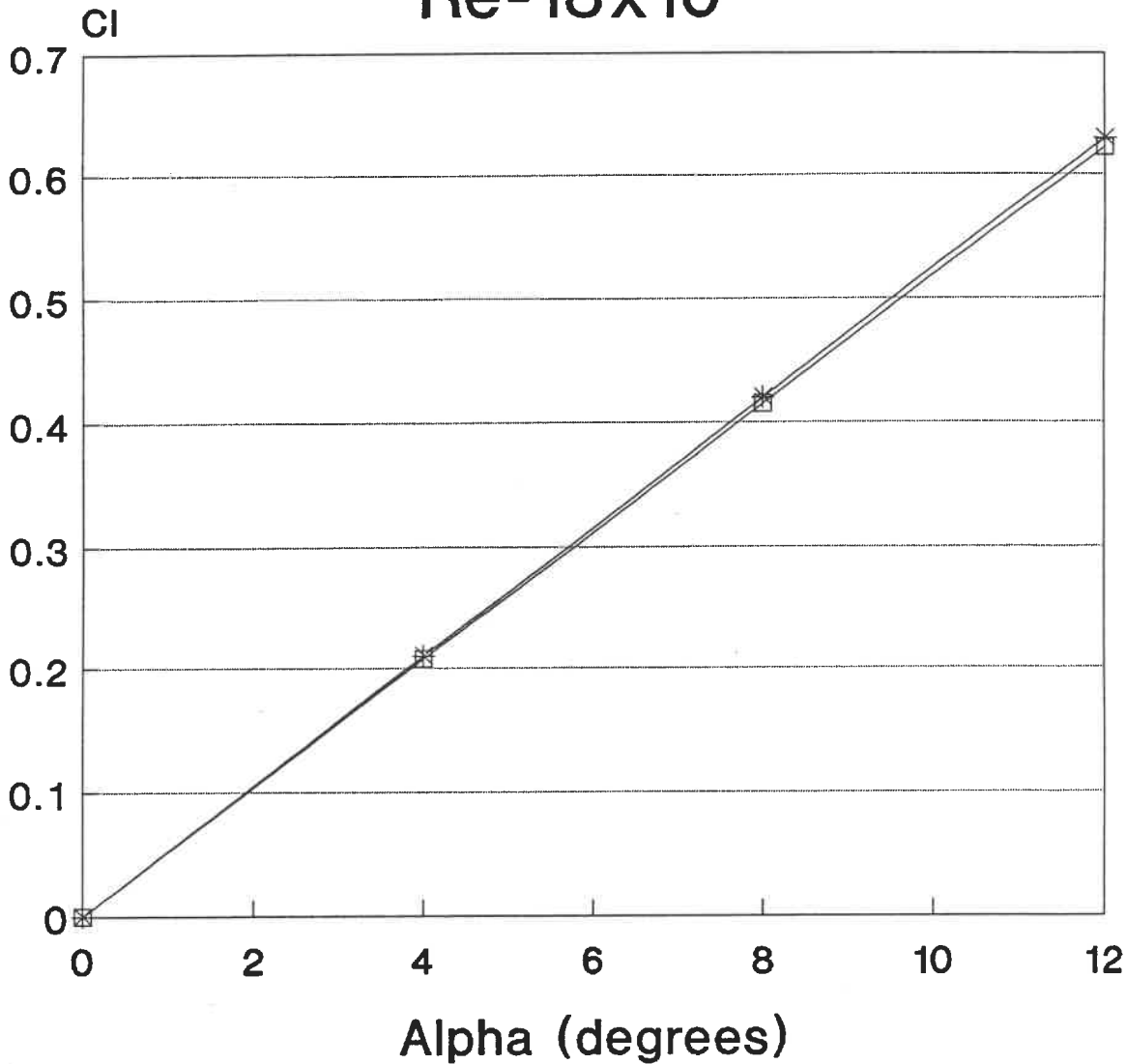
Fig. 21:Comparison of Lift Distribution VII vs Experimental

A.R.=3.0 T.R.=0.5 Sw=45.0
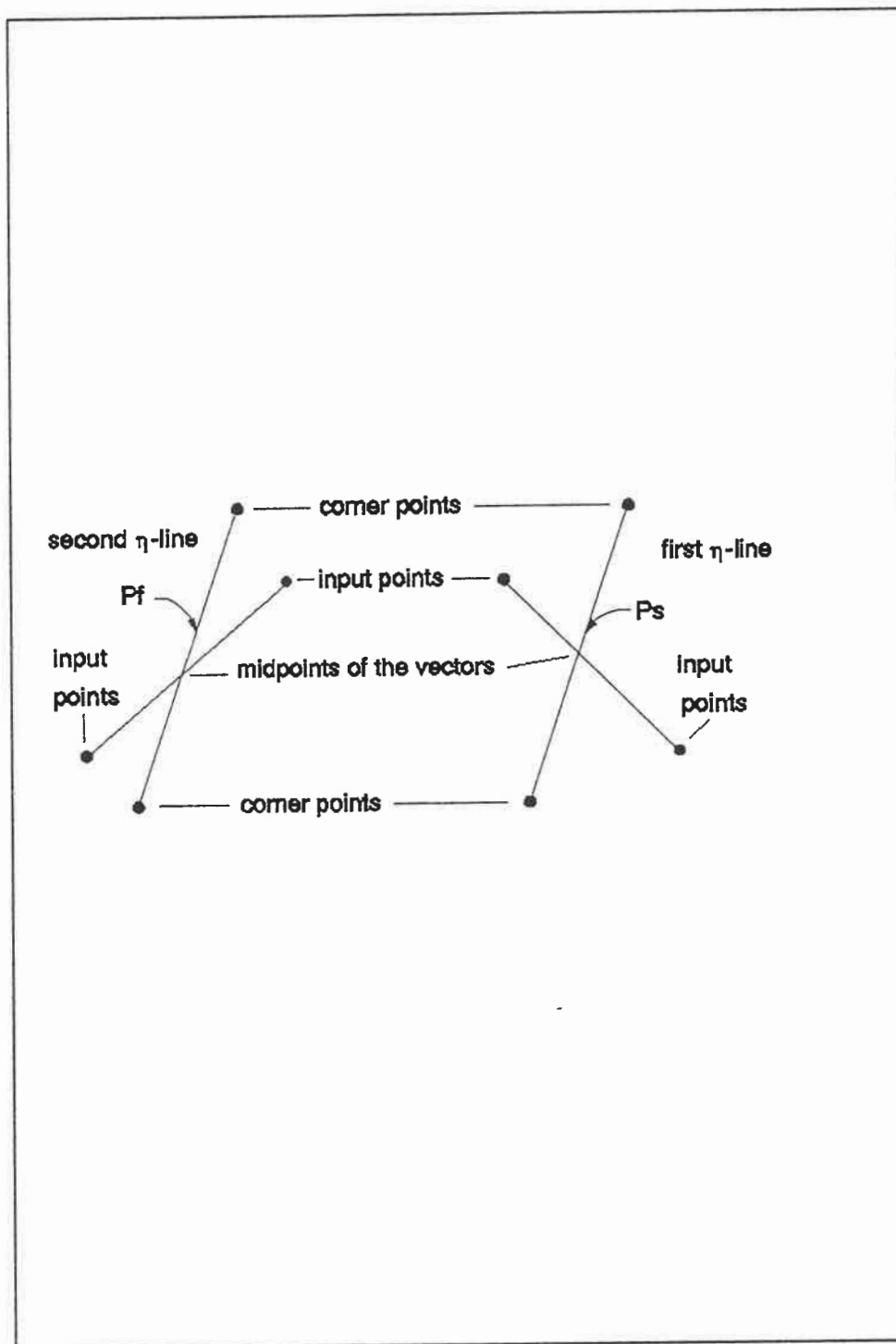
Figure 22 Input Points Forming a Trapezoidal
Element
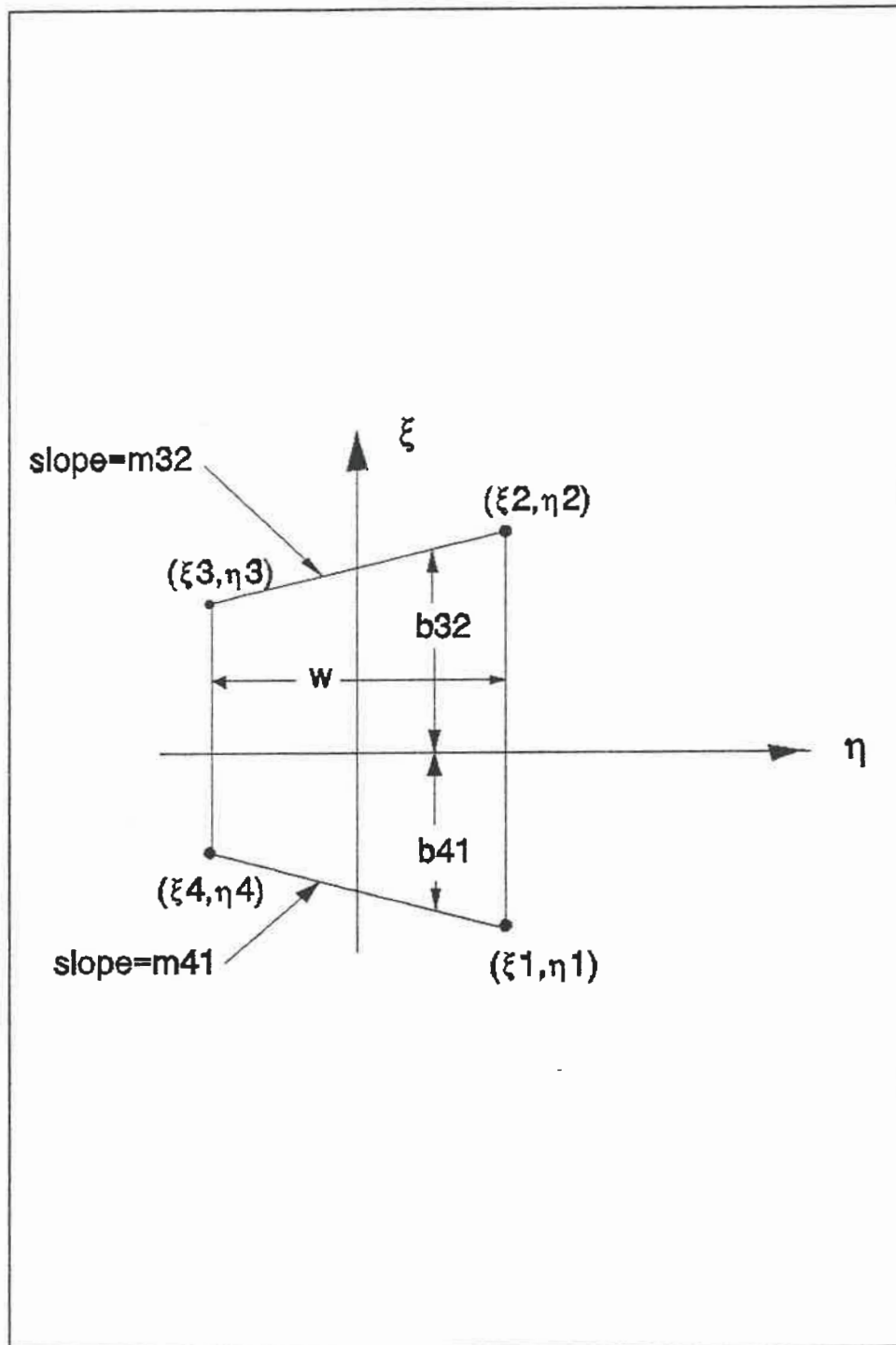
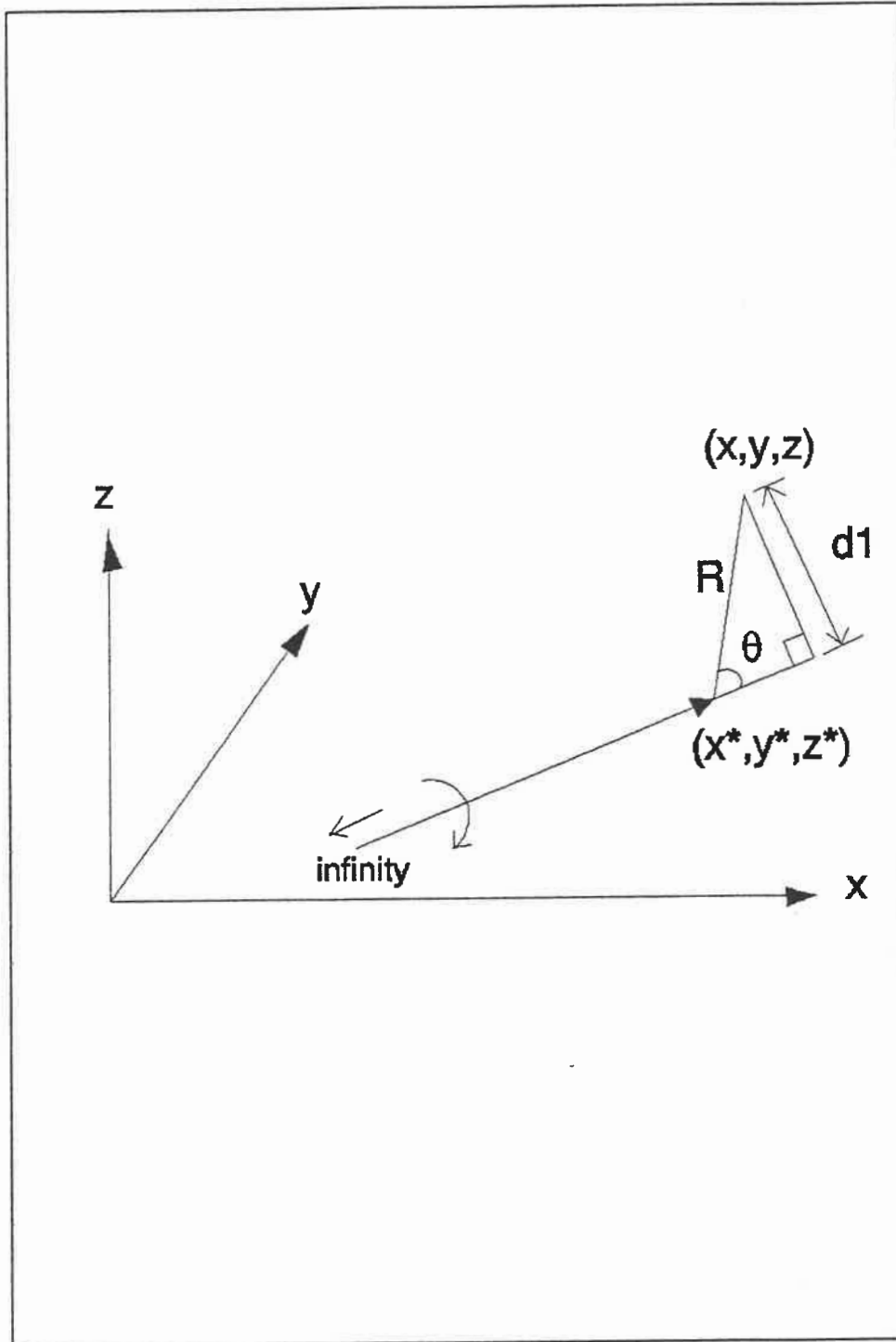Figure 23 Plane Trapezoidal Element
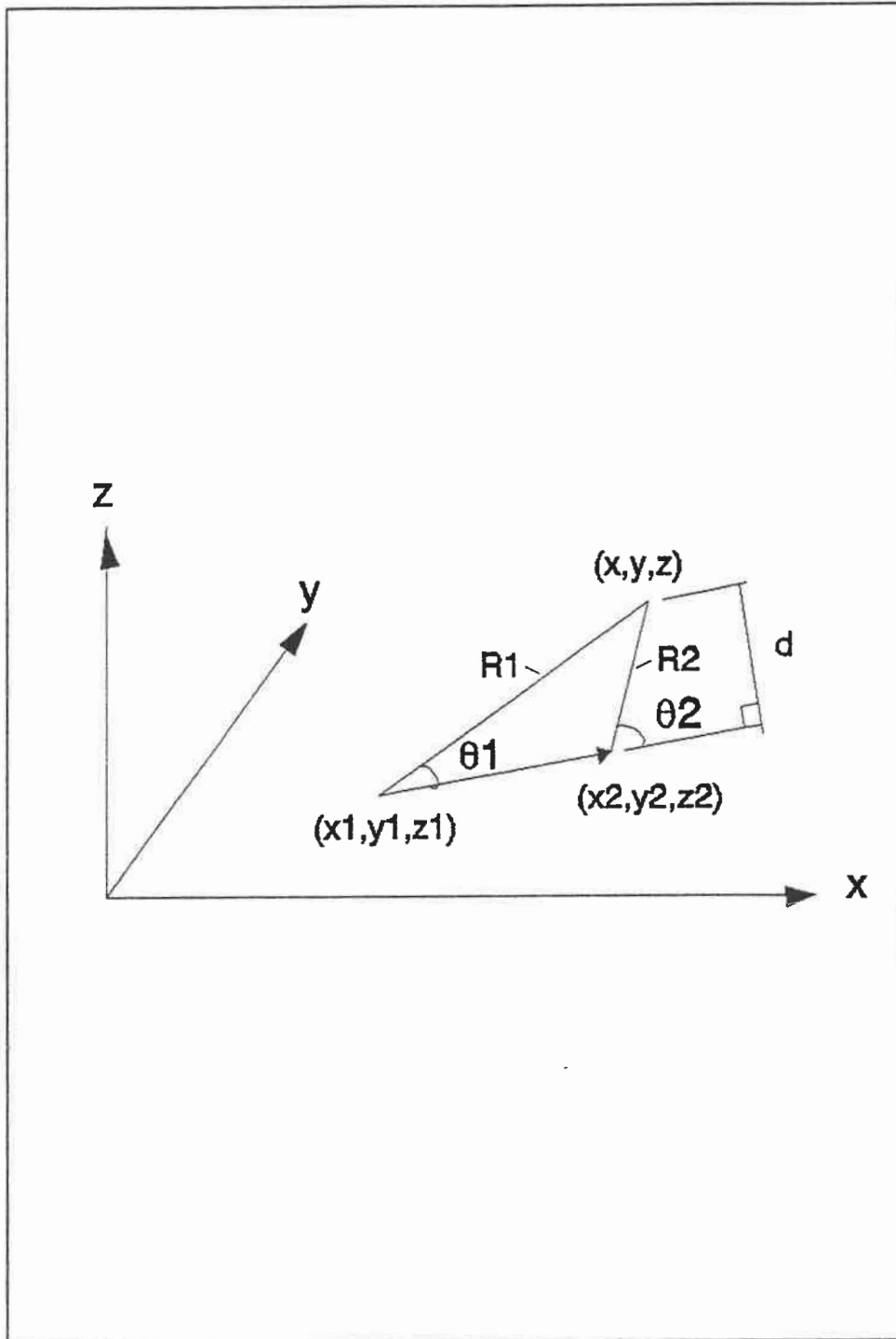
Figure 24 Vortex Segment

Figure 25 Semi-Infinite Vortex Line
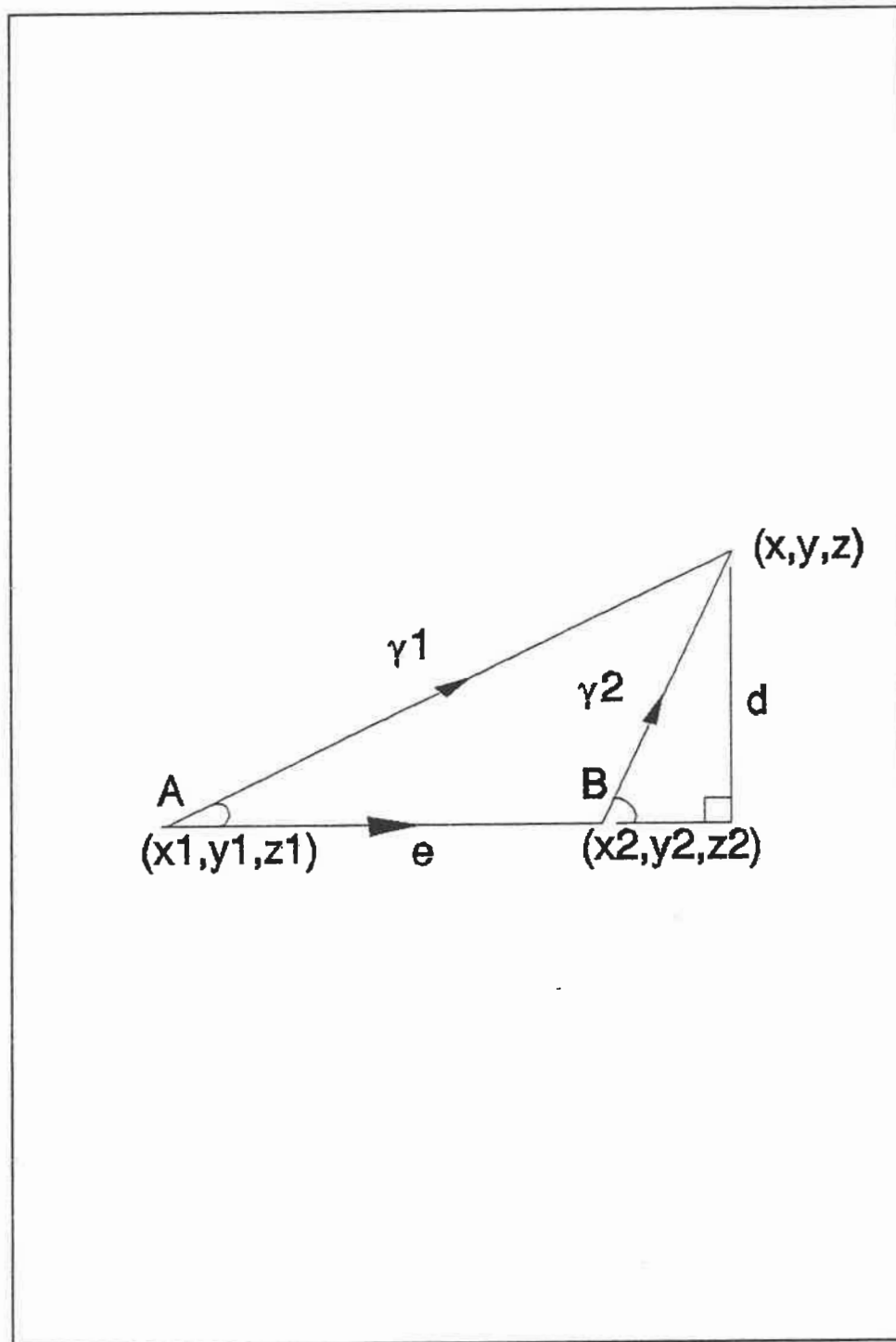
Figure 26 Line Source Segment